Role of Wnt/Planar Cell Polarity Genes in Migration of Facial Branchiomotor Neurons

---

A Thesis Presented to

the Faculty of the Graduate School

at the University of Missouri

In Partial Fulfillment

of the Requirements for the Degree

Master of Arts

---

by

WHITNEY ANN PIKE

Dr. Anand Chandrasekhar, Thesis Advisor

DECEMBER 2013

The undersigned, appointed by the Dean of the Graduate School, have examined the thesis entitled

Role of Wnt/Planar Cell Polarity Genes in
Migration of Facial Branchiomotor Neurons

presented by Whitney Ann Pike,
a candidate for the degree of Master of Arts of Biological Sciences,

and hereby certify that, in their opinion, it is worthy of acceptance.

_____

Professor Anand Chandrasekhar

_____

Professor Dawn Cornelison

_____

Professor Elizabeth Bryda

ACKNOWLEDGEMENTS

There are so many people who have helped me along this journey that I cannot easily list all of them. Thank you so much to all of you, especially:

Anand Chandrasekhar - Thank you for allowing me the opportunity to work with you. I have greatly enjoyed my time in your lab and have learned so much over the past three years. You are a great example of a scientist and mentor, and skills you have taught me will remain with me forever.

My committee members, D. Cornelison and Elizabeth Bryda – Thank you for providing your insight into my projects, and all of the help you gave me over the course of the past three years. You truly challenged me to think and develop as a scientist.

The members of the Chandrasekhar lab, past and present – Derrick Glasco for sparking my interest in the mouse model system; Vinoth Sittaramane for excellent guidance and support; Suman Gurung and James Allen for discussion; Taybor Parker, Trevor Karasek, and Thao Le for their help in the mouse colony maintenance, as well as several other undergraduates for their support in managing the lab.

My family and friends – for everything you have done for me, thank you does not seem to say enough. Thank you to my parents, for allowing me the opportunity to dream and seek out my potential. My sisters and friends for their unwavering support. My husband for being there for me everyday. And finally to

my sister and my son, I take much comfort in knowing that you are always looking down on me, and I miss you so much. I love you all!

TABLE OF CONTENTS

LIST OF FIGURES AND TABLES

ABSTRACT

During brain development, newborn neurons must migrate to precise locations in order to establish functional circuitry. Defective neuronal migration underlies several human brain disorders. The facial branchiomotor (FBM) neurons providing an intriguing model to examine neuronal migration mechanisms. Migration of these neurons requires the function of components of the Wnt/Planar Cell Polarity (PCP) signaling pathway. In the mouse, these neurons are born in rhombomere 4 (r4) of the hindbrain, and migrate caudally into r6 to form the facial motor nucleus. In mice carrying mutations in the gene encoding the Wnt/PCP cadherin *Ceslr1*, caudal migration is intact, but a significant subset of neurons inappropriately migrates rostrally, suggesting that *Celsr1* regulates the directionality of migration. Tissue-specific *Celsr1* knockouts indicate that *Celsr1* likely functions within the ventricular zone of rhombomeres 3 and 4. These and other data suggest that Wnt-mediated signaling may inappropriately attract FBM neurons into r3 in *Celsr1* mutants, and that such attraction is normally suppressed in wild type embryos. In *Celsr1* mutants, the inactivation of *Dvl* suppresses the rostral migration phenotype, suggesting that rostral migration is *Dvl*-dependent. Therefore, we hypothesized that FBM neurons can potentially respond to the chemoattractant Wnt5a in r3 through a *Dvl*-dependent pathway, but that *Celsr1* in the rostral hindbrain normally suppresses *Wnt* activity, preventing inappropriate rostral migration.

FBM neurons of wild type mice can be attracted towards ectopic sources of Wnt5a placed in the rostral hindbrain. Consistent with our hypothesis, migration of FBM neurons towards Wnt5a coated beads placed in r3 in *Dvl2*$^{-/-}$ hindbrain explants was greatly reduced compared to migration in *Dvl2*$^{+/+}$ and *Dvl2*$^{+/-}$ explants. Thus it appears that the suppression of responsiveness to *Wnt5a* could be preventing the neurons from responding to the chemoattractant signal in r3 and blocking rostral migration. If *Celsr1* is acting in r3 and r4 to suppress attraction toward Wnts in r3, it is possible that Celsr1 is upstream of a Wnt antagonist. Therefore, we hypothesized that in the absence of Wnt antagonists, the rostral migration phenotype will be recapitulated because Wnt is able to attract the FBM neurons rostrally. Hence, we analyzed the roles of Wnt antagonists like the *secreted Frizzled Related Proteins (sFRPs)* in the migration of FBM neurons. *sFRP1* expression significantly overlaps that of Wnt5a in the mouse hindbrain. In *sFRP1; sFRP2* compound mutants, inappropriate rostral migration was not observed. However, FBM neurons exit the migratory stream precociously during caudal migration, suggesting that sFRPs may constrain the behavior of caudally migrating FBM neurons.

To further elucidate the mechanisms regulating rostral migration of FBM neurons, we performed an expression profiling screen (RNA-seq) to identify genes that are misregulated in *Celsr1*$^{+/Crash}$ hindbrains. RNA-sequencing was performed using the Illumina platform, and analyzed using TopHat, Cufflinks, and CuffDiff. Candidate genes were further short-listed using various criteria, and several candidates have been identified for future analyses.

CHAPTER 1: Introduction

Cellular migration is a critical process in the development of many systems, and can have severe impacts on disease. For example, during early embryonic development, gastrulation occurs via the movement of blastula cells to develop a multi-layered body plan. Later in development, cell movements control such processes as neurulation, organogenesis, and immune responses. Several diseases are associated with incorrect cell movements. For instance, many different cancers arise from the movement of cells to form tumors that can invade different tissues and metastasize.

The adult brain is an incredibly complex tissue with several layers of organization. During development, the migration of neurons within the central nervous system is essential to establishing the complex neuronal circuitry of the brain. When neuronal migration is defective, it can have severe impacts on development and is associated with several human disorders. Given the important role of the nervous system, it is crucial to understand the mechanisms that regulate neuronal migration.

1.1. Neuronal Migration

1.1.1. Overview of Neuronal Migration

Neuronal migration has been well characterized in cortical neurons. During this process, an individual neuron determines the direction in which to migrate by interpreting signal from the environment, and extends a leading process in that direction. Next, the nucleus and perinuclear material move toward the leading process, leaving behind a trailing process which is later retracted (Lambert de Rouvroit and Goffinet, 2001). While this explains general cell movements, different classes of neurons may alter these mechanisms depending upon their location (Valiente and Marin, 2010).

During this process of migration, neurons must make several decisions, including the initiation of migration, determining the direction in which to migrate, and deciding when to stop migration. Initiation and direction of migration depends largely upon environmental cues. As the neuron begins migration it may come into contact with and adhere to specific substrates, such as the extracellular matrix, which provide navigational information. In addition, protein guidance cues can be found which have the ability to either attract or repel neurons in a specific direction (Valiente and Marin, 2010). Radial and tangential movements are two specific mechanisms by which neurons can migrate. Radial migration is when neurons use the fibers of the radial glial cells as the substrate on which they migrate (**Figure 1.1 a, b**). Tangential migration, on the other hand, is the migration of neurons in a glia-independent fashion, which can utilize

several diverse substrates for guidance (**Figure 1.1 c**) (Marin and Rubenstein, 2003)

1.1.2. Radial Migration

Radial migration is necessary for the formation of the layers of the cerebral cortex. Neocortical neurons and glia cells are born in an area near the cerebral ventricle known as the proliferative or ventricular zone, the layer of epithelium that is facing the brain vesicles, where neuronal progenitors undergo mitosis. Glial cell bodies remain in the ventricular zone and extend long processes through the developing cortex to form the intermediate and marginal zones. When neuronal progenitors exit mitosis and become specified as neurons, they lose their attachment to the ventricular surface and are free to migrate out of the ventricular zone by attaching to radial glial cells, which have extended long radial processes from the ventricular zone to the pial surface. Thus, neurons are able to migrate from the ventricular zone, through the intermediate and subplate zones, and come to rest upon reaching the cortical plate, after detaching from the glial fibers (Sidman & Rakic, 1973; Rakic, 1988). As newer neurons migrate away from the ventricular zone, they move over and beyond the older neurons that have already settled at the pial surface, thus making a highly organized “inside out” laminated arrangement of neurons (Park et al 2002).

Figure 1.1. Radial and Tangential Migration

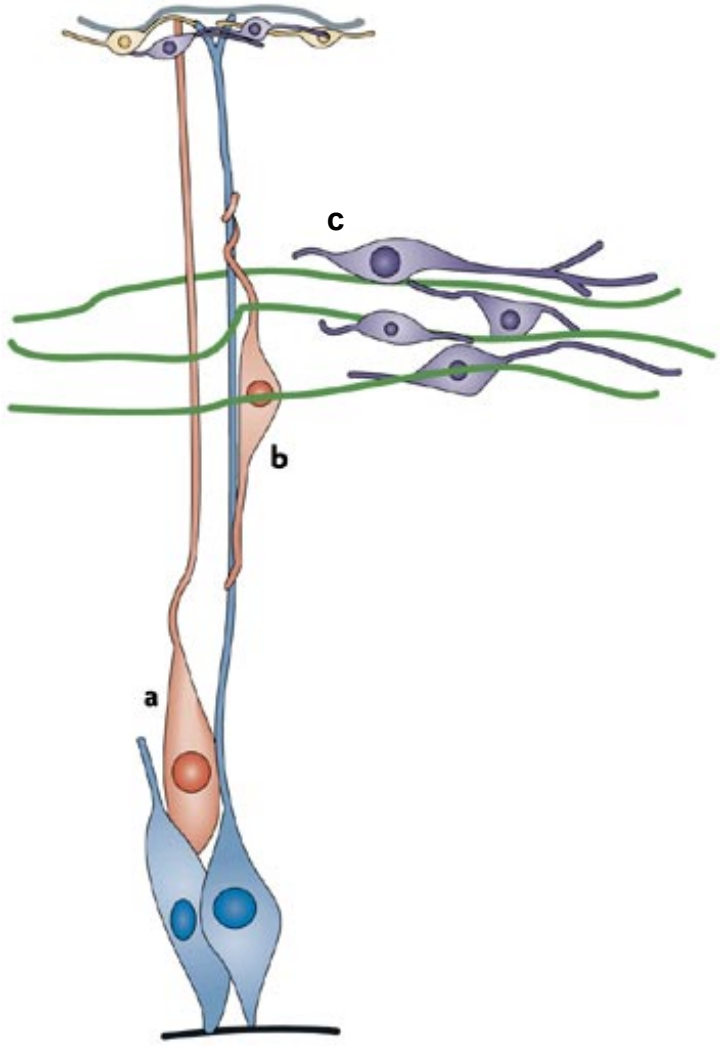

Reprinted by permission from Macmillan Publishers Ltd: *Nature Reviews Neuroscience (Ghashghaei et al., 2007),* copyright 2007.

Figure 1.1. Radial and Tangential Migration

Mechanisms of neuronal migration include radial and tangential migration. (**a, b**) During radial migration, neurons (red) use fibers of radial cells (blue) as a substrate. (**c**) In contrast, tangential migration (purple) is orthogonal to radial migration, and can use substrates such as other fibers or the pial membrane of other cells (green) to migrate. Modified from Ghashghaei *et al. Nature Reviews Neuroscience* **8**, 141–151 (February 2007), doi:10.1038/nrn2074.

1.1.3. Tangential Migration

Tangential migration does not depend upon radial glial cells. Tangentially migrating neurons can attach to many different substrates, such as neighboring cells or axons, and move orthogonal to the direction of radial migration. Several adhesion molecules, such as laminin, have been identified in the migratory route of neurons by providing an interaction between the migrating cells and the extracellular matrix (Marin and Rubenstein, 2003). In addition, chemorepulsive and chemoattractant signals may be involved in the regulation of this migration by guiding the direction in which neurons migrate For example, Hypothalamic gonadotropin-releasing hormone (GnRH) neurons undergo ventrally directed tangential migration towards the diffusible factor netrin1 in the forebrain, indicating that netrin1 acts as a chemoattractant (Murakami et al., 2010). Directed tangential migration of interneurons within the cerebral cortex appear to be regulated by the chemorepulsive effects of interactions between Neuropilin and Semaphorin by signaling the axon to change direction (Marin and Rubenstein, 2001, 2003)

1.1.4. Defective Neuronal Migration

Several human brain disorders have been associated with defective neuronal migration. These disorders are rare and can vary greatly in severity, including symptoms such as cognitive problems, microcephaly, epilepsy, and ataxia. Examples of neuronal migration disorders include lissencephaly and periventricular heterotopia, in which the cortical neurons fail to either terminate or

initiate migration, respectively (Dobyns and Das, 2009; Guerrini and Parrini, 2010). Thus, lissencephaly leads to a thickened and disorganized cortex, resulting in severe mental retardation and developmental delays. Periventricular heterotopia is characterized by the accumulation of differentiated neurons at the ventricular zone. This disorder has been linked to *Filamen A (FLNA),* which is present on the X chromosome, resulting in embryonic lethality in males, and epilepsy in females (Guerrini and Parrini, 2010). Considering the severe consequences that arise when neuronal migration is defective, it is important to understand the mechanisms that regulate migration.

1.1.5. FBM Neuron Migration

The facial branchiomotor (FBM) neurons represent an intriguing example of neuronal migration because they undergo both tangential and radial migration, and have been used to study the initiation of neuronal migration, and more recently, the direction in which neurons migrate. All subtypes of cranial motor neurons in the hindbrain are born within the ventricular zone and undergo radial migration towards the pial surface. One subset, the FBM neurons, also undergoes a characteristic tangential migration. FBM neurons are born in rhombomere 4 (r4) of the hindbrain. The axons of the FBM neurons exit out of r4 to the second branchial arch and innervate muscles that are responsible for facial expression and jaw movements. In mouse, at embryonic day 10.5 (E10.5), the FBM cell bodies begin migrating caudally along the midline in a manner orthogonal to the radial fibers. When the neurons reach r6 by E12.5, they begin

to migrate dorsolaterally and transition to radial migration to form the facial motor nucleus by E14.5 (Chandrasekhar, 2004; Song, 2007). Migration in this manner indicates that the cell bodies must have some sort of directional cue in order to stay within the constraints of the migratory pathway.

Several molecules have been identified as potential guidance cues regulating neuronal migration in the mouse. For instance, Sdf1a acts as a chemoattractant cue for neural progenitors migrating to the dentate gyrus (Bhattacharyya et al., 2008). Neuropilin 1 activates both Semaphorin 3A to guide the movements of the facial branchiomotor axons and VEGF which acts as a chemoattractant for neural cell bodies in the formation of the facial nerve (Schwarz et al., 2004; Schwarz et al., 2008). Wnt5a acts as a chemorepulsive agent in the guidance of corticospinal and commissural axons (Charron and Tessier-Lavigne, 2005; Keeble et al., 2006), but has also been shown to be a chemoattractant in mouse hindbrain explants studies in which FBM neurons migrate towards exogenous Wnt5a (Vivancos et al., 2009).

1.2. Non-Canonical Wnt/PCP Signaling in FBM Neuron Migration

1.2.1 Wnt Signaling Pathways

In Wnt signaling, Wnt, a secreted glycoprotein, binds to Frizzled (Fzd), a seven-pass transmembrane receptor in order to activate the phosphoprotein Dishevelled (Dvl). In the canonical Wnt signaling pathway, this leads to the accumulation of β-catenin, which is then translocated to the nucleus and forms a

complex with LEF or TCF DNA-binding proteins to activate transcription of Wnt target genes (Behrens et al., 1996; Cadigan and Nusse, 1997). In the non-canonical Wnt/planar cell polarity (PCP) pathway (**Figure 1.2**), Dvl can active the small GTPases RhoA and Rac, which will then activate ROCK and Jun kinases, impacting cytoskeletal arrangements, or cell polarity and movements, respectively. The Wnt/PCP pathway is important in establishing the polarity of several different cell types. For instance, epithelial cells have an apical-basal polarity, neurons have a spatial design allowing for propagation of a signal in only one direction, and many cells are able to migrate because they have established leading and tailing edges. PCP mechanisms were first described in the *Drosophila* wing, in which Fzd recruits Dvl to the membrane of one cell, leading to the accumulation of Van-gogh (Vangl)/Prickle (Pk) complexes at the membrane of an adjacent cell, resulting in a polarized formation of wing hairs throughout the wing (Barrow, 2006). Bristle development on *Drosophila* wings (Barrow, 2006), hair patterns in mice (Devenport and Fuchs, 2008), and orientation of cilia in the inner ear (Curtin et al., 2003) are a few examples of PCP processes. In addition, the non-canonical Wnt/PCP pathway has been studied extensively in the migration of the FBM neurons.

1.2.2. Role of Wnt/PCP Components in FBM Neuron Migration

The zebrafish model has provided much insight into the role of the Wnt/PCP signaling pathway in neuronal migration. Among the Wnt/PCP molecules, several are important for the caudal migration of FBM neurons.

Figure 1.2. Non-canonical Wnt/PCP Signaling Pathway

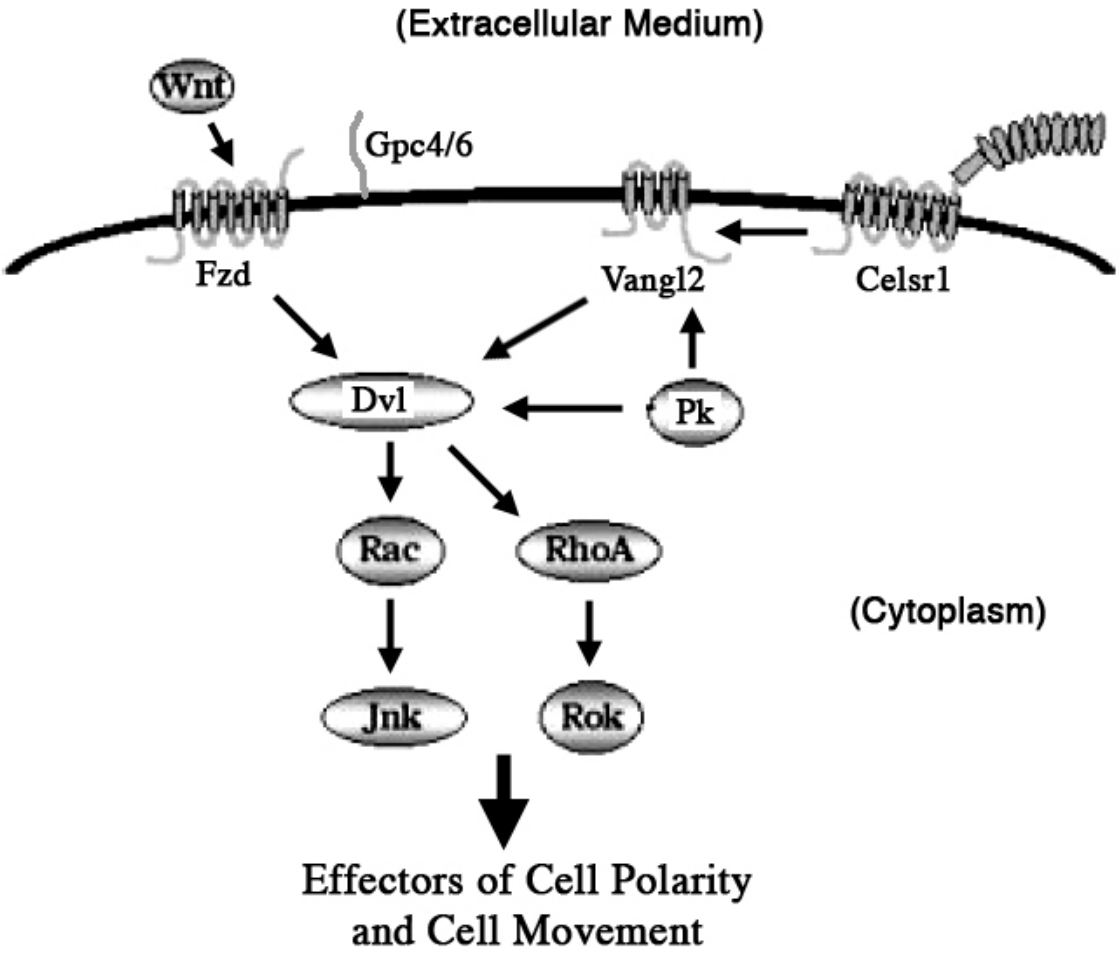

Figure 1.2. Non-canonical Wnt/PCP Signaling Pathway

In the non-canonical Wnt/PCP signaling pathway, Wnt binds to the 7-pass transmembrane receptor Fzd in order to recruit Dvl to the membrane. Celsr1 and Vangl2 are critical to this non-canonical pathway by allowing for further activation of Dvl. Dvl functions to activate small GTPases Rac and RhoA, which then activates kinases Jnk and Rok. This leads to phosphorylation of proteins involved in cytoskeletal rearrangements, cell polarity, and cell movements.

Caudal migration of the FBM neurons in zebrafish has been shown to require components such as *stbm/vangl2*, *celsr1a/1b/2*, *pk1a/b*, and *fzd3a*, but *wnt5a/11* and *dvl* are not required (Bingham et al., 2002; Carreira-Barbosa et al., 2003; Jessen et al., 2002; Mapp et al., 2010; Wada et al., 2006). In the mouse, it has been shown that *Vangl2*, *Ptk7*, *Celsr1-3*, *Fzd3*, and *Scrb1* all play a role in the migration of FBM neurons (Glasco, 2011; Glasco et al., 2012; Qu et al., 2010; Vivancos et al., 2009). Interestingly, a subset of FBM neurons in *Celsr1* mouse mutants are able to migrate rostrally, a phenotype that has never been described in other zebrafish or mouse mutations (Qu et al., 2010). In addition, *Dvl* signaling may be dispensable for caudal migration in both the zebrafish and mouse, but is necessary for rostral migration of FBM neurons in mouse (Glasco, 2011; Glasco et al., 2012).

1.3. *Celsr1* Mediates the Suppression of Rostral Migration of FBM Neurons

1.3.1. Redundant Roles of *Celsr* Genes in Caudal Migration of FBM Neurons

The Wnt/PCP pathway has been shown to play a critical role in the migration of FBM neurons. The *Celsr* genes are a family of atypical cadherins that belong to a family of G-protein-coupled receptors (GPCRs) important for cell adhesion and cell-cell communication. In zebrafish, combinatorial loss of function mutations in *celsr1a*, *celsr1b*, and *celsr2* results in a block of caudal

FBM neuron migration, indicating that the *celsr* genes are critical for caudal migration of FBM neurons (Qu et al., 2010; Wada et al., 2006). In the mouse, *Celsr1-3* homologs are expressed in complementary patterns. *Celsr1* is expressed throughout the ventricular zone and in the floor plate cells of the hindbrain during embryonic development, while *Celsr3* is expressed in post-mitotic neuronal cells, and *Celsr2* is found in both the ventricular zone and post-mitotic neural cells (Qu et al., 2010; Tissir and Goffinet, 2006, 2013). Mutant mice containing the null *Celsr2*^{tm1Dgen} allele (Tissir et al., 2010) *(Celsr2*$^{-/-}$*),* display FBM neurons that prematurely migrate laterally in r5, forming elongated facial nuclei. Mutant mice containing the null *Celsr3*^{tm1Agof} allele (Tissir et al., 2005) (*Celsr3*$^{KO/KO}$) exhibit normal FBM neuron migration, but in *Celsr2*$^{-/-}$*; Celsr3*$^{KO/KO}$ mice, the neurons migrate early as in the *Celsr2*$^{-/-}$ mice, but the facial nucleus is considerably smaller due to cell death upon inactivation of both copies of *Celsr*. These data indicate that *Celsr2* and *Celsr3* function together to regulate caudal migration (Glasco, 2011; Qu et al., 2010).

1.3.2. Some FBM neurons undergo abnormal rostral migration in *Celsr1*^{Crash} and *Celsr1*^{KO} mice

In the mouse, *Celsr1-3* may regulate caudal migration, but *Celsr1* also appears to play a more unique role (Qu et al., 2010). Normally, the FBM neurons in the mouse are born within r4 of the hindbrain, and migrate caudally towards r6. In mice heterozygous for the dominant negative *Celsr1*^{Crash} allele, most of the FBM neurons migrate caudally out of r4 in a normal fashion. However, a small

but significant subset of neurons migrates abnormally in a rostral direction towards r2. This rostral migration phenotype is also evident in the null allele *Celsr1*^{KO} mutant mice (Qu et al., 2010). Thus, it appears that *Celsr1* normally acts within the rostral hindbrain in order to suppress the rostral migration of FBM neurons (**Chapter 3**, **Figure 3.1**).

1.3.3. Celsr1 Functions Within the Ventricular Zone of r3-5 to Suppress Rostral Migration

The *Celsr1* expression pattern was characterized in detail in order to further elucidate the mechanisms by which *Celsr1* could be acting to suppress rostral migration of FBM neurons. *Celsr1* mRNA is expressed within the neuroepithelium and the floor plate of the developing mouse hindbrain. Celsr1 protein is expressed in neuroepithelial cells, intermingled with Islet1 (Isl1)-positive FBM neurons in r4 at E9.5-10.5. By E11.5, Celsr1 is expressed in the floor plate cells, and no longer colocalized with Isl1 cells in the FBM neurons (Qu et al., 2010).

Given its broad expression in the hindbrain, we created several *Celsr1* conditional mutants to determine the spatial requirements of *Celsr1* in FBM neuron migration. The Cre-lox system was utilized to create knockouts in areas overlapping the *Celsr1* expression domain. Mice with a floxed allele for *Celsr1* (Celsr1^{tm1Fati}) were bred to transgenic mice that expressed Cre recombinase under the control of different tissue specific promoters. Thus, in the progeny, in the areas where Cre is expressed, the exons between the LoxP sites are

excised, generating cells that are null for Celsr1 in specific areas. In this manner, the *r4-Cre* line knocked out *Celsr1* specifically in rhombomere 4 (provided by Michèle Studer, U. of Nice; France) (Di Bonito et al., 2013; Studer et al., 1998), *Krox20-Cre* (provided by Susan Dymecki, Harvard) (Voiculescu et al., 2000) in rhombomeres 3 and 5, and *Shh-Cre* (Jackson Laboratory) (Harfe et al., 2004) in the floor plate cells. Both the *r4-Cre* and the *Krox20-Cre* conditional knockouts display a rostral migration phenotype similar to the Celsr1 mutants, while conditionally inactivating *Celsr1* in the floor plate using a *Shh-Cre* line did not affect FBM neuron migration. Together these results indicate that *Celsr1* functions specifically within rhombomeres 3-4 to specify FBM neuron directionality (Glasco, 2011). Given the rostral migration phenotype in the absence of *Celsr1*, it is possible that *Celsr1* normally acts within the r3-r4 region to suppress rostral migration of the FBM neurons.

1.3.4. FBM Neurons of *Celsr1*^{Crash} Mutants Respond to a Local Guidance Cue

To investigate further a role for specific rhombomeres in rostral migration, we examined the origin of the rostrally migrating neurons. Rostral migration upon the loss of *Celsr1* could be due to either a random loss of polarity of the neurons, or a guidance cue capable of attracting the FBM neurons. To further understand the mechanisms regulating the suppression of rostral migration, anterograde labeling of the migrating neurons in *Celsr*$^{+/Crash}$ mice was performed. If rostral migration is due to a random loss of polarity, rostrally migrating FBM

neurons could potentially be born anywhere within r4. However, if rostral migration is due to a guidance cue in the rostral hindbrain, it is likely that the rostrally migrating neurons would be found only in the anterior portion of r4 so that they are in closer proximity to the guidance cue. The results indicate that rostrally migrating neurons are born solely within the upper portion of r4, and are consistent for a role for Celsr1 in r4. Together, this data give support for a model for rostral migration occurring in response to a local guidance cue in the rostral hindbrain, which is normally suppressed in wild type embryos (Glasco, 2011; Qu et al., 2010).

1.3.5 Rationale

We propose a model in which *Ceslr1* normally acts in the rostral hindbrain to suppress a guidance cue from attracting the FBM neurons in that direction. To further elucidate this model of *Celsr1* mediating rostral suppression of FBM neurons, it is important to understand the molecular mechanisms by which *Celsr1* is functioning. The abnormal rostral migration evident in *Celsr1* mutant mice is completely suppressed upon the inactivation of *Dvl2*, indicating that Dvl is required for rostral migration to occur. Explant studies using a chemoattractant placed in the rostral hindbrain allowed us to further examine the roles of Wnt and Dvl in rostral migration (**Chapter 3**). It is possible that there are other candidate molecules in the rostral hindbrain whose expression may be differentially misregulated upon the loss of *Celsr1*. Thus, a high-throughput sequencing, RNA-

seq, was performed to identify candidate molecules involved in the *Celsr1*-mediated suppression of rostral migration (**Chapter 4**).

CHAPTER 2: Material and Methods

*Unless otherwise indicated, all protocols were followed as previously described (Glasco, 2011). In each protocol, reagents are referred to in their abbreviated forms; please see **Section 2.7** for a detailed list of components and instructions to prepare each one.*

2.1. Animal Maintenance

2.1.1. Mouse strains

Listed below are strains or alleles of the animals used in our studies, and the abbreviated name they are referred to by (**Table 2.1**):

2.1.2. Mouse colony maintenance

Mouse colonies were maintained using standard protocols approved by the Animal Care and Use Committee at the University of Missouri. Mice were housed in a 72-73°C room with 30-70% humidity and a 12 hour light/dark cycle. Conventional cages contained corncob bedding and one source of housing enrichment. Mice were kept in groups, with the exception of males designated for timed matings. To maintain specific mouse lines in the colony, breeding trios containing one male and two females were kept at all times, along with a stock of genotyped males and females under one year of age.

Table 2.1. Mouse Strains

Strain	Shortened Name	Source
B6.CD1-*Tg(Hoxb1-cre)*^{r4Mist}/Cnrm	*r4-Cre*	Michèle Studer (University of Nice, France)
B6.129S6-*Shh*$^{tm2(cre/ERT2)Cjt}$/J	*Shh-Cre*	Jackson Laboratory (stock #005622)
B6-*Egr2*$^{tm2(cre)Pch}$/Dym	*Krox20-Cre*	Susan Dymecki (Harvard University)
B6-*Celsr1*^{tm1Fati}	*Celsr1*^{fl}	Fadel Tissir (University of Louvain, Belgium)
B6-*Celsr1*$^{tm1.1Fati}$	*Celsr1*^{KO}	Fadel Tissir (University of Louvain, Belgium)
C-*Celsr1*^{Crsh}/Murd	*Celsr1*^{Crash}	Jennifer Murdoch (MRC; UK)
129S-*Dvl1*^{tm1Awb}/J	*Dvl1*	Jackson Laboratory (stock #007965)
129S-*Dvl2*^{tm1Awb}/J	*SE1::GFP*	Samuel Pfaff (Salk Institute)
B6-*Gt(ROSA)26Sor*$^{tm4ACTB-tdTomato,-EGFP)Luo}$	*ROSA26mTmG*	Dawn Cornelison (University of Missouri)
B6-Sfrp1^{tm1Bsk}	*sFRP1*	Kamana Misra (University of Medicine & Dentistry, New Jersey)
B6-Sfrp2^{tm1Sato}	*sFRP2*	Kamana Misra (University of Medicine & Dentistry, New Jersey)

2.1.3. ID Tagging

In order to track and genotype individual mice, each mouse was ID tagged between 18 and 21 days, prior to weaning. The mouse was restrained by hand, and the edge of the ear was held with a blunt forceps. A small animal ear tag (National Band & Tag, No. 1005-1) soaked in 70% ethanol was applied midway down the pinna of the ear using a stainless steel applicator (National Band & Tag, No. 1005s1). The ear tag number for each mouse was recorded in a custom Excel database, and the same number was used when collecting tissue for genotyping.

2.1.4. Tissue collection and genomic DNA isolation

Mice were genotyped using tail biopsies collected at post-natal day 18 (P18) to P21. The mouse was restrained by hand, and using a clean razor blade, a 0.5 mm piece was cut from the end of the tail. The tail tissue was placed in a 1.5 mL tube labeled with the mouse's ear tag number. The tail was held in styptic powder (Kwik Stop, 18821) to stop any bleeding. Mice were returned to the breeding cage until weaning at P21.

In some cases, ear biopsies were taken from adult mice for genotyping purposes. These were taken by restraining the mouse by hand, and using an ear punch to clip a 1 mm circle from the pinna of the ear. The ear punch (National

Band & Tag, No. 1005s1) was cleaned with 70% ethanol between animals. The tissues could be stored at -20°C for up to one week before DNA isolation.

2.1.5. Euthanization

Adult animals were euthanized by asphyxiation in a carbon dioxide chamber containing enough room for each animal to maintain its normal posture. The chamber was flooded with 100% carbon dioxide until all animals were unconscious. Mice euthanized because of age or colony reduction were left in the carbon dioxide chamber for 10-20 minutes. Pregnant mice with embryos for collection were kept in the chamber for only two minutes so that the embryonic tissue remained as fresh as possible. Cervical dislocation was performed after CO_2 treatment as a secondary means to ensure death. All animal procedures were approved by the University of Missouri Animal Care and Use Committee.

2.1.6. Embryo Collection

Timed matings were utilized to collect embryos at specific time points during development. Two females were set up with one embryo breeder male, and copulation plugs were checked daily. The day of plug was designated as embryonic day E0.5. To ensure pregnancy before dissection, the female was weighed on E0.5, by placing the mouse in a 500 mL beaker lined with a paper towel, and returned to a stock cage until E7.5, at which point the animal was weighed daily until the day of dissection (generally E11.5-E12.5). Pregnancy was identified by a minimum 20% increase in weight from E0.5 to E12.5. If the

mouse had gained sufficient weight, we concluded that she was pregnant, and the mouse was euthanized in a carbon dioxide chamber, followed by cervical dislocation to obtain embryos of the correct embryonic age. This protocol for identifying pregnancy was extremely accurate, broadly applicable over a range of litter sizes, and avoided needless euthanization of non-pregnant females of valuable genetic backgrounds. The abdomen was cleaned with 70% ethanol, and sterilized surgical scissors were used to make longitudinal incisions from the vagina to the rib cage, being careful to cut just underneath the skin. Blunt forceps were used to remove the uterus from the abdomen, carefully cutting the blood vessels and connective tissue away. The uterus was placed in ice-cold 1X-PBS-DEPC in a 100 mm x 15 mm petri dish (Fisher, 0875712) and opened by sliding thin forceps along the entire length of the uterine muscle. This was done quickly in order to relieve any pressure the uterine muscles may be putting on the embryos. Individual embryonic sacs were then broken open using two pairs of blunt forceps, and the embryos were removed by cutting the umbilical cord. The embryos were then transferred to a fresh petri dish filled with ice-cold 1X-PBS-DEPC in order to confirm the age, based upon Thieler staging. The embryos could then be processed for fixation or used for further tissue dissection.

The method for fixation varied depending upon the application, but in general, embryos were fixed overnight in 4% PFA in 1X-PBS-DEPC. If fixing whole embryos, the fourth ventricle was opened prior to fixation to allow the solution to penetrate all tissues. Fixation was performed immediately after the gross dissection. Embryos were transferred to 1X-PBS-DEPC and stored at 4°C

for immediate use or dehydrated through a methanol series and stored at -20°C indefinitely.

2.2. Genotyping

All genotyping protocols were performed as previously described (Glasco, 2011) with the following changes.

2.2.1. DNA Isolation

The method of DNA isolation differed for adult and embryonic tissues. For adult mice, tail biopsies were taken at postnatal day 18, and DNA was isolated using the Qiagen DNAeasy blood and tissue kit (Qiagen, 69504). Briefly, tail tissue was lysed overnight using Proteinase K and incubating at 37°C. The following day, the DNA is bound to the silicone membrane of a spin column via centrifugation, followed by a series of washes to eliminate contaminates. The washes were performed using AW1 and AW2 wash buffers, and each wash was repeated twice. The purified DNA was then eluted using 100 µL EB buffer, and stored at 4°C.

To genotype embryos, the handplate was collected during dissection. To minimize contamination between samples, forceps were cleaned with 70% ethanol between each sample. The handplate was removed and collected in a 1.5-mL microcentrifuge tube filled with 1X-PBS. The 1X-PBS was removed, replaced with 100 µL of lysis buffer, and incubated at 55°C for two hours with occasional mixing. DNA was precipitated by adding 1 µL of glycogen (Roche,

catalog number 10901393001) plus 200 µL of 100% ethanol per sample, gently mixed, then stored at -20°C overnight. The following day, the DNA was pelleted at 14,000 rpm for 5 minutes, washed in 250 µL of 70% ethanol, air dried at 37°C, and resuspended in 35 µL of QIAGEN buffer EB.

2.2.2. 129S-*Dvl2*^{tm1Awb}/J

Dishevelled 2 genotyping was performed by standard PCR using protocol from Jackson Labs (50 µL reaction). (http://jaxmice.jax.org/protocolsdb/f?p=116:2:4281157126504667::NO:2:P2_MASTER_PROTOCOL_ID,P2_JRS_CODE:1482,008001). The multiplex assay was designed such that the widltype (WT) and mutant amplicons are only ~50 base pairs apart, and so it was extremely important to run the gels long enough to allow band separation. The WT amplicon is 263 bp, mutant is 209 bp, and the heterozygotes will have both amplicons. Initially, gel electrophoresis with 3% agarose gels was performed at 100 mV for 1 hour, as indicated in Glasco, 2011. However, as our experiments progressed, we found that the amplicons needed to be separated further to allow for proper identification of the genotypes. Because the bands were so close together, it became difficult to differentiate between the different genotypes. For instance, a WT band was easily confused with a heterozygote in which the lower band was not separated from the top band completely and appeared to be one large band. Thus, we began to use 3% agarose gels ran at 70 mV for 4 hours to allow for greater separation (**Figure 2.1**).

Figure 2.1. *Dvl2* genotyping

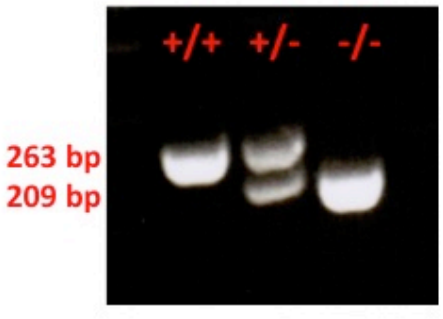

Figure 2.1. *Dvl2* genotyping

Dvl2 genotyping was performed using standard PCR protocol, and analyzed on a 3% agarose gel. The wild type *Dvl2* allele is indicated by a 263 bp amplicon, and the mutant allele is indicated by a 209 bp allele. Both amplicons will be present in samples for heterozygous animals (+/-), the 263 bp amplicon only for wild type animals (+/+), and the 209 bp only for homozygous mutant animals (-/-).

2.2.3. *B6-Sfrp1^{tm1Bsk}*

sFRP1 mutant mice were obtained from Kamana Misra (University of Medicine & Dentistry of New Jersey, Piscataway, NJ). The *sFRP1* line was produced by deletion of 1176 bp of exon 1 and replaced by a LacZ/MC1-Neo selection cassette. This mutation disrupts the CDR domain in the sFRP1 protein and results in a null allele (Bodine et al., 2004). Homozygous mice are viable and fertile. Genotyping was performed by standard PCR amplification as follows (50 µL reaction):

Component	[Stock]	[Final]	µL/reaction
nuclease-free water	--	--	13
GoTaq Green Master Mix (Promega M7123)	2X	1X	25
Forward primer (WT allele) 5'- CGGCCAGCGAGTACGACTACGTGAGC -3'	10 µM	0.5 µM	2.5
Reverse primer (WT allele) 5'- GCATCTCGGGCCAGTAGAAGCCGAAG -3'	10 µM	0.5 µM	2.5
Forward primer (Mutant allele) 5'- ACGGCATGGTGCCAATGAATCGTCTG -3'	10 µM	0.5 µM	2.5

Reverse primer (Mutant allele)	10 µM	0.5 µM	2.5
5'- CAAATAATATCGGTGGCCGTGGTGTC -3'			
genomic DNA	--	--	2

Thermocycler Conditions:

(94 ˚C, 2 min) x1; [(94 ˚C, 30 sec), (55.0 ˚C, 30 sec), (72 ˚C, 1 min)] x 35 cycles; (72 ˚C, 5 min) x1; (4 ˚C, HOLD)

The resulting product is analyzed on a 3% agarose 0.5X TBE gel. The WT allele produces a 379-bp amplicon, and the mutant allele produces a 212-bp amplicon. Heterozygous mice show both 379 bp and 212 bp amplicons (**Figure 2.2**)

2.2.4. B6-Sfrp2^{tm1Sato}

sFRP2 mice were provided by Kamana Misra. Null mice were generated using standard gene-targeting methods. The first coding exon was replaced with *lacZ,* deleting the endogenous translational initiation ATG codon and creating a loss of function allele. Homozygous mice are viable and fertile (Kobayashi et al., 2009; Lei et al., 2006).

Genotyping was performed by standard PCR amplification as follows (50 µL reaction):

Figure 2.2. *sFRP1* genotyping results

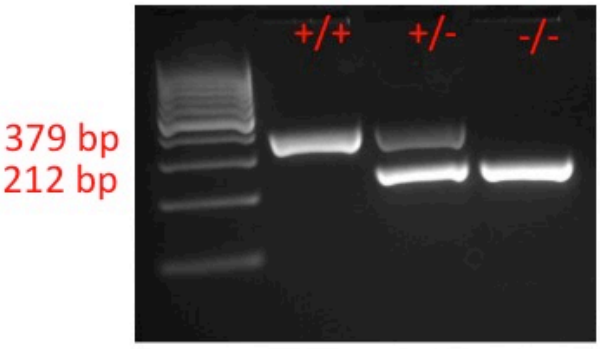

Figure 2.2. *sFRP1* genotyping results

sFRP1 genotyping was performed using standard PCR protocol, and analyzed on a 3% agarose gel. The wild type *sFRP1* allele is indicated by a 379 bp amplicon, and the mutant allele is indicated by a 212 bp allele. Both amplicons will be present in samples for heterozygous animals (+/-), the 379 bp amplicon only for wild type animals (+/+), and the 212 bp only for homozygous mutant animals (-/-).

Component	[Stock]	[Final]	µL/reaction
Nuclease-free water	--	--	13
GoTaq Green Master Mix (Promega, M7123)	2X	1X	25
Forward primer (WT allele) 5'- CTGGACGCCTGCGAAGTTTG -3'	10 µM	0.5 µM	2.5
Reverse primer (WT allele) 5'- TGGGCTTACAGCTATCAGTC -3'	10 µM	0.5 µM	2.5
Forward primer (Mutant allele) 5'- AGGCGATTAAGTTGGGTAACG -3'	10 µM	0.5 µM	2.5
Reverse primer (Mutant allele) 5'- ACGAGCAGAGCGAGGGAGTC -3'	10 µM	0.5 µM	2.5
genomic DNA	--	--	2

Thermocycler Conditions:

(94 ˚C, 5 min) x1; [(94 ˚C, 40 sec), (57.0 ˚C, 40 sec), (72 ˚C, 1 min)] x 35 cycles; (72 ˚C, 10 min) x1; (4 ˚C, HOLD)

The resulting product is analyzed on a 3% agarose 0.5X TBE gel. The WT allele produces a 379-bp amplicon, and the mutant allele produces a 212-bp amplicon. Heterozygous mice show both 379 bp and 212 bp amplicons (**Figure 2.3**).

2.3. Hindbrain Dissections

Timed matings were used to collect embryos at specific developmental stages, specifically E11.5 and E12.5. One at a time, embryos were transferred to a petri dish containing either 1X-PBS-DEPC or L-15 media. Sharp forceps were sterilized with 70% ethanol. If genotyping was required, the hand plate was removed and placed temporarily in a 1.5 mL microcentrifuge tube containing cold 1X-PBS-DEPC. To remove the hindbrain, first the head was cut away from the body by holding one pair of forceps above the level of the arm, and a second pair to slice the head away from the body. Next, the same principle was applied to remove the facial tissue. One set of forceps was held above eye level at a diagonal slant down the head to avoid hitting the hindbrain. The second set of forceps was then used to remove the face and tissues on the pial side of the hindbrain. The hindbrain was turned dorsal up to allow for visualization of the fourth ventricle. The thin tissue overlaying the ventricle was opened using two forceps. The forceps could then be inserted down the length of the spinal cord to create an “open book” preparation. The surrounding tissue was then peeled away from the pial surface, and any excess tissue (i.e., trigeminal root, excess spinal cord, forebrain) was cut off. Care was taken while dissecting around the

Figure 2.3. *sFRP2* genotyping

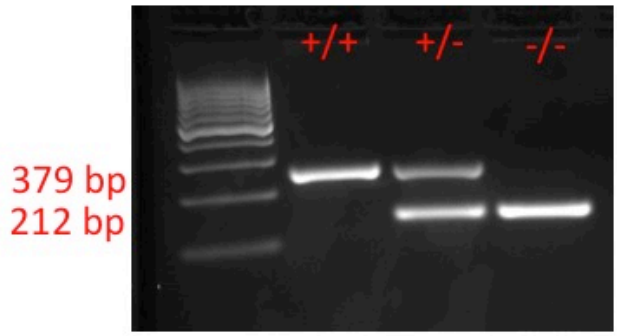

Figure 2.3. *sFRP2* genotyping

sFRP2 genotyping was performed using standard PCR protocol, and analyzed on a 3% agarose gel. The wild type *sFRP2* allele is indicated by a 379 bp amplicon, and the mutant allele is indicated by a 212 bp allele. Both amplicons will be present in samples for heterozygous animals (+/-), the 379 bp amplicon only for wild type animals (+/+), and the 212 bp only for homozygous mutant animals (-/-).

trigeminal root because of its fragility. The hindbrain was then transferred to a 1.5 mL microcentrifuge tube containing 4% PFA, fixed overnight, and processed accordingly.

2.4. Expression Analysis

2.4.1. In Situ Hybridization

Whole mount in situ hybridization was performed according to previously described protocols (Glasco, 2011). Generally, the color reaction was performed using the NBT/BCIP substrate. After the color reaction, embryos were fixed in 4% PFA-DEPC and processed according to their appropriate application.

2.4.2. In Situ Hybridization/ Immunohistochemistry

For some embryos, it was necessary to do a double in situ hybridization/ immunohistochemistry to determine the rhombomere boundaries of expression. In this case, the in situ hybridization was performed as previously described, using fresh tissue from *SE1::GFP* embryos that had not been exposed to methanol. The color reaction was performed using FastRed substrate (Sigma, F4523). The FastRed substrate fluoresces in the rhodamine channel. FastRed solution was replaced four times, followed by an overnight incubation at room temperature if necessary. After the color reaction, embryos were fixed in 4% PFA-DEPC overnight, and immediately followed with immunohistochemistry (IHC) for GFP protein in order to label the FBM neuron migratory stream.

IHC was performed at 4°C in 0.5 mL tubes while gently rocking in the dark. The hindbrain tissues were washed 6 times in 500 µL PBST for 15 minutes each, followed by a 2-3 hour incubation in 400 µL PBST containing 2% BSA. The primary antibody (rabbit anti-GFP, Invitrogen A11122, 1:400 dilution in PBST containing 2% BSA) was added and allowed to incubate for four nights. On the fifth day, the samples were washed in PBST six times for one hour each, followed by an overnight incubation in PBST, to allow for removal of the primary antibody. The next day, the samples were washed once in PBST for 15 minutes, and then incubated overnight in the secondary antibody (AlexaFluor 488-chicken anti-rabbit, Invitrogen A21441, 1:200 dilution in PBST). The following day, the secondary antibody was removed by washing the samples in PBST 7-8 times for an hour each, followed by an overnight wash in PBST. On the final day, the samples were brought to room temperature and washed in PBST for 15 minutes. They were then transferred to foil-covered 12 well plates and washed 1-2 more times with PBST. The hindbrains were post-fixed in 4% PFA-DEPC for at least 2 hours, or overnight if desired. They were then mounted in MOWIOL mounting medium (prepared by University of Missouri Molecular Cytology Core). Z-stack images were taken on a confocal microscope (University of Missouri Molecular Cytology Core, Zeiss LSM 510 META NLO) to visualize the pattern of gene expression (RITC channel) and the distribution of FBM neurons (FITC channel). This allowed us to define the boundaries of the gene expression relative to specific rhombomeres.

2.4.3. In situ Hybridization Sectioning

Certain experiments required that the expression be analyzed on cross sections of the hindbrain. Following in situ hybridization, hindbrains were fixed overnight and slowly moved to 70% glycerol through a graded series of glycerol diluted in dH_2O. Thick sections were cut by hand using microscissors (Fine Science Tools, 15006-09) at various locations. Sections were then mounted in 70% glycerol and imaged.

2.5. Dvl2 Explants

2.5.1. Obtaining *Dvl2*$^{-/-}$; *GFP*$^{+/-}$ embryos

To investigate a role for *Dvl2* in the rostral migration of FBM neurons, ectopic or supernumerary sources of Wnt were created in the rostral hindbrain using protein coated agarose beads. To properly place the beads on the hindbrain explant relative to the various rhombomeres and the FBM neurons in r4, it was important to be able to visualize the FBM neurons. *Dvl2* mice (129S-*Dvl2*^{tm1Awb}/J) were obtained from the Jackson Laboratory (http://jaxmice.jax.org/strain/008001.html). 50% of *Dvl2* homozygous mutants are viable and fertile (Hamblet et al., 2002). *Dvl2*$^{-/-}$ mice were crossed into the *SE1::GFP* line, which expresses GFP in the branchiomotor neurons, and allows for visualization of the FBM neurons in live tissue (Shirasaki et al., 2006; Song et al., 2006). The resulting *Dvl2*$^{+/-}$; *GFP*$^{+/-}$ mice were intercrossed to obtain *Dvl2*$^{-/-}$; *GFP*$^{+/-}$ embryos at embryonic day E11.5 (**Figure 2.4**). Since *Dvl2*$^{-/-}$ embryos

Figure 2.4. Breeding scheme for the collection of *Dvl2*$^{-/-}$ embryos

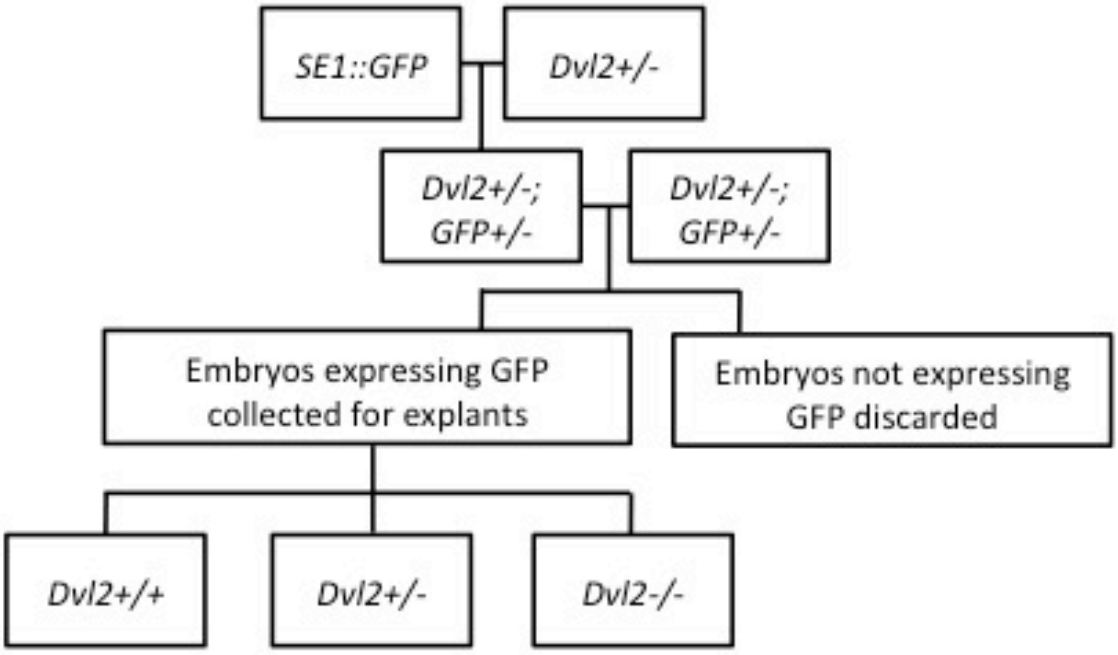

Figure 2.4. Breeding scheme for the collection of *Dvl2*$^{-/-}$ embryos

Live imaging of explants required that the *Dvl2* mouse line was bred into the *SE1::GFP* background so that the FBM neurons would express GFP. The mutant allele is indicated by -, and + indicates the wild type allele. Once *Dvl2*$^{+/-}$; *GFP*$^{+/-}$ mice were obtained, they were intercrossed in order to collect *Dvl2*$^{+/+}$, *Dvl2*$^{+/-}$, *and Dvl2*$^{-/-}$ littermates that expressed GFP for use in explant tissue culture. Because the GFP expression in FBM neurons was used to determine the proper placement of beads, all GFP negative embryos were discarded immediately.

display no overt morphological defects (Hamblet et al., 2002), genotyping was performed after the analysis so that blind scoring of the rostral migration phenotype could be performed by one individual. GFP expression in FBM neurons was determined by visualizing the hindbrain using a fluorescent microscope. Embryos that did not express GFP were discarded. Embryos were collected at E11.5 so that embryos were viable for at least 48 hours, and this time point was sufficiently early in development that many FBM neurons had not yet begun caudal migration. Initial experiments using explants from E10.5 embryos, the day at which FBM neuron migration begins, were discontinued since the tissues did not remain healthy after 24 hours.

2.5.2. Preparing Wnt5a-soaked beads

Affi-gel blue gel (Bio-Rad, 153-7301, stored at 4°C) is composed of agarose beads cross-linked to a blue dye that allows for the specific binding of proteins. To allow efficient protein binding, the beads were soaked in Wnt5a protein or 1X-PBS-DEPC for 24 hours before use. To prepare the beads, 200 µL of beads were centrifuged at 5000 rpm (Eppendorf microfuge, 5424) in 1.5 mL tubes at room temperature for 2 minutes, the supernatant was discarded, and the beads were washed in 1X-PBS-DEPC two times. Clean beads were stored in 400 µL 1X-PBS-DEPC at 4°C for up to one week. Twenty µL of clean beads were then placed in a 35 mm petridish, and the 1X-PBS-DEPC was carefully removed. Five µL of Wnt5a protein (R&D, 645-WN, stored at -80°C), carrier free Wnt5a proteins (R&D, 645-WN/CF, stored at -80°C) or 1X-PBS-DEPC was then

pipetted onto the beads. The petri dish was then sealed and placed inside of a larger dish containing 1X-PBS-DEPC to prevent the protein from drying out. The beads were stored at 4°C overnight.

As a control, we used beads that were coated in 1X-PBS-DEPC on the *SE1::GFP* embryos. Rostral migration did not occur in any of the explants with 1X-PBS-DEPC-coated beads. In contrast, in 50% of the explants with Wnt5a coated beads, FBM neurons migrated toward the beads within 24 hours, similar to previous studies (Vivancos et al., 2009). To test whether carrier free Wnt5a protein (not containing BSA) may be more efficacious than Wnt5a constituted in BSA, we tried a few experiments with beads coated with carrier-free Wnt5a. However, carrier free protein did not increase the rostral migration phenotype (3/21 explants exhibit rostral migration), and so Wnt5a constituted in BSA was used in all explants.

2.5.3. Hindbrain dissection

Embryos were collected at E11.5. The hindbrains were dissected in cold L-15 media (Gibco, 21083-027, stored at 4°C). Since *Dvl2*$^{-/-}$ embryos display no overt morphological defects (Hamblet et al., 2002), hand plates were taken from each embryo for genotyping at the same time the hindbrain was removed, and genotyping was performed only after blind scoring of the rostral migration phenotype was completed. Once the hindbrains were removed, they were viewed under GFP. All GFP positive hindbrains were cut down to a smaller sized

explant by removing excess spinal cord, midbrain, and surrounding tissue and kept in L-15 media until bead placement and hindbrain culture.

2.5.4. Hindbrain Cultures

Before beginning the dissection, a 6 well plate containing 8.0 µm polycarbonate membrane inserts (Corning costar, 3428) was prepared by placing 200 µL laminin (Sigma, L2020, prepared at 0.003 µg/µL in 1X-PBS-DEPC) on each filter and placed in a 37°C, 5% CO_2 incubator (Heraeus, Hera Cell 150). Neurobasal mix was prepared and warmed to 37°C (refer to **Section 2.7.3** for recipe). After the hindbrain dissection was complete, the 6 well plate was removed from the incubator, and the laminin was gently removed from the inserts. Inserts were processed one at a time by removing the insert from the plate and blotting it on a clean KimWipe to remove the laminin. The insert was then placed on top of two cover slips in a dry petri dish so that the bottom of the insert did not come into contact with the petri dish. One hindbrain explant was placed on each insert, positioning the explant so that it was as flat as possible, and removing all excess liquids by micropipette. After the beads were placed, 340 µL of Neurobasal mix was placed in the well, the insert was replaced into the well by allowing the medium to gently wet the underside of the filter, and the plate was returned to the 37°C, 5% CO_2 incubator to allow the explant to adhere to the filter. The beads were placed on the hindbrains placed on the inserts using a stereomicroscope equipped with epifluorescence to visualize the GFP-

expressing motor neurons. Explants were viable for 72 hours under these conditions.

To determine the best conditions for culturing the tissue, *SE1::GFP* embryos were processed under several conditions. During the first trials, beads were placed immediately after the hindbrain was positioned, and the hindbrains were imaged at time 0 before the insert was replaced in the well with neurobasal mix. Although the beads were positioned rostrally to the FBM neuron migratory stream in r2/3, as visualized by GFP, by 24 hours, the beads appeared to have moved so that they overlapped the neurons in r4. This made scoring for a rostral phenotype difficult. Placing the beads in r1 seemed to have a similar movement, and rostral migration was never seen, perhaps because the Wnt source was too far away from the FBM neurons to be able to attract them. We considered that perhaps the tissue was changing its shape once placed in the media and warmed to 37°C, and so we began placing the beads immediately after the hindbrain was placed on the insert, returning the well plates to the incubator, and imaging the explants 1 hour after bead placement in the neurobasal media. This allowed us to move the beads slightly if the tissue changed shape and displaced the beads. The beads did not move after they were repositioned. These conditions were used to culture all of the *Dvl2* explants.

2.5.5. Bead placement

Affi-gel blue gel (Bio-Rad, 153-7301, stored at 4°C) beads were soaked in Wnt5a protein or 1X-PBS-DEPC for 24 hours before use. Once an explant was

positioned on the filter, and all liquids were removed, the tissue was ready for bead placement. Clean forceps were used to pick up a few beads, and place them carefully on the tissue. Using GFP fluorescence as a reference, beads were placed above and lateral to the r3/r4 border. No beads were placed in the caudal half of r3 to ensure that the beads did not overlap with the FBM neurons. Handling the beads was difficult because they tended to clump together, making it almost impossible to pick up only 1-2 beads. Instead, forceps were used to pick up several beads, which were then dropped onto the hindbrain explant above the FBM neurons. The beads would then spread out as they came in contact with liquid. It was important to remove as much liquid as possible before placing the beads so that they did not float off of the explant. Once the beads were placed on the explant, they were manipulated very gently by using either forceps or a tungsten needle to roll the bead to a new location, taking great care not to damage the tissue. On average, about 20 beads were placed on each explant, although it appeared that the number was not as important as the distance the beads were placed from the FBM neurons. Once beads were placed, the filter was returned to the 6 well plate containing Neurobasal Mix. This process was repeated for each explant. The beads dry out very quickly, and thus it was important to keep them in a covered dish containing 1X-PBS between each explant. Because of this, it is not advisable to use the beads for more than one day. However, on the *SE1::GFP* explants, there were occasions in which the beads were not dry, and so were stored at 4°C and attempted for use the

following day. In these cases, rostral migration was still evident using the Wnt5a coated beads, so long as the beads had not dried out overnight.

2.5.6. Imaging explants and scoring migration phenotype

After the beads were placed in the explants, they were incubated at 37°C for one hour to allow the tissue to adhere to the filter. Explants were first imaged at this time, designated as time zero. Explants were incubated (37°C, 5% CO_2 incubator, Heraeus, Hera Cell 150) and imaged 24 hr and 48 hr later. Images were acquired under brightfield illumination (Olympus SZX12 stereomicroscope) to observe the health of the tissue and the bead placement, and under GFP fluorescence to observe the migration of the FBM neurons. The distribution of FBM neurons at the three time points was compared before genotyping, and enabled blind scoring of rostral migration phenotype. GFP positive cells anterior to the r4 boundary were considered to have migrated rostrally. This was confirmed by comparing the images to the zero time point image to ensure that the GFP positive cells had moved into the rostral area (r3) after bead placement. In most cases, the FBM neurons migrated up to and surrounding the most caudally placed beads in r3.

2.5.7. *Dvl2* Genotyping

During dissections to prepare hindbrain explants, the hand plate of each embryo was collected and given the same code as the embryo. The tissue was

digested overnight and DNA was purified the following day (Qiagen, 69504). Genotyping was performed after the explants were imaged at 48 hours by standard PCR as previously described (Glasco, 2011).

2.6. RNA Sequencing

The methods described below are outlined in **Figure 2.5**.

2.6.1. Tissue collection

RNA from hindbrains collected from wild type and *Celsr1*$^{+/Crash}$ littermates was submitted for RNA sequencing to identify genes that are differentially expressed, and may be involved in generating the rostral migration phenotype. To reduce the effect of genetic variability on gene expression, *Celsr1*$^{+/Crash}$ females, all siblings from one breeding pair, were bred against a single *SE1::GFP* male. Since we were interested in identifying gene expression differences in the r3-r4 region between *Celsr1*$^{+/Crash}$ embryos and their siblings at the time when abnormal rostral migration occurs, we considered harvesting hindbrain tissues at E10.5 and E11.5. At E10.5, the trigeminal motor neurons in r2 and r3 are migrating mediolaterally, and abnormal rostral migration into r3 is not very evident. Due to these factors, it was difficult to unambiguously identify *Celsr1*$^{+/Crash}$; *GFP*$^{+/-}$ embryos. At E11.5, *Celsr1*$^{+/Crash}$; *GFP*$^{+/-}$ embryos are easily identifiable based on the rostral migration phenotype of the GFP-expressing FBM neurons (**Figure 2.6b**). By E12.5, caudal migration (and defective rostral

Figure 2.5. Overview of RNA Sequencing Protocol

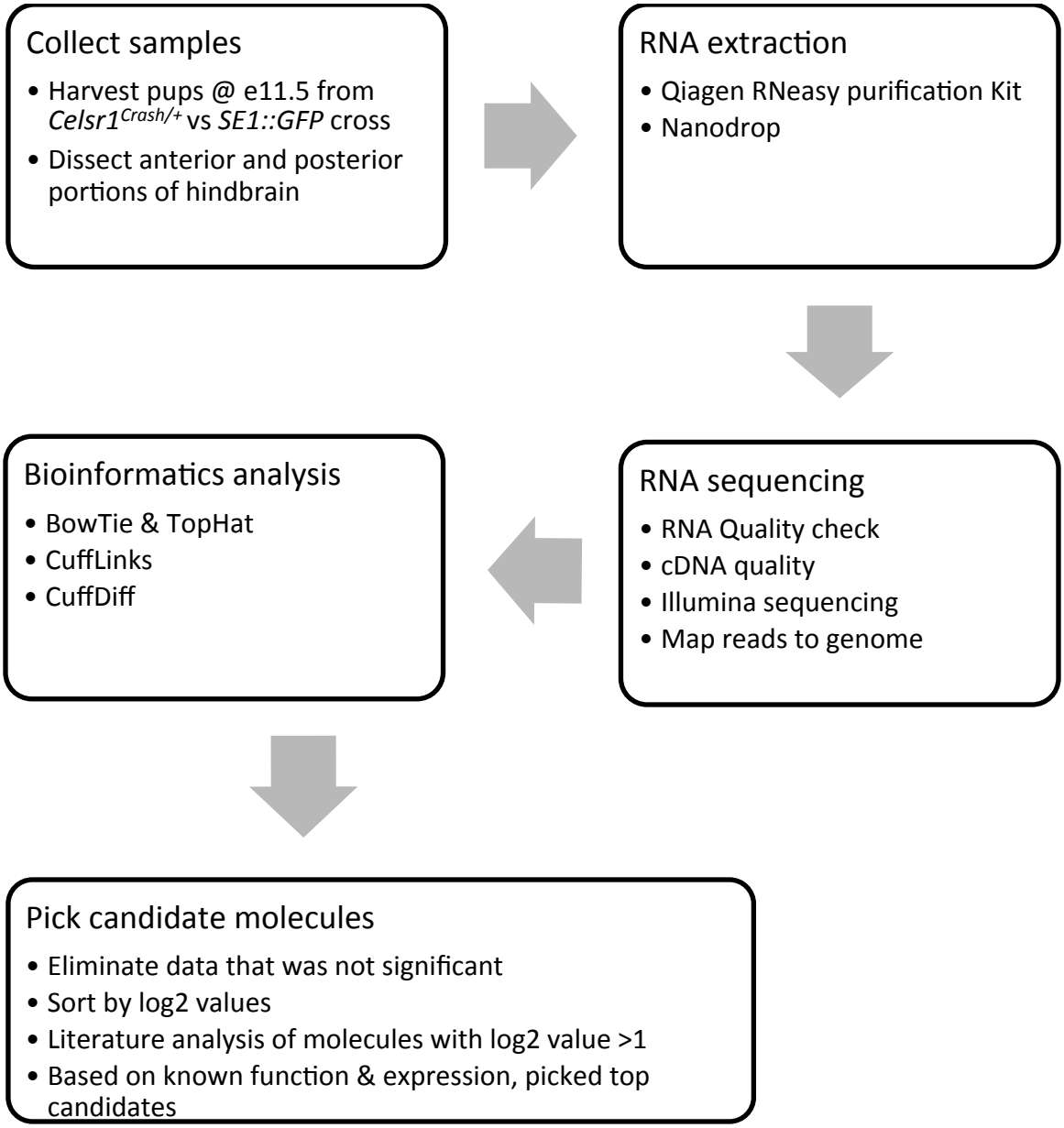

Figure 2.5. Overview of RNA Sequencing Protocol

Schematic of protocol for submission of samples for RNA sequencing and bioinformatics analysis to identify candidate molecules.

migration) is essentially complete, decreasing the likelihood of detecting gene expression changes relevant to migration. Immediately after E11.5 embryos were harvested, the hindbrain from each embryo was carefully dissected in ice-cold 1X-PBS-DEPC in a large petri dish. 1X-PBS-DEPC was kept on ice and replaced after every 2-3 dissections. Hindbrains were sorted under GFP epifluorescence for the rostral migration phenotype into either *Celsr1*$^{+/+}$*; GFP*$^{+/-}$ or *Celsr1*$^{+/Crash}$*; GFP*$^{+/-}$ pools in 1X-PBS-DEPC containing 0.5x pen-strep. All tools used in the dissection were flame sterilized and treated with RNaseOut (G Biosciences, 786-70). Using tungsten needles (Tungsten wire, 0.016 OD, Small Parts Inc., Part # TW-016-60-05) (Brady, 1965) or micro-scissors (Fine Science Tools, 15006-09) to cut the hindbrain, the r2 to mid-r4 (anterior) region and the mid-r4 to r6 (posterior) regions were carefully dissected (**Figure 2.6**, indicated by dashed red lines). To determine the location of the cuts, we used the anterior and posterior boundaries of r4 as landmarks because the FBM neuron cell bodies occupy the entire extent of r4, and their axons can be easily seen exiting the hindbrain in this rhombomere. The r4 region was cut in half so that the rostral and caudal halves would be included in the anterior and the posterior tissue fragments, respectively. Next, the tissues lateral to the FBM neuron migratory stream were removed (**Figure 2.6**, indicated by dashed red lines). The rostral hindbrain fragment was then cut at approximately the r2/r1 border, using the trigeminal motor nucleus in r2 as a landmark. The caudal hindbrain fragment was cut caudal to r6, which was identified by the presence of the nascent facial motor nucleus. These dissections generated four samples: Wa (**W**ildtype:

Figure 2.6. Anterior and posterior portions of WT and mutant hindbrains collected for RNA sequencing

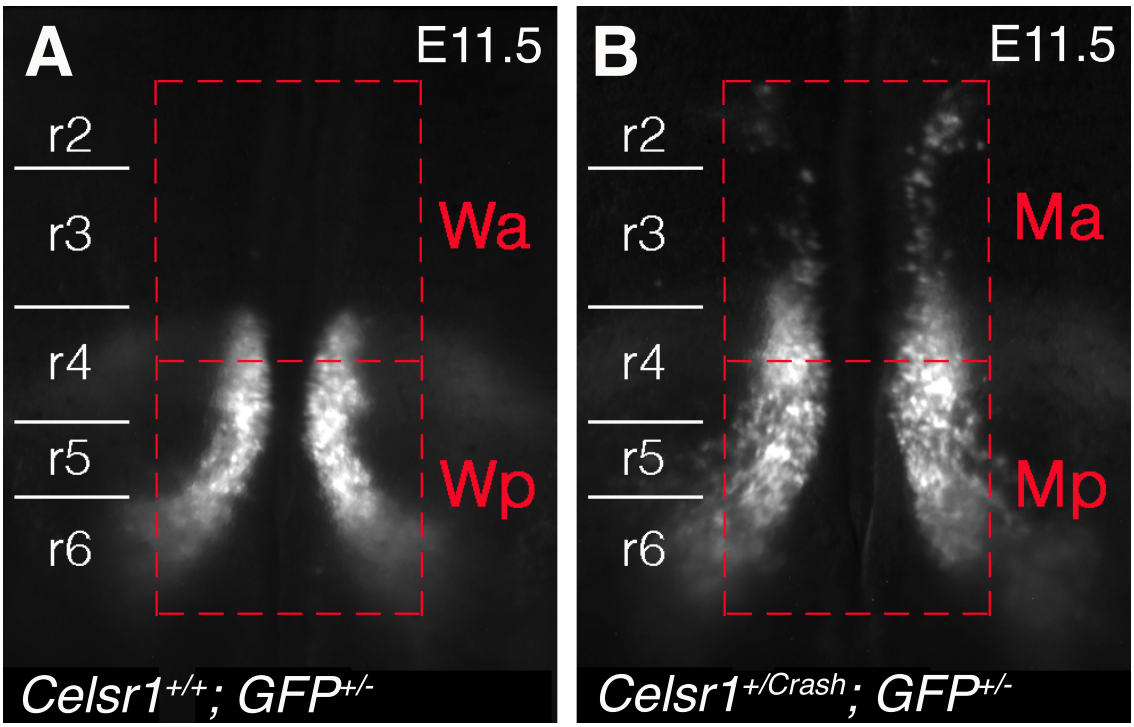

Figure 2.6. Anterior and posterior portions of WT and mutant hindbrains collected for RNA sequencing

Live images of (**A**) *Celsr1*$^{+/+}$*; GFP*$^{+/-}$ (W) and (**B**) *Celsr1*$^{+/Crash}$*; GFP*$^{+/-}$ (M) E11.5 hindbrains. Red dashes indicate where tissue was cut to collect samples for RNA extraction. Tissue was cut using GFP as a guideline for rhombomere boundaries. In both WT and mutant, the r2-mid-r4 regions and the r4-r6 regions of each hindbrain was carefully removed and used for RNA synthesis. RNA was isolated from each sample and submitted for RNA quality checks and RNA sequencing.

Abbreviations: W: WT, or *GFP*$^{+/-}$. M: mutant, or *Celsr1*$^{+/Crash}$*; GFP*$^{+/-}$. a: anterior hindbrain, from r2-mid r4. p: posterior hindbrain, from mid r4-r6.

Celsr1$^{+/+}$*; GFP*$^{+/-}$ **a**nterior hindbrain fragment), Wp (**W**ildtype: *Celsr1*$^{+/+}$*; GFP*$^{+/-}$; **p**osterior hindbrain fragment), Ma (**M**utant: *Celsr1*$^{+/Crash}$*; GFP*$^{+/-}$; **a**nterior hindbrain fragment), and Mp (**M**utant: *Celsr1*$^{+/Crash}$*; GFP*$^{+/-}$; **p**osterior hindbrain fragment) (**Figure 2.6**). The tissues were placed in separate 1.5 mL microcentrifuge tubes containing 500 µL RNA*later* RNA Stabilization Reagent (Qiagen, 76104) to minimize RNA degradation. This process was repeated for each hindbrain, alternating between *Celsr1*$^{+/+}$*; GFP*$^{+/-}$ and *Celsr1*$^{+/Crash}$*; GFP*$^{+/-}$ embryos to minimize systematic errors resulting from tissue degradation. Tissue extracts from the same genotype were pooled in order to obtain enough tissue for RNA extraction.

2.6.2. Total RNA preparation

For the high throughput RNA sequencing, it is important to have high quality RNA. We tried two methods of isolating total RNA using wild type tissue. The first method was a modification of a protocol for isolating RNA from zebrafish embryos for RNA sequencing. The samples were centrifuged at 15,000 rpm for 10 minutes at room temperature to pellet the tissue and remove the RNAlater (Ambion, AM7020). 1-4 hindbrain tissues were homogenized using a small pestle grinder (Fisher, 03-392-106) in 200 µL RNAzol (Molecular Research Center, RN 190). Another 300 µL RNAzol and 200 µL DEPC-treated dH_2O were added and mixed, and the samples were incubated for 10 minutes at room temperature. The samples were centrifuged at 12,000 rpm for 15 minutes at room temperature and the supernatant was collected in a fresh tube. An equal volume of

isopropanol was added to the supernatant, mixed and incubated for 10 minutes at room temperature, and pelleted at 12,000 rpm for 15 minutes at room temperature. The supernatant was discarded and the pellet was washed twice in 70% ethanol, air-dried, and dissolved in 20 µL RNase-free water.

In the second method, total RNA was isolated and purified from the hindbrain fragments using the Qiagen RNeasy mini kit (Qiagen, 74104) following the removal of the RNAlater. The samples were centrifuged at 15,000 rpm for 10 minutes at room temperature to pellet the tissue and the RNAlater was removed. The tissue was homogenized in 250 µL of lysis Buffer RLT in a 1.5 mL microcentrifuge tube using the small pestle grinder for 30-60 seconds or until all tissue was disrupted. An additional 350 µL of lysis Buffer RLT was added to bring the total volume to 600 µL and the tube was inverted to mix. The lysate was transferred to a QIAshredder spin column in a 2 mL collection tube and spun down at room temperature in a microcentrifuge for two minutes at full speed. One volume of 70% ethanol was added to the lysate and mixed by pipetting. 700 µL of the sample was then transferred to an RNeasy spin column in a 2 mL collection tube and centrifuged at room temperature for 15 seconds at 8000 x g. The flow-through was discarded, and this step was repeated by transferring the remaining lysate to the same spin column. 700 µL Buffer RW1 was added to the spin column and centrifuged at room temperature for 15 seconds at 8000 x g to wash the spin column membrane. A second wash was performed using 500 µL Buffer RPE and centrifuging at room temperature for 15 seconds at 8000 x g. After each wash the flow-through was discarded. To dry the membrane, 500 µL

Buffer RPE was added to the column and was centrifgued at room temperature for 2 minutes at 8000 x g. To ensure that no ethanol is carried over during RNA elution, the spin column was carefully removed from the used collection tube, transferred to a new 2 mL collection tube, and centrifuged again at room temperature for 1 minute at full speed. The spin column was then placed in a 1.5 mL collection tube and 30 µL of RNase-free water was pipetted directly onto the spin column membrane. The RNA was eluted by centrifugation at room temperature for 1 minute at 8000 x g. RNA was stored at -80°C. In pilot experiments using wild type tissues, we found that RNA quality (**Section 4.2.3**) was substantially higher with the RNeasy kit, which was adopted for isolating RNA from the dissected hindbrain fragments from *Celsr1*$^{+/+}$*; GFP*$^{+/-}$ and *Celsr1*$^{+/Crash}$*; GFP*$^{+/-}$ embryos.

2.6.3. Submission guidelines for RNA

For RNA sequencing, the University of Missouri DNA Core guidelines require that the amount of RNA submitted is equal to at least 100 ng/µL of RNA in a total volume of 50 µL. After RNA isolation was completed, the DNA Core performed an RNA integrity test to ensure quality and amount of RNA (**Chapter 4**). Every sample was validated individually. Based on these results we combined the RNA samples from 8 *Celsr1*$^{+/+}$*; GFP*$^{+/-}$ and 8 *Celsr1*$^{+/Crash}$*; GFP*$^{+/-}$ embryos for RNA sequencing.

2.6.4. RNA sequencing

Sequencing was performed by the University of Missouri DNA Core using the Illumina HiSeq2000, a high-throughput sequencer. During this process the total RNA is converted to a cDNA library. This library is composed of 200-500 base pair fragments of cDNAs. Each fragment is then sequenced, creating "reads" of 30-400 base pairs. Reads can then be aligned to a reference genome, in this case the Genome Reference Consortium Mouse Build 38 patch release 1 (GRCm38.p1) (http://www.ncbi.nlm.nih.gov/assembly/GCF_000001635.21/), in order to make a transcriptional map of the genome which contains transcription structure and expression levels of each (Wang et al., 2009) (Described in **Chapter 4**).

2.6.5. Expression Analysis

To facilitate the analysis of genome-wide expression patterns in a set of biological samples, the MU Informatics Research Core Facility (IRCF) leverages several existing resources and develops novel ones as necessary. Specifically, the University of Missouri Research Support Computing (RSC, http://doit.missouri.edu/research/) maintains an extensive and well-managed computational infrastructure that supports the analysis of high-throughput data. The UMBC Lewis cluster has more than 1200 processing cores and 1.2PB of shared disk space available to store, process and analyze the RNA-Seq data generated by the Illumina DNA sequencer housed in the MU DNA Core. The IRCF staff has extensive expertise in exploiting these computational resources to

analyze RNAseq data using a collection of open source software; including the bowtie-based TopHat suite, which contains Cufflinks and Cuffdiff (Trapnell et al., 2009; Trapnell et al., 2010), velvet and oases (Zerbino and Birney, 2008), RSEM (Li and Dewey, 2011) and the various R packages specialized for RNAseq, such as DESeq (Anders and Huber, 2010), and edgeR (Robinson et al., 2010). Upstream of the analysis, the IRCF staff use a three-phase quality control pipeline: 1) reads are trimmed of low-confidence nucleotides, 2) reads are filtered based on proportion of low confidence nucleotides, and 3) reads are removed that match ribosomal RNA, mitochondrial genomes, repeat elements and reads of otherwise dubious origin.

2.7. Solutions and Reagents

2.7.1. Immunohistochemistry

PBST (50 mL)

Component	Amount	[Stock]	[Final]
Triton X-100 (in 1X-PBS-DEPC)	500 µL	10%	0.1%
1X-PBS-DEPC	45.5 mL	-	-

Do not autoclave. Make fresh during procedure.

PBST containing 2& BSA (50 mL)

Component	Amount	[Stock]	[Final]
BSA (Sigma A7906)	100 mg	100%	2%

Triton X-100 (Fisher BP151)	50 µL	100%	0.1%
1X-PBS-DEPC	to 50 mL	-	-

Make fresh and use immediately.

2.7.2. Explant Culture

Neurobasal Mix (4 mL)

Component	Amount	[Stock]	[Final]
Neurobasal media (4° C) (Invitrogen 12348-017)	3.4 mL	1x	0.85x
GDNF in Neurobasal media (-20° C) (R&D 212GD)	340 µL	0.0001%	0.00085%
Antibiotic Antimycotic (AA) (-20° C) (Sigma A5955)	34 µL	100x	0.85x
GlutaMAX (Room Temperature) (Invitrogen 35050-061)	34 µL	100x	0.85x
B-27 (-20° C) (Invitrogen 17504-044)	68 µL	50x	0.85x

Note: GDNF stock was reconstituted at 10 µg/100 µL in sterile 1X PBS containing 0.1% BSA and stored in 5 µL aliquots at -20°C until diluted 1:1000 in neurobasal media. The dilution could be stored at 4°C for up to one month.

Laminin (Sigma L2020)

Laminin was purchased at a concentration of 1 mg/mL in Tris buffered NaCl, and stored in 50 µL aliquots at -20°C. To use, it was diluted 3:1000 in 1X-PBS-DEPC, and could be stored at 4°C for one month.

2.7.3. RNA Sequencing

1X-PBS-DEPC containing 0.05x Pen-Strep

Component	Amount	[Stock]	[Final]
1X-PBS-DEPC	30 mL	1x	0.95x
Penicillin-Streptomycin (Gibco,15140-122)	150 µL	1x	0.05x

CHAPTER 3: Potential Roles for *Dvl* signaling and *sFRP* function in FBM Neuron Migration

Manuscript under preparation:

Glasco, D. M., Bryant-Pike, W., Qu, Y., Reustle, L., Misra, K., Di Bonito, M, Studer, M., Fritzsch, B., Goffinet, A., Tissir, F. and Chandrasekhar, A. The PCP cadherin Celsr1 blocks anterior migration of facial branchiomotor neurons by suppressing responsiveness to Wnts.

3.1. Introduction

3.1.1. Some FBM neurons undergo abnormal rostral migration in *Celsr1*$^{+/Crash}$ and *Celsr1*$^{KO/KO}$ mice

Facial branchiomotor (FBM) neurons in the mouse are born within rhombomere 4 (r4) of the hindbrain, and migrate caudally towards r6 where they form the facial motor nucleus, which innervates muscles involved in jaw movements and facial expression. The non-canonical Wnt/PCP pathway has been studied extensively for roles in the migration of these neurons. In zebrafish, *celsr1a*, *celsr1b*, and *celsr2* are important for the caudal migration of the FBM neurons (Qu et al., 2010; Wada et al., 2006). In mice heterozygous for the dominant negative *Celsr1*^{Crash} allele, most of the FBM neurons migrate caudally out of r4 in a normal fashion. However, a small but significant subset of neurons

migrates abnormally in a rostral direction towards r2 (**Figure 3.1**). *Celsr1*$^{KO/KO}$ mutant animals containing the *Celsr1* null allele also display a rostral migration phenotype (Qu et al., 2010). These results suggest that *Celsr1* may support caudal migration of FBM neurons by suppressing rostral migration. This is the first and thus far only description of a genetic or experimental condition that results in an abnormal rostral migration of FBM neurons in zebrafish or mice. Therefore, it promises to provide insight into the mechanisms that ensure caudal neuronal migration.

3.1.2. *Celsr1* expression in the mouse hindbrain

Given the novel migration defect in *Celsr1* mutants, the *Celsr1* expression pattern was characterized in detail. *Celsr1* is expressed in the neuroepithelium and the floor plate of the developing mouse hindbrain at E10.5 at all axial levels (**Figure 3.2 A-D**). By E12.5, expression is downregulated at the r4 level but remains strong in the floor plate of r5 and caudally. This coincides with the developmental stage at which most FBM neurons have already migrated out of r4. Celsr1 is expressed in the ventricular zone at E9.5, and is restricted to the floor plate by E11.5. By this stage, immunostaining reveals that Celsr1 does not colocalize with Isl1, a marker for FBM neurons. Since Celsr1 is not expressed within the migrating FBM neurons, it is important to determine the tissues in which *Celsr1* functions to suppress rostral migration of FBM neurons (Glasco, 2011; Qu et al., 2010).

Figure 3.1. FBM neurons migrate rostrally in *Celsr1*^{Crash} embryos

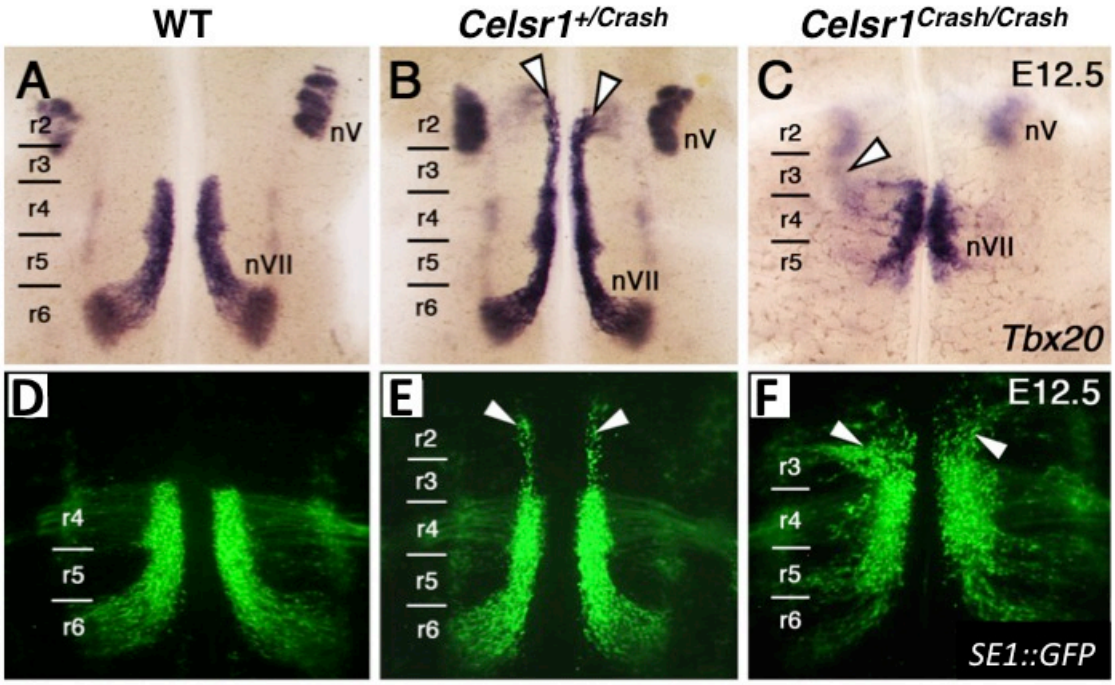

Reprinted by permission from Society for Neuroscience: *Journal of Neuroscience (Qu et al., 2010),* copyright 2010.

Figure 3.1. FBM neurons migrate rostrally in *Celsr1*^{Crash} embryos

Ventricular views of flat mounted hindbrains processed for ISH using *Tbx20* (**A-C**). **A**, In a WT embryo at E12.5, FBM neurons can be seen distributed throughout their migratory pathway spanning r4-r6. Within r6, the neurons migrate radially to form the facial (nVII) nucleus. **B**, In a *Celsr1*$^{+/Crash}$ embryo, caudal migration is intact, but a significant number of neurons migrate rostrally into r2 and r3. **C**, In a *Celsr1*$^{Crash/Crash}$ embryo, most FBM neurons remain in r4. **D, E**, In *SE1::GFP* transgenic *WT* and *Celsr1*$^{+/ Crash}$ embryos, FBM neuron migration is identical to *Tbx20* ISHs (**A, B**). In *Celsr1*$^{Crash/Crash}$, the *SE1::GFP* indicates rostral FBM neuron migration into r2 and r3. Arrowheads indicate rostral migration. Scale bars: (in ***C***), ***A***–***C***, ***G***–***I***, 300 μm; (in ***F***) ***D***–***F***, 375 μm; (in ***J***), ***J***–***M***, 375 μm. Figure modified from Qu, Y. et al. Atypical cadherins Celsr1-3 differentially regulate migration of facial branchiomotor neurons in mice. *J Neurosci, 30*(28), 9392-9401 (2010).

Figure 3.2. Cre lines used to inactivate *Celsr1* in tissue specific regions

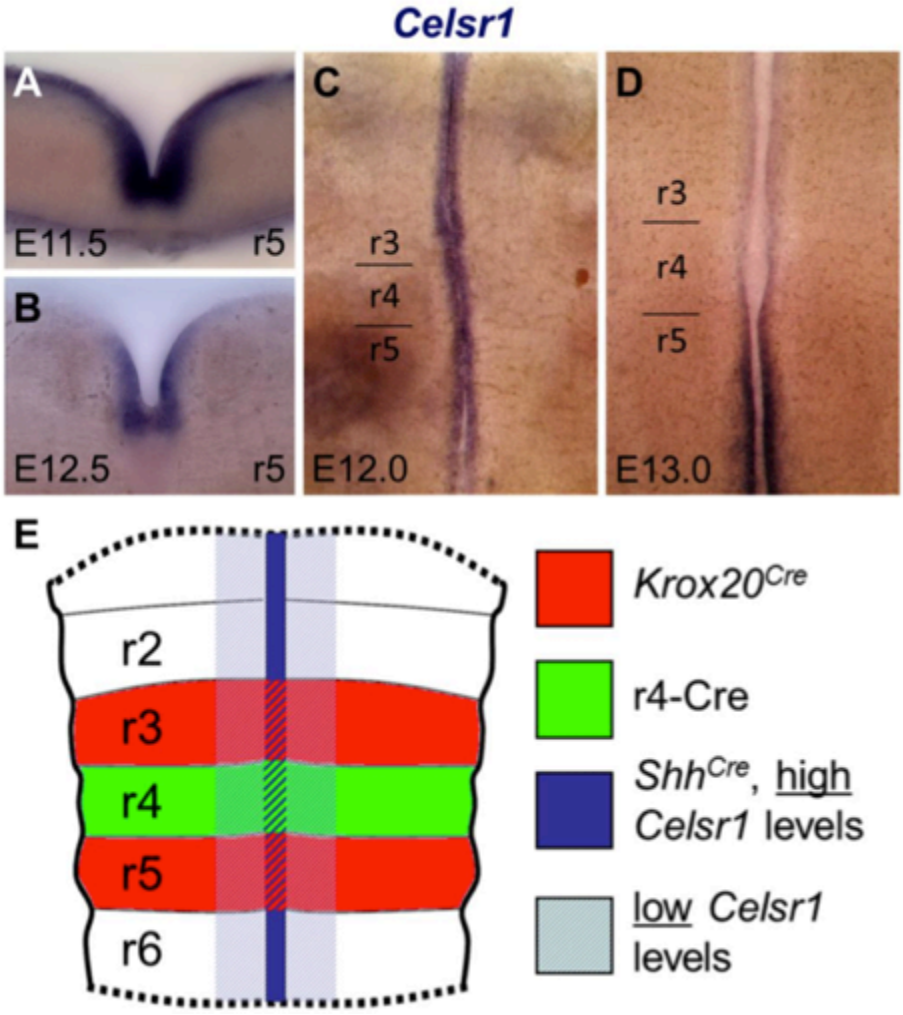

Figure 3.2. Cre lines used to inactivate Celsr1 in tissue specific regions

A-D, Whole mount and sections of E11.5-E13.0 WT embryos processed for *Celsr1* ISH. *Celsr1* is expressed throughout the ventricular zone of the developing mouse hindbrain at all axial levels. **E**, Several inducible Cre lines overlap the expression domain of *Celsr1 (Di Bonito et al., 2013; Glasco, 2011; Harfe et al., 2004; Studer et al., 1998; Voiculescu et al., 2000)*, and will be utilized to generate *Celsr1* conditional knockouts using the Cre-lox system.

3.1.3. Tissue specific knockouts to determine spatial requirement of *Celsr1*

To determine the identity of the tissues within which *Celsr1* functions to suppress rostral migration of FBM neurons, we undertook a conditional knockout approach by examining the consequences of inactivating *Celsr1* in subsets of its expression domain. *Celsr1* was conditionally inactivated in different locations by crossing the *Celsr1*^{floxed} allele (Ravni et al., 2009) into a series of Cre lines that are under the control of promoters for tissues overlapping *Celsr1* expression (**Fig. 3.2 E**). To ensure that the Cre drivers reported reliably on Cre activity coincident with their expression domains, we crossed the Cre lines into the Rosa26^{mTmG} binary reporter line (Muzumdar et al., 2007), where membrane Tomato and membrane GFP expression respectively label Cre-negative and Cre-expressing tissues (**Fig. 3.3 A-D**). FBM neuron migration was analyzed in conditional mutant embryos and control siblings to determine the spatial requirement for *Celsr1* activity. Disruption of *Celsr1* in r3/5 using *Krox20*^{Cre} (provided by Susan Dymecki, Harvard University) (Voiculescu et al., 2000) resulted in rostral migration of the FBM neurons into r2 and r3 in ~50% of mutant embryos (**Figure 3.3 E, F**). An *r4*^{Cre} line, deleting *Celsr1* specifically in rhombomere 4 (provided by Michèle Studer, University of Nice; France) (Di Bonito et al., 2013) was also able to partially recapitulate the rostral migration phenotype, with FBM neurons moving into r3 in 75% of mutant embryos. When a *Shh*^{Cre} line was used to inactive *Celsr1* activity in the floor plate cells (Jackson Laboratory) (Harfe et al., 2004), the FBM neurons migrated normally with no

Figure 3.3. *Celsr1* functions within the ventricular zone of r3/r4 to suppress rostral migration

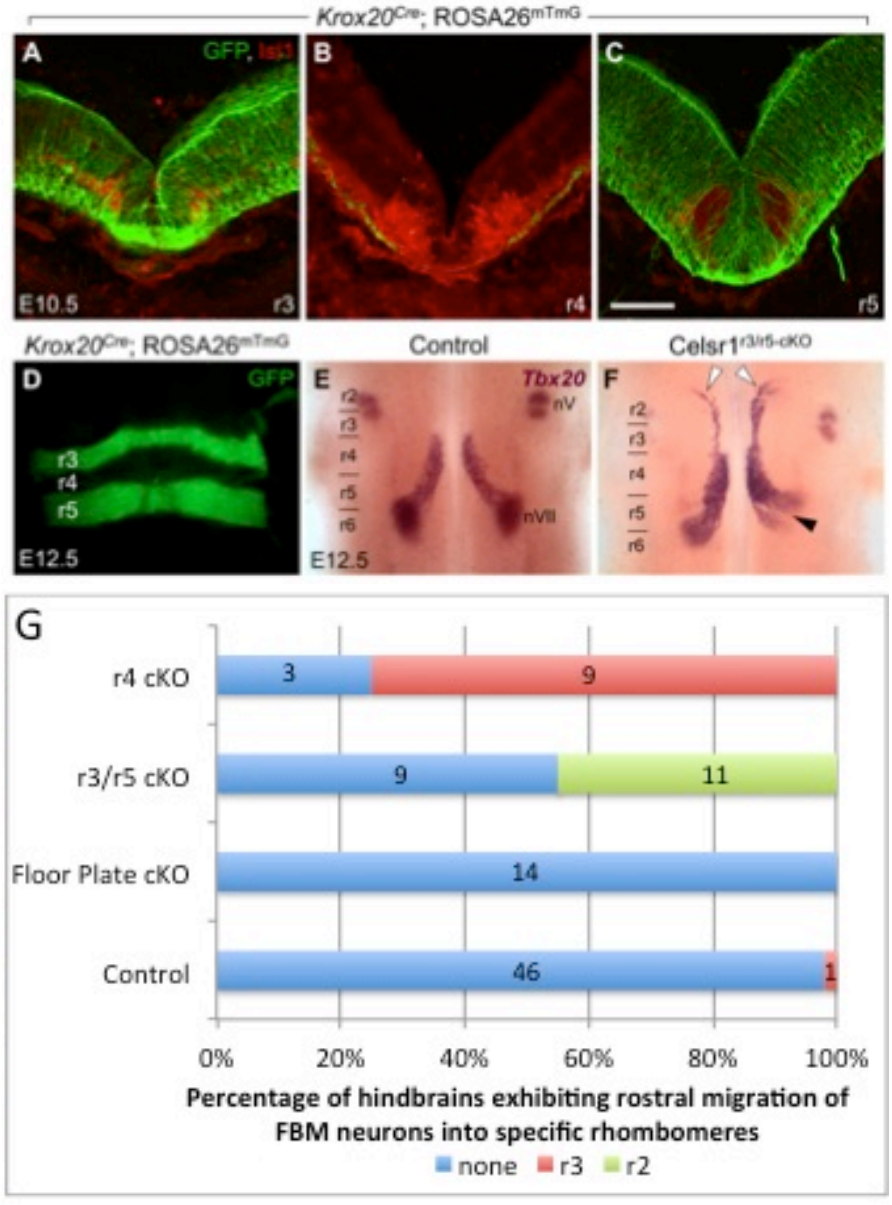

Figure 3.3. *Celsr1* functions within the ventricular zone of r3/r4 to suppress rostral migration

Conditional knockouts of *Celsr1* were generated using specific Cre drivers that overlapped *Celsr1* expression. A *ROSA26*^{mTmG} line was used to verify Cre activity. The rosa allele contains LoxP sites surrounding a mT allele which are excised by Cre recombinase, and upon excision, allows for expression of membrane-targeted GFP (mG). In cells without Cre activity, membrane-targeted tandem dimer Tomato (mT) is expressed. **A-F**, Example of one of the conditional knockouts, *Krox20-Cre*. **A-C**, sections through r3-5, confirm that Cre recombinase was active in r3 and r5 (**A, C**), and inactive in r4 (**B**). **D**, Whole mount embryo indicating *Krox20-Cre* activity in r3 and r5. **E, F**, *Tbx20* ISHs of *WT* and *Krox20-Cre* conditional mutants. Inactivation of r3 and r5 recapitulate the *Celsr1*^{Crash} rostral migration phenotype (**F**). **G**, Graph displaying the migration phenotypes of each *Celsr1* conditional knockout. *r4-Cre* was also able to recapitulate the rostral migration phenotype, while FBM neurons migrated normally in the floor plate *Shh-Cre* line.rostral migration phenotypes (**Figure 3.3 G**). This was surprising, given the strong *Celsr1* domain of expression in the floor plate (**Figure 3.2**), as well as data indicating that the floor plate cells are required for caudal migration of the FBM neurons in zebrafish (Sittaramane et al., 2013). The conditional knockout data suggest strongly that *Celsr1* functions specifically within rhombomeres 3-5 to suppress the rostral migration of FBM neurons in wild type embryos. However, *Celsr1* expression in r5 is unlikely to mediate suppression of rostral migration into the r2-r3 region. Moreover,

conditional inactivation of *Celsr1* in the ventricular zone using an *Nkx6.2:Cre* line (Fogarty et al., 2007) recapitulates the *Celsr1*$^{KO/KO}$ phenotype (Y. Qu, A. Goffinet and F. Tissir, University of Louvain, personal communication). Based on these observations, we propose that *Celsr1* functions in the ventricular zone of r3 and r4 to suppress the rostral migration of FBM neurons

3.1.4. Rostrally migrating neurons in *Celsr1* mutants may be responding to a guidance cue

The conditional knockout analyses suggest that *Celsr1* functions in the ventricular zone of r3 and r4 to suppress rostral migration of FBM neurons. At least two mechanisms could generate the rostral migration phenotype of *Celsr1* mutants. First, *Celsr1* inactivation may cause FBM neurons to lose their polarity such that neurons at any location in r4 would have the ability to migrate either rostrally (into r3) or caudally (into r5). Alternatively, following Celsr1 inactivation, a motor neuron chemoattractant may be unmasked in the rostral hindbrain, resulting in rostral migration of FBM neurons from a small region adjacent to the r3-r4 boundary. To differentiate between the two mechanisms, anterograde labeling of the rostrally and caudally migrating neurons in *Celsr1*$^{+/Crash}$ mice was performed using different colored lipophilic dyes (Fritzsch et al., 2005). The data indicate that rostrally FBM neurons in *Celsr1* mutants originate from the anterior aspect of rhombomere 4, adjacent to r3, suggesting strongly that the rostrally migrating neurons in *Celsr1* mutants are responding to a locally expressed guidance cue in the rostral hindbrain (Glasco, 2011). Thus, *Celsr1* may normally

suppress rostral migration of FBM neurons by blocking the expression or activity of a chemoattractive cue in the rostral hindbrain.

3.1.5. *Celsr1* and *Wnt5a* expression domains overlap in the rostral hindbrain

One potential candidate for the guidance cue attracting FBM neurons to the rostral hindbrain is Wnt5a. Wnt5a is a chemoattractant that is expressed broadly in r5 and caudally (Vivancos et al., 2009). Interestingly, *Wnt5a* and *Celsr1* expression significantly overlap within the rostral hindbrain. *Celsr1* is expressed along the midline through the entire hindbrain, while *Wnt5a* expression is along the midline rostrally to r3. Thus, it is possible that Celsr1 is acting to inhibit Wnt5a, thereby suppressing rostral migration in wild type mice.

3.1.6. Model for *Celsr1*-mediated suppression of rostral migration

Given that Wnt5a is a chemoattractant that is expressed broadly in r5 and r6 in the caudal hindbrain, it is possible that FBM neurons migrate caudally in response to this signal (Vivancos et al., 2009). Since rostral migration occurs in *Celsr1*-deficient embryos, we hypothesize that in wild type embryos, Celsr1 along the midline in r4 and rostral rhombomeres acts to suppress the activity of Wnt5a, which overlaps in expression with *Celsr1* in the rostral hindbrain. Suppression of responsiveness to Wnt5a could prevent the neurons from responding to the

chemoattractant signal in r3 and block rostral migration. In *Celsr1* mutants, the Wnt5a signal is not suppressed, leading to inappropriate rostral migration of FBM neurons (**Figure 3.4**).

3.1.7 Rostral Migration is Dvl-dependent

Several components of the Wnt/PCP signaling pathway has been shown to play a role in the migration of the FBM neurons (Bingham et al., 2002; Carreira-Barbosa et al., 2003; Glasco, 2011; Jessen et al., 2002; Qu et al., 2010; Sittaramane et al., 2009; Vivancos et al., 2009; Wada et al., 2006). While Dishevelled (Dvl) function is critical for Wnt/PCP signaling, its role in FBM neuron migration remained unclear. We showed that disruption of Dvl signaling in zebrafish embryos using dominant negative constructs generated PCP defects, such as a shortened body axis, but FBM neurons migrated normally (Glasco et al., 2012). In addition, FBM neurons migrated normally in *Dvl1/2* double mutant mice, despite a fully open neural tube, a bona fide PCP defect. These data suggest strongly that Dvl function is not required for caudal migration of FBM neurons. Interestingly, we found that *Dvl2* function appears to be required for the abnormal rostral migration of FBM neurons seen in *Celsr1*^{Crash} mutants. The deletion of one copy of *Dvl2* in *Celsr1*$^{+/Crash}$ mice has no effect on rostral migration, but deletion of both copies completely suppresses the rostral migration phenotype (Glasco et al., 2012). We hypothesize that *Celsr1* function in the rostral hindbrain antagonizes Wnt5a activity, preventing Fzd (and Dvl) activation in FBM neurons, and thereby suppressing rostral migration. In *Celsr1* mutants,

Figure 3.4. Model for Celsr1-Mediated Suppression of Rostral FBM Neuron Migration

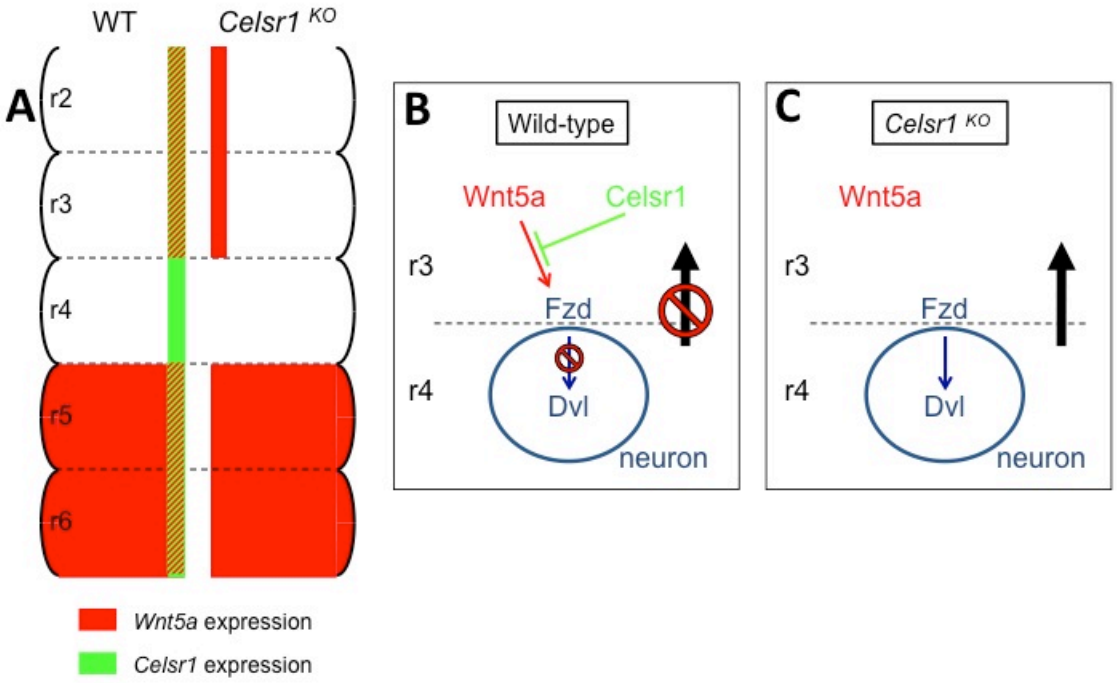

Figure 3.4. Model for *Celsr1*-Mediated Suppression of Rostral FBM Neuron Migration

Proposed model for *Celsr1*-mediated suppression of migration. Schematic of *Wnt5a* and *Celsr1* expression in the hindbrain, indicating that *Celsr1* and *Wnt5a* expression overlap along the midline through the entire hindbrain, with the exception of r4 (**A**). Our data indicate that Celsr1 in the rostral hindbrain may be inhibiting Wnt from binding to Fzd and thus suppressing migration in that direction (**B**). In the absence of *Celsr1*, Wnt inhibition is relieved and neurons migrate rostrally (**C**).

Wnt5a can activate Fzd (and Dvl) in FBM neurons, which migrate rostrally toward the Wnt5a source in r3 (**Figure 3.4**).

Wnt5a has been shown to act as a guidance cue in several systems, including the repulsion of corticospinal and commissural axons (Charron and Tessier-Lavigne, 2005; Fenstermaker et al., 2010; Keeble et al., 2006), and the attraction of FBM neurons (Vivancos et al., 2009). In explant studies, beads soaked in Wnt5a protein and placed lateral to the migratory stream of FBM neurons in r4 are sufficient to induce migration of FBM neurons towards the beads (Vivancos et al., 2009), indicating that the antero-lateral migration of FBM neurons may be Wnt-dependent. If Dvl function is necessary within FBM neurons for rostral migration (**Figure 3.4**), we would predict that FBM neurons would not migrate toward Wnt5a-soaked beads placed in the r3 region of *Dvl2*-deficient hindbrain explants.

3.2. Results

3.2.1. *Dvl3* expression is not altered in *Dvl1/2* double mutants

Dishevelled (Dvl) is an essential intracellular signaling component in the Wnt pathway (Gao and Chen, 2010; Jessen et al., 2002; Penton et al., 2002). While several Wnt/PCP genes are required for caudal migration of FBM neurons in zebrafish and mice (Bingham et al., 2002; Carreira-Barbosa et al., 2003; Glasco et al., 2012; Jessen et al., 2002; Qu et al., 2010; Sittaramane et al., 2009; Vivancos et al., 2009; Wada et al., 2006), Dvl plays little or no role in FBM

migration in zebrafish (Jessen et al., 2002). In the mouse, combined deletion of *Dvl1* and *Dvl2* does not disrupt caudal migration of the FBM neurons, indicating that they are dispensable for caudal migration (Glasco et al., 2012). Despite the lack of a migration phenotype, *Dvl1/2* double mutant mice display profound PCP defects, including an open neural tube and misorientation of stereociliary bundles in the inner ear hair cells (Etheridge et al., 2008; Hamblet et al., 2002; Wang et al., 2005). In the mouse, there are three *Dvl* genes (*Dvl1-3*) that are expressed in partially overlapping patterns throughout development (Tissir and Goffinet, 2006). Thus, the lack of a neuronal migration phenotype could result from *Dvl3* compensating for the loss of *Dvl1,2* in double mutants. Therefore, we examined *Dvl3* expression in *Dvl1/2* double mutants (**Figure 3.5**). E12.5 and E14.5 embryos were processed for *Dvl*3 whole-mount in situ hybridization, and sectioned by hand at various rhombomere levels. At E12.5, *Dvl3* is expressed only within the ventricular zone, and is absent from the region of the migrating FBM neurons (**Figure 3.5 A**). At E14.5, after migration is complete, *Dvl3* expression persists in the ventricular zone, and is absent in the region where the facial motor nucleus is located (**Figure 3.5 C**). Importantly, this expression pattern is not affected in *Dvl1/2* double mutant embryos (**Figure 3.5 B, D**), indicating that *Dvl*3 likely does not function in redundant fashion with *Dvl1* and Dvl*2* to regulate caudal migration. These data suggest strongly that Dvl function is not required for caudal migration of FBM neurons in mouse (Glasco et al., 2012).

Figure 3.5. *Dvl3* expression is not affected in *Dvl1/2* double mutants.

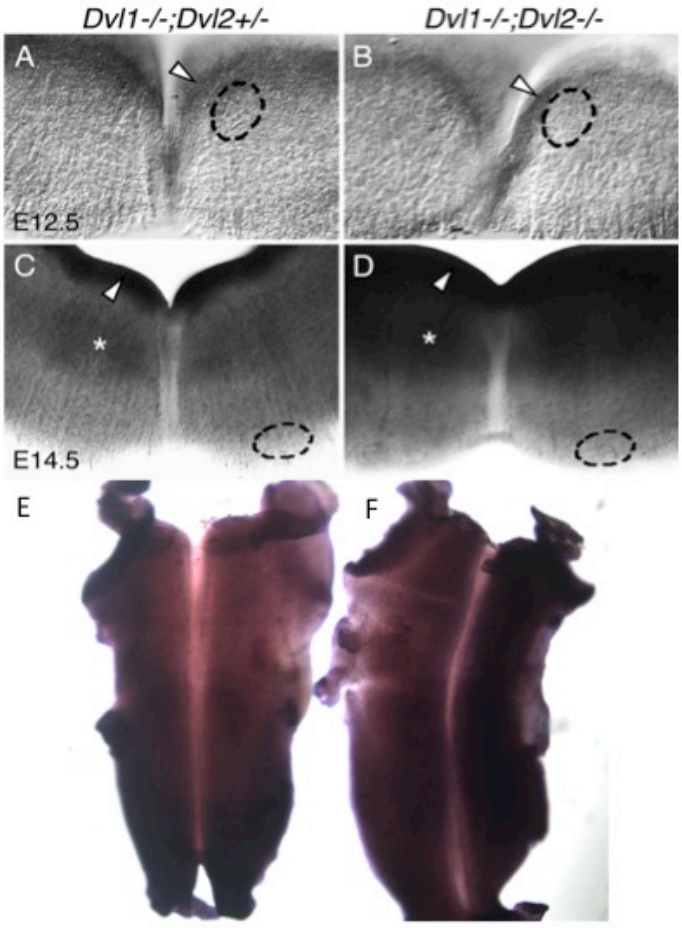

Figure 3.5. *Dvl3* expression is not affected in *Dvl1/2* double mutants.

Thick (~100 µm) cross sections (dorsal at top) of E12.5 (**A**, **B**) and E14.5 (**C**, **D**) hindbrains. Embryos were processed for *Dvl3* whole-mount ISH, then hand-sectioned. In an E12.5 *Dvl1*$^{-/-}$*; Dvl2*$^{+/-}$ control embryo (**A**), *Dvl3* expression at the r4 level is confined to the ventricular zone (arrowhead), and excluded from the region where FBM neurons would be located (nVII, dotted circle). This expression pattern is not affected in a *Dvl1*$^{-/-}$*; Dvl2*$^{-/-}$ mutant embryo (**B**). In an E14.5 *Dvl1*$^{-/-}$*; Dvl2*$^{+/-}$ embryo (**C**), *Dvl3* expression at the r6 level is confined to the ventricular zone (arrowhead) and the mantle zone (asterisk), and excluded from the pial surface where the facial motor nucleus would be located (nVII, dotted circle). This expression pattern is not affected in a *Dvl1*$^{-/-}$*; Dvl2*$^{-/-}$ mutant embryo (**D**). (**E, F**) E12.5 whole mount hindbrains before hand sectioning. (**E**) *Dvl1*$^{-/-}$*; Dvl2*$^{+/-}$, (**F**) *Dvl1*$^{-/-}$*; Dvl2*$^{+/-}$.

3.2.2. *Dvl2* mutant FBM neurons exhibit reduced responsiveness toward Wnt5a beads

While Dvl function may not be required for caudal migration, analysis of *Celsr1*$^{+/Crash}$*; Dvl2*$^{-/-}$ mice hindbrains suggests that *Dvl2* plays a role in the abnormal rostral migration of FBM neurons toward a potential Wnt5a source in r3 in *Celsr1* mutants (Glasco et al., 2012). Here, we directly test two elements of this model; first, whether FBM neurons can be induced to move rostrally toward a Wnt5a source, and second, whether such induced rostral migration is dependent on Dvl function. We performed these studies using hindbrain explants prepared from wild type and *Dvl2* mutant embryos. It was shown previously that in wild type explants, Wnt5a-coated beads placed near the lateral margin of the hindbrain near the r3-r4 boundary are able to attract FBM neurons (Vivancos et al., 2009). We performed similar experiments by placing the Wnt5a beads in the central region of r3, rather than at the lateral margins. *SE1::GFP* embryos were collected at E11.5 and hindbrain explants were cultured on filters with either 1X-PBS-DEPC- or Wnt5a-coated beads. While 1X-PBS-DEPC-coated beads failed to elicit migration of GFP-expressing FBM neurons from anterior r4, Wnt5a-coated beads definitively attracted FBM neurons rostrally out of r4 in 50% of the explants (**Figure 3.6**). These data suggest that excess Wnt5a provided by the beads is sufficient to overcome the putative antagonism mediated by Celsr1 that normally suppresses rostral migration.

To test whether the rostral migration induced by Wnt5a beads is Dvl-dependent, *Dvl2*$^{+/-}$*; GFP*$^{+/-}$ mice were incrossed to obtain *Dvl2*$^{+/+}$*; GFP*$^{+/-}$, *Dvl2*$^{+/-}$*;*

Figure 3.6. Wnt5a-coated beads induce the rostral migration of FBM neurons

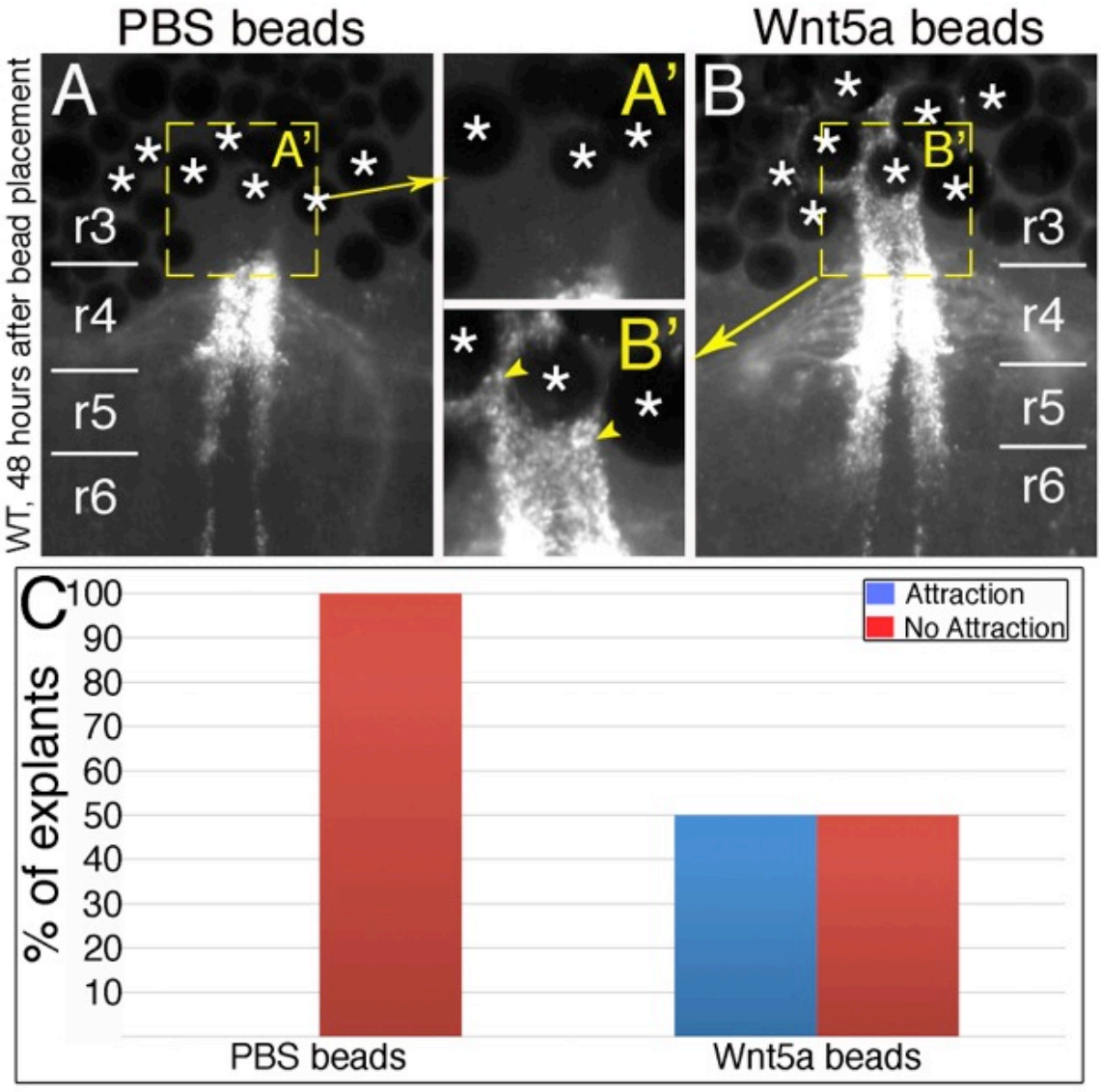

Figure 3.6. Wnt5a-coated beads induce the rostral migration of FBM neurons

SE1::GFP hindbrains were collected for explants using 1X-PBS-DEPC- or Wnt5a-coated beads (**A, B** respectively). Beads were placed above r3 and laterally to the FBM neurons. 100% of explants with 1X-PBS-DEPC beads failed to induce rostral migration (**A, A'**). Wnt5a beads were able to induce rostral migration of the FBM neurons 50% of the time (**B, B'**). Graph of percent of explants with rostral migration show a significant change in the Wnt5a beads compared to the 1X-PBS-DEPC beads (**C**, 1X-PBS-DEPC: n=29, Wnt5a: n=97). Asterisks, coated-beads. Arrowheads, rostrally migrating FBM neurons.

GFP$^{+/-}$ and *Dvl2*$^{-/-}$*; GFP*$^{+/-}$ embryos at E11.5, and hindbrain explants were cultured for 24-48 hours after placement of Wnt5a-coated beads (**Figure 2.4**). In both the *Dvl2*$^{+/+}$; GFP$^{+/-}$ and *Dvl2*$^{+/-}$; GFP$^{+/-}$ mice, rostral migration was evident 24 hours after bead placement (**Figure 3.7 A, C**, *Dvl2*$^{+/+}$; GFP$^{+/-}$ 48% attraction, n=10; Dvl2$^{+/-}$; GFP$^{+/-}$ 66% attraction, n=21). In contrast, rostral migration was greatly reduced in *Dvl2*$^{-/-}$*; GFP*$^{+/-}$ explants (20% attraction, n=1), suggesting that rostral migration induced by Wnt5a beads is Dvl-dependent (**Figure 3.7 B, C**). These results further support our model that Celsr1 normally suppresses Dvl-dependent rostral migration of FBM neurons by antagonizing Wnt5a activity in anterior rhombomeres.

3.2.3. *sFRPs* as candidate molecules involved in the suppression of Wnt signaling in the rostral hindbrain

Wnt5a is a guidance cue capable of inducing the rostral migration of FBM neurons in hindbrain explants. While our data thus far are consistent with a role for Celsr1 in suppressing rostral migration of FBM neurons by antagonizing Wnt function, the molecular mechanism of this antagonistic effect remains obscure. Therefore, we are considering candidate molecules that could potentially be involved in this mechanism. One of these is a family of Wnt antagonists called the *secreted Frizzled Related Proteins (sFRPs)*. There are five *sFRP* genes in mouse, with *sFRP1* and *sFPR2* being expressed in the hindbrain (Leimeister et al., 1998; Misra and Matise, 2010). It is possible that *sFRP* activity/expression in the rostral hindbrain is positively regulated by Celsr1, and that the sFRPs bind

Figure 3.7. Rostral migration is reduced in *Dvl2*$^{-/-}$ explants

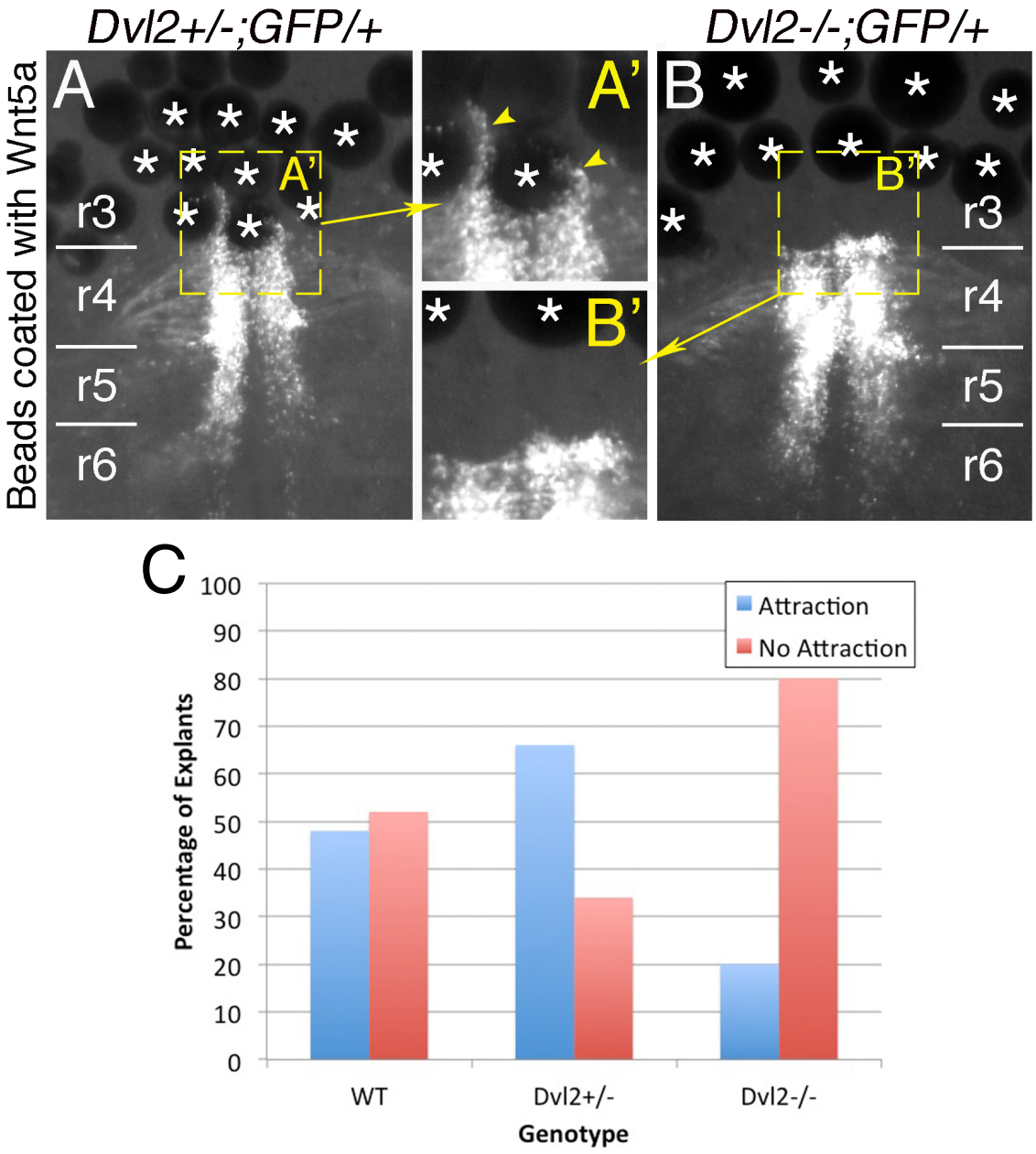

Figure 3.7. Rostral migration is reduced in *Dvl2*$^{-/-}$ explants

Littermates form *Dvl2*$^{+/-}$; *GFP*$^{+/-}$ incrosses were collected at E11.5 and cultured in the presence of Wnt5a-coated beads in the rostral hindbrain. FBM neurons of the *GFP*$^{+/-}$ and *Dvl2*$^{+/-}$; *GFP*$^{+/-}$ embryos were able to migrate rostrally towards the beads (**A, A'**). In *Dvl2*$^{-/-}$; *GFP*$^{+/-}$ explants, Wnt5a-coated beads were unable to induce the rostral migration of the FBM neurons (**B, B'**). Chi square analysis show that the rostral migration seen in WT embryos with Wnt5a-coated beads was not significant from the *Dvl2*$^{+/-}$; *GFP*$^{+/-}$ embryos. Initial results indicate that there was a significant reduction in the number of explants displaying rostral migration in the *Dvl2*$^{-/-}$; *GFP*$^{+/-}$ compared to the *Dvl2*$^{+/+}$; *GFP*$^{+/-}$ and *Dvl2*$^{+/-}$; *GFP*$^{+/-}$ explants (**C**, *Dvl2*$^{+/+}$; *GFP*$^{+/-}$: n=23, *Dvl2*$^{+/-}$; *GFP*$^{+/-}$: n=32, *Dvl2*$^{-/-}$; *GFP*$^{+/-}$: n=5. $P<0.001$).

Wnt5a in the rostral hindbrain, thereby preempting attraction of FBM neurons. To explore these possibilities, we characterized in detail *sFRP1* and *sFRP2* expression in the wild type hindbrain, and examined FBM neuron migration in *sFRP1/2* compound mutants.

3.2.4. *sFRP1* and *sFRP2* are expressed in broad, overlapping patterns in the hindbrain

To examine their expression in the vicinity of the FBM neurons, we performed whole mount in situ hybridization of WT embryos for *sFRP1* and *sFRP2*. *sFRP1* expression overlaps significantly with that of *Wnt5a*, with a broad domain in the caudal hindbrain, and a smaller domain along the midline extending rostrally from the r2/r3 boundary (**Figure 3.8 A**). To determine whether specific features of the *sFRP1* expression domain coincided with rhombomere boundaries, *SE1::GFP* embryos were first processed for an *sFRP1* in situ, using a FastRed substrate which fluoresces in the rhodamine channel (573 λ). After fixation, the tissues were processed for immunofluorescence using an anti-GFP antibody (AlexaFluor 488-chicken anti-rabbit, Invitrogen A21441). Confocal imaging showed that the caudal domain of *sFRP1* expression has a sharp boundary at the r3/r4 boundary, and *sFRP1* is expressed throughout the caudal hindbrain (**Figure 3.8 B**). The rostral domain of *sFRP1* seen in the NBT/BCIP in situ could not be reliably imaged by epifluorescence.

sFRP2 is expressed along the lateral margins of the hindbrain, with domains of expression extending medially in r5 and r6 (**Figure 3.8 C**).

Figure 3.8. Expression analysis of *sFRP1* and *sFRP2* in the developing mouse hindbrain

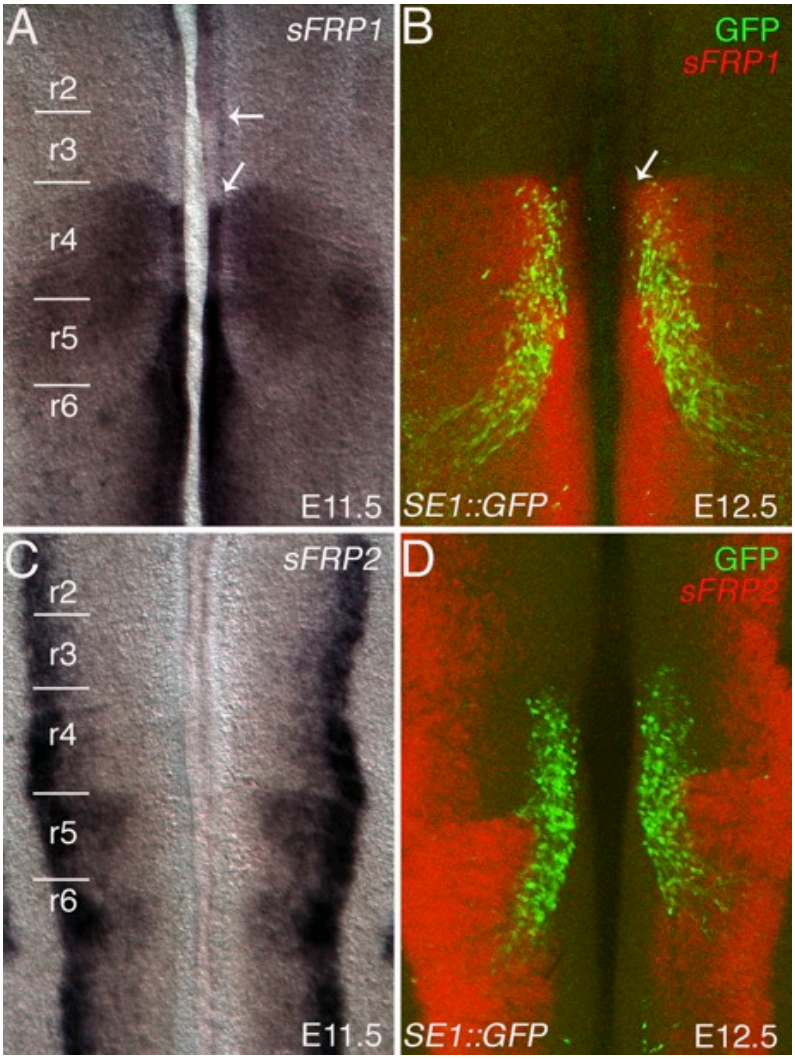

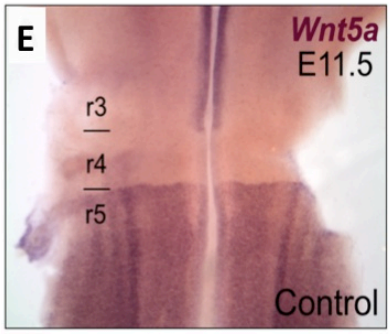

Figure 3.8. Expression analysis of *sFRP1* and *sFRP2* in the developing mouse hindbrain

NBT/BCIP in situ hybridization of WT embryos at E11.5 (**A,C**) indicate that *sFRP1* is expressed along the midline in the rostral hindbrain, as well as in large domains caudally (**A,** arrows). *sFRP2* expression is more restrained to lateral regions of the hindbrain (**C**). To determine the precise rhombomere boundaries of expression, *SE1::GFP* embryos were processed for in situ hybridization using a Fast Red fluorescent substrate for *sFRP* expression, followed by immunohistochemistry using a GFP antibody to label the FBM neurons (**B,D**). These experiments indicated that the caudal region of *sFRP1* expression begins at the r4/r5 boundary (**B**, arrow). The caudal domain of *sFRP1* expression was never seen when using the Fast Red substrate. *sFRP2* is expressed along both sides of the lateral hindbrain, with some medial expansion of expression within rhombomeres 5 and 6 which appear to form a border surrounding the lateral edges of the stream of caudally migrating FBM neurons (**D**). *sFRP1* expression overlaps with that of Wnt5a (**E**).

Fluorescence in situ and anti-GFP immunofluorescence indicates that the *sFRP2* expression domain abuts the column of migrating FBM neurons in r5 and r6. The partly complementary, but also overlapping expression patterns of *sFRP1* and *sFRP2* in r4, r5 and r6 is consistent with the potential for *sFRPs* to act in concert with Wnt5a to constrain the caudal migration of FBM neurons (**Figure 3.8 D**).

3.2.5. *sFRP1* and *sFRP2* mutant mice

sFRP1$^{-/-}$ and *sFRP2*$^{-/-}$ mice were obtained from Kamana Misra (University of Medicine & Dentistry of New Jersey, Piscataway, NJ) and crossed to obtain *sFRP1*$^{+/-}$; *sFRP2*$^{+/-}$ mice . The *sFRP1*$^{-/-}$ mouse line was generated by targeted deletion of exon 1 of the gene, including the cystein-rich domain (CRD), resulting in the loss of mRNA expression. *sFRP1*$^{-/-}$ mice are homozygous viable and do not display any overt phenotypes (Bodine et al., 2004). The *sFRP2*$^{-/-}$ line was also generated by targeted deletion of the first coding exon, including the translation initiation codon, leading to the loss of mRNA expression. *sFRP2*$^{-/-}$ mice are viable and fertile (Kobayashi et al., 2009; Lei et al., 2006). Using the breeding scheme outlined (**Figure 3.9**), we generated double heterozygotes. Intercrosses of double heterozygote siblings generated embryos that were missing 0-2 copies of *sFRP1* and 0-2 copies of *sFRP2* (**Figure 3.9**). We collected embryos at E11.5 and E12.5, and examined FBM neuron migration by performing in situ hybridization for *Tbx20* (Song et al., 2006).

Figure 3.9. *sFRP* Breeding scheme

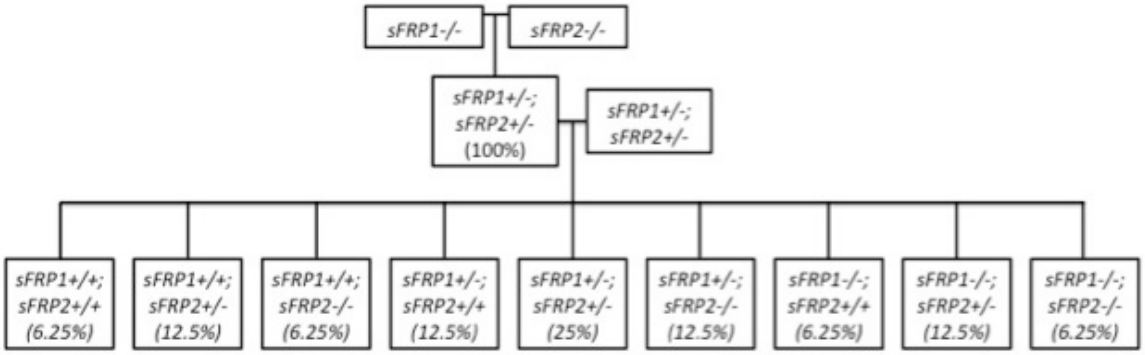

Figure 3.9. *sFRP* Breeding scheme

Schematic of breeding scheme to obtain *sFRP1/2* compound mutants. The mutant allele is indicated by -, and + indicates the wild type allele. *sFRP1*$^{-/-}$ and *sFRP2*$^{-/-}$ mice were crossed to obtain *sFRP1*$^{+/-}$; *sFRP2*$^{+/-}$ mice. These were then intercrossed to obtain embryos at E11.5 and E12.5 lacking anywhere from 0-2 copies of *sFRP1* and 0-2 copies of *sFRP2.* The expected percentage of each genotype is indicated.

3.2.6. FBM neuron migration in *sFRP1/2* compound embryos

To investigate a role for the *sFRPs* in FBM neuron migration, we collected compound *sFRP1/2* mutant embryos (**Figure 3.9**) and examined neuronal migration using *Tbx20* whole mount in situ hybridization. We hypothesized that sFRPs are activated by Celsr1 to suppress Wnt activity. Thus, we would expect that inactivation of *sFRP1/2* will recapitulate the rostral migration phenotype seen in *Celsr1* mutants. In E11.5 embryos lacking 0-2 copies of *sFRP1* and 0-2 copies of *sFRP2*, small streams of cells that were positive for Tbx20 were frequently seen in r3, consistent with a rostral migration defect (**Figure 3.10**). However, this phenotype was not seen in E12.5 compound mutants (**Figure 3.11**). *Tbx20* in situs of WT embryos ranging in age from E11.0 to E12.5 indicate that the *Tbx20* positive cells likely represent trigeminal neurons in r3 that had not yet initiated lateral migration to form the trigeminal motor nucleus (Song et al., 2006). Importantly, these cells are very likely not FBM neurons.

To further investigate a potential role for sFRPs in the *Celsr1*-mediated suppression of rostral migration, *sFRP1/2* compound mutant mice were crossed to the $Celsr1^{KO}$ line (**Figure 3.12**). If sFRPs played a role in suppressing the rostral migration phenotype, we hypothesized that a reduction in *sFRP* gene dosage may exacerbate the rostral migration phenotype seen in the *Celsr1* deficient embryos. We attempted to collect embryos at E11.5 and E12.5 to use for *Tbx20* ISH to analyze the FBM neuron migration patterns. *sFPR1/2* compound mutant females were bred to $Celsr1^{KO/fl}$ male mice. Mating was successful, as indicated by a positive plug, but very few females were pregnant

Figure 3.10. *Tbx20* positive cells in rhombomere 3 of E11.5 *sFRP* compound mutants

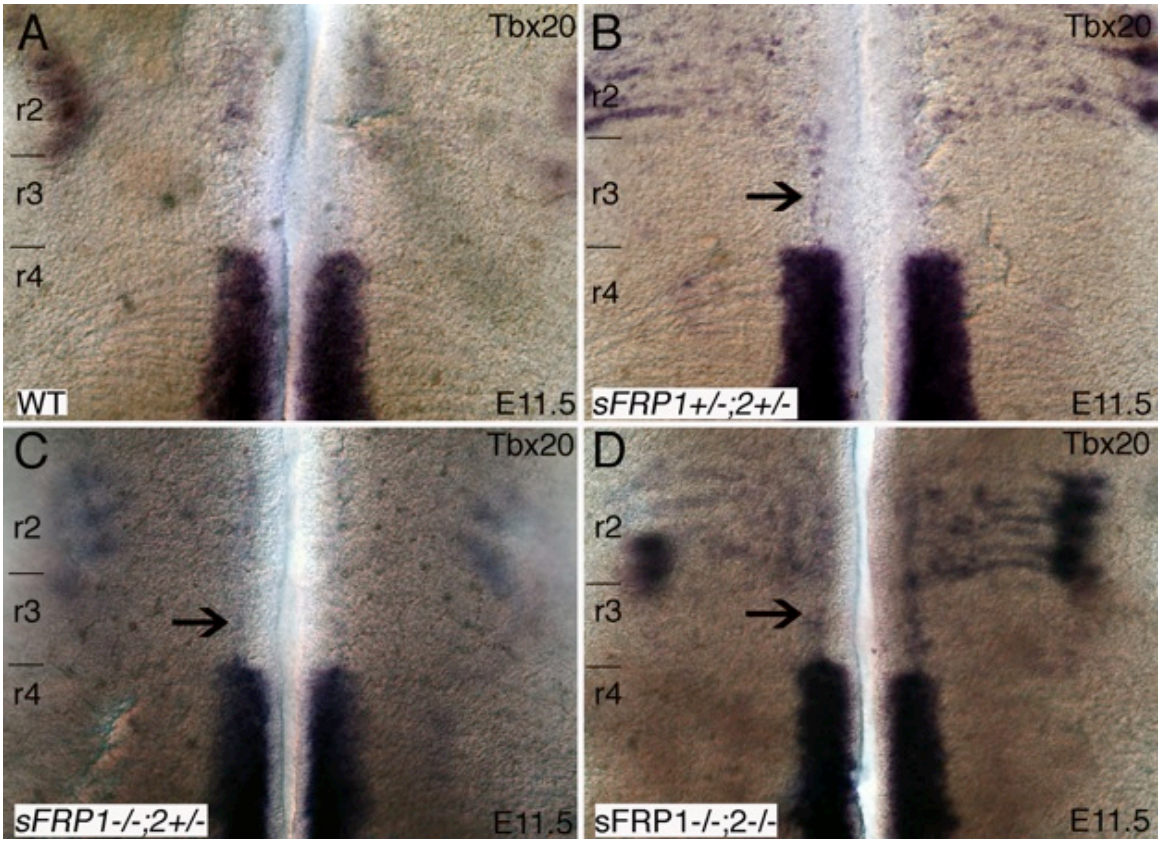

Figure 3.10. *Tbx20* positive cells in rhombomere 3 of E11.5 *sFRP* compound mutants

sFRP compound mutant embryos at E11.5 were processed for Tbx20 in situ hybridization to analyze the FBM neuron migration patterns. Compared to WT embryos (**A**), embryos lacking 1-4 copies of *sFRP1/2* have cells that express Tbx20 in rhombomere 3 (**B-D**, arrow), indicating a weak rostral migration phenotype.

Figure 3.11. *sFRP* is not required for abnormal rostral migration, but may be involved in caudal migration of FBM neurons

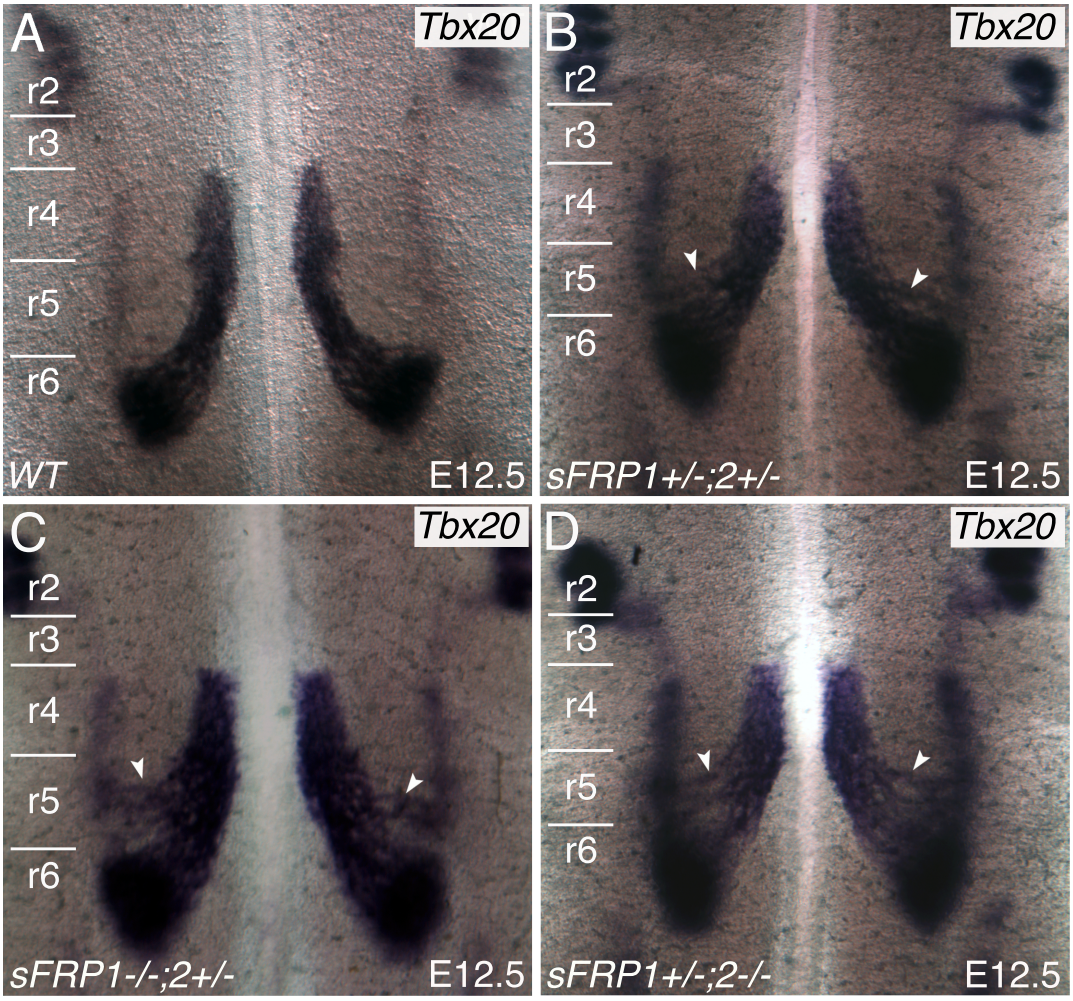

Figure 3.11. *sFRP* is not required for abnormal rostral migration, but may be involved in caudal migration of FBM neurons

sFRP compound mutant embryos at E12.5 were processed for *Tbx20* in situ hybridization to further analyze the rostral FBM neuron migration pattern. *Tbx20* positive cells were absent from r3 in all cases (**A-D**). All compound *sFRP* mutants display a precocious lateral migration phenotype (**B-D**, arrowheads), in which the caudally migrating FBM neurons exit the migratory stream prematurely, forming an expanded facial nucleus into rhombomere 5.

Figure 3.12. *sFRP; Celsr1* Breeding scheme

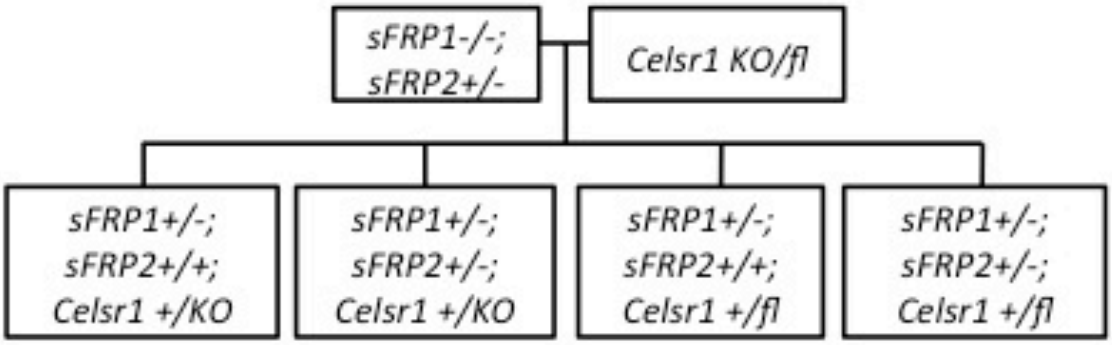

Figure 3.12. *sFRP; Celsr1* Breeding scheme

Schematic of breeding scheme to obtain *sFRP1/2; Celsr1*$^{+/KO}$ compound mutant embryos to determine if *sFRPs* are able to alter the rostral migration phenotype evident in *Celsr1K*$^{O/+}$ mice. *sFRP1*$^{-/-}$*;2*$^{+/-}$ mice were crossed to *Celsr1*$^{KO/fl}$ mice to obtain E11.5 and E12.5 embryos. *Celsr1*$^{fl/+}$ mice do not have an FBM neuron migration phenotype, and so were used as a control.

by E11.5, which could be indicative of embryonic lethality at an earlier stage. As a result, we could obtain only a small number of E11.5 embryos for analysis. While *Celsr1*$^{+/KO}$ embryos displayed a weak rostral migration phenotype similar to E11.5 *sFRP* mutants, *Celsr1*$^{+/fl}$ embryos exhibited no migration defects (**Table 3.1**). There was not a significant difference observed between the *sFRP1*$^{+/-}$*; 2*$^{+/-}$*; Celsr1*$^{+/KO}$ and the *sFRP1*$^{+/-}$*; 2*$^{+/-}$*; Celsr1*$^{+/fl}$ embryos. *Tbx20* positive cells were seen in r3 in almost all embryos, giving further evidence that the possible rostral migration phenotype seen in the *sFRP* embryos at E11.5 is an artifact of the trigeminal neurons.

Similar to *Wnt5a* mutant mice (Vivancos et al., 2009), FBM neurons of compound *sFRP1/2* mutants exit the migratory stream early in rhombomere 5 to form an expanded facial nucleus (**Figures 3.11, 3.13, Table 3.1**). This precocious lateral migration suggests a role for *sFRP1* and *sFRP2* in regulating the caudal migration of FBM neurons.

3.4. Conclusions

We propose that *Celsr1* function somehow suppresses the rostral migration of FBM neurons toward the Wnt5a source in r3 (**Figure 3.4**). When *Celsr1* is inactivated, rostral migration occurs, but intriguingly is dependent on *Dvl2* function. In order to test this further, we employed an explant system to analyze FBM neuron migration patterns in response to ectopic sources of the putative chemoattractant Wnt5a. In *Dvl2*$^{+/+}$ and *Dvl2*$^{+/-}$ littermates, ectopic Wnt5a

Table 3.1. FBM neuron migration phenotypes in *sFRP1/2* compound mutants

A) Rostral Migration Phenotype

	E11.5		E12.5	
Genotype	**Normal migration**	***Tbx20*+ cells in r2/r3**[1]	**Normal migration**	***Tbx20*+ cells in r2/r3**[2]
***sFRP1*$^{+/-}$; *sFRP2*$^{+/-}$**	5/11	6/11	6/6	0/6
***sFRP1*$^{+/-}$; *sFRP2*$^{-/-}$**	2/4	2/4	2/2	0/2
***sFRP1*$^{+/-}$; *sFPR2*$^{+/+}$**	0/1	1/1	0/0	0/0
***sFRP1*$^{-/-}$; *sFRP2*$^{+/-}$**	1/2	1/2	1/1	0/1
***sFRP1*$^{-/-}$; *sFRP2*$^{+/+}$**	0/1	1/1	3/3	0/3
***sFRP1*$^{-/-}$; *sFRP2*$^{-/-}$**	1/2	1/2	2/2	0/2
***sFRP1*$^{+/-}$; *sFRP2*$^{+/-}$; *Celsr1*$^{fl/+}$**	1/5	4/5		
***sFRP1*$^{+/-}$; *sFRP2*$^{+/-}$; *Celsr1*$^{KO/+}$**	0/6	6/6		

[1,2] Tbx20 positive cells in r2 and r3, likely trigeminal neurons that have not initiated lateral migration

[1] refer to **Figure 3.10**

[2] refer to **Figure 3.11**

B) Caudal Migration Phenotype

	E11.5		E12.5	
Genotype	**Normal migration**	**Precocious lateral migration**[3]	**Normal migration**	**Precocious lateral migration**[4]
sFRP1$^{+/-}$; sFRP2$^{+/-}$	8/11	3/11	1/6	5/6
sFRP1$^{+/-}$; sFRP2$^{-/-}$	3/4	1/4	1/2	1/2
sFRP1$^{+/-}$; sFPR2$^{+/+}$	1/1	0/1	0/0	0/0
sFRP1$^{-/-}$; sFRP2$^{+/-}$	1/2	1/2	0/1	1/1
sFRP1$^{-/-}$; sFRP2$^{+/+}$	1/1	0/1	1/3	2/3
sFRP1$^{-/-}$; sFRP2$^{-/-}$	2/2	0/2	0/2	2/2
sFRP1$^{+/-}$; sFRP2$^{+/-}$; Celsr1$^{fl/+}$	4/5	1/5		
sFRP1$^{+/-}$; sFRP2$^{+/-}$; Celsr1$^{KO/+}$	6/6	0/6		

[3,4] Caudally migrating FBM neurons that exit the migratory stream early in r5

[3] refer to **Figure 3.13**

[4] refer to **Figure 3.11**

Table 3.1. FBM neuron migration phenotypes in *sFRP1/2* compound mutants

Table indicating the FBM neuron migration patterns in E11.5 and E12.5 *sFRP1/2* compound mutants. The *Tbx20* expressing cells evident at E11.5 were originally thought to be rostrally migrating FBM neurons. However, this phenotype was completely resolved by E12.5, indicating that the *Tbx20* positive cells in the rostral hindbrain were likely trigeminal neurons that had not yet completed migration. *sFRP1; sFRP2; Celsr1* compound mutant embryos were collected at E11.5 to determine if the rostral migration phenotype would be exacerbated. There were no significant differences observed between the $sFRP1^{+/-}$; $sFRP2^{+/-}$; $Celsr1^{KO/+}$ and the $sFRP1^{+/-}$; $sFRP2^{+/-}$; $Celsr1^{fl/+}$embryos.

Precocious lateral migration was scored as being Tbx20 positive cells that migrated out of the caudal migratory stream early in r5, instead of r6 as normal. This phenotype is evident in embryos lacking any number of copies of *sFRP1* or *sFPR2*, and indicates a role for *sFRPs* in caudal migration.

Figure 3.13. *sFRP* is not required for abnormal rostral migration, but may be involved in caudal migration of FBM neurons

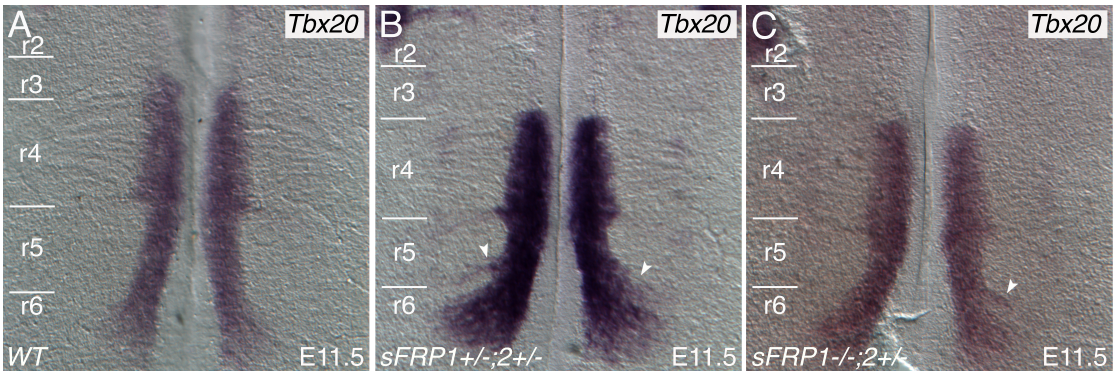

Figure 3.13. *sFRP* is not required for abnormal rostral migration, but may be involved in caudal migration of FBM neurons

sFRP compound mutant embryos at E11.5 were processed for *Tbx20* in situ hybridization to further analyze the rostral FBM neuron migration pattern. *Tbx20* positive cells were absent from r3 in all cases (**A-D**). All compound *sFRP* mutants display a precocious lateral migration phenotype (**B-D**, arrowheads), in which the caudally migrating FBM neurons exit the migratory stream prematurely, forming an expanded facial nucleus into rhombomere 5.

in the rostral hindbrain was able to frequently induce the migration of FBM neurons in that direction (**Figure 3.6**). In contrast, the FBM neurons in *Dvl2*$^{-/-}$ explants rarely migrated rostrally in response to ectopic Wnt5a (**Figure 3.7**). These data give further support to our model of *Celsr1*-mediated suppression, but it is still unclear exactly how *Celsr1* mediates this suppression.

Other candidate molecules were tested for a potential role in this model, including the secreted Frizzled Related Proteins (sFRPs). *sFRP1* and *sFRP2* are expressed in overlapping patterns in the hindbrain (**Figure 3.8**), and appear to play a role in the caudal migration of the FBM neurons, but are dispensable for rostral migration (**Figure 3.11, 3.13**).

CHAPTER 4: Identification of Genes with Potential Roles in FBM Neuron Migration

4.1. Introduction

4.1.1. Rostral migration in *Celsr1*$^{+/Crash}$ mice

During the development of the mouse brain, facial branchiomotor (FBM) neurons are born within a segment of the hindbrain, rhombomere 4 (r4). These neurons then migrate caudally towards r6, where they form the facial motor nucleus. In *Celsr1*$^{+/Crash}$ and *Celsr1*$^{KO/KO}$ mice, most of the FBM neurons migrate towards r5/6 in a normal fashion, but a significant subset migrates abnormally in a rostral direction towards r2/3. Thus, it is possible that in wild type embryos, *Celsr1* acts to suppress the rostral migration of the FBM neurons.

4.1.2. Rationale

Analyses presented in **Chapter 3** suggest that *Celsr1* functions within the ventricular zone of rhombomeres 3 and 4 to suppress the rostral migration of FBM neurons, and that only neurons born in the anterior portion of r4 migrate rostrally in *Celsr1*$^{+/Crash}$ mice. In addition, the data suggest that Celsr1 may suppress rostral migration by antagonizing Wnt activity. Therefore, we evaluated whether *secreted Frizzled Related Proteins* (*sFRPs*), a family of Wnt antagonists, played any role in FBM neuron migration. Our data suggest that although *sFRP1*

and *sFPR2* are expressed at the right place and time, they are likely not involved in suppressing rostral migration of FBM neurons (**Chapter 3**). Hence it is possible that *Celsr1* acts directly or indirectly to control the expression of other genes that may be involved in the suppression of rostral migration.

In our model (**Figure 3.4**), *Celsr1* normally inhibits Wnt5a from activating Dvl-dependent signaling in FBM neurons, thus suppressing rostral migration. In the absence of *Celsr1*, Wnt5a activates signaling within FBM neurons, resulting in rostral migration. However, how Wnt5a activity is normally suppressed by Celsr1 remains obscure. We also cannot rule out that other guidance cues may be affected by loss of *Celsr1*. To better understand how *Celsr1* regulates FBM neuron migration, we performed high-throughput expression profiling using RNA-seq to identify candidate genes regulating FBM neuron migration, in particular, the suppression of rostral migration. By comparing expression levels of genes in the anterior hindbrain between a normal mouse and a mouse with a rostral migration phenotype, we have identified several candidate genes with potential roles in FBM neuron migration.

4.2. Methods

4.2.1. Tissue collection

In order to identify differentially expressed genes potentially associated with FBM neuron migration, including abnormal rostral migration, hindbrain tissue was collected from *Celsr1*$^{+/+}$*; GFP*$^{+/-}$ and *Celsr1*$^{+/Crash}$*; GFP*$^{+/-}$ littermates. Since

most FBM neurons migrate from r4 caudally to r6 in *Celsr1* mutants, and since rostrally migrating neurons move from r4 to r2, we wanted to enrich for genes that may be differentially expressed in rostrally versus caudally migrating neurons, and/or in the environment. Furthermore, we wanted to avoid enriching for genes that would be expressed in differentiating FBM neurons (rostrally or caudally migrating), which would not be expected to change across genetic backgrounds. Therefore, fragments of hindbrain tissue from the r2-r4 (anterior) and the r4-r6 (posterior) regions of *Celsr1*$^{+/+}$*; GFP*$^{+/-}$ and *Celsr1*$^{+/Crash}$*; GFP*$^{+/-}$ mice were carefully dissected using tungsten needles, and used to make RNA (**Section 2.6, Figure 2.6**). A small portion of r4 was included in both the anterior and posterior fragments so that genes expressed at similar levels in r4 of wild type and *Celsr1* mutants, such as motor neuron-specific and r4-specific genes, were less likely to be identified during the bioinformatics analyses.

4.2.2. RNA quality

After RNA extraction, RNA concentrations were estimated using a Nanodrop spectrophotometer (model #ND-1000), and samples were submitted to the University of Missouri DNA Core for an RNA integrity test (Bio-Rad Experion, RNA StdSens chip) to determine if the RNA was sufficiently high quality for high throughput sequencing using the Illumina system. The tests indicated that the RNA purified using the Qiagen RNeasy kit was of higher quality than that purified using the RNAzol method (example of quality test results: **Figure 4.1**). The

Figure 4.1. RNA integrity test validates RNA quality for high-throughput sequencing

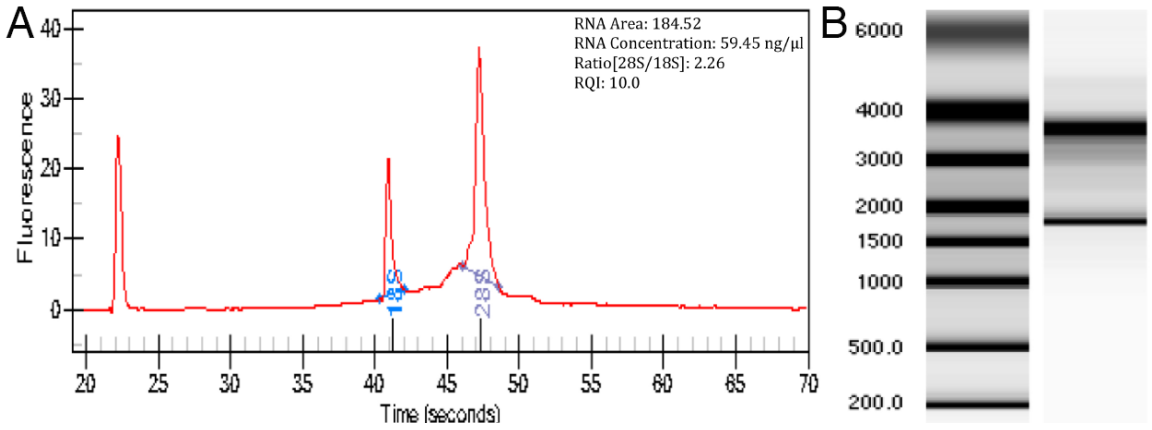

Figure 4.1. RNA integrity test validates RNA quality for high-throughput sequencing

Sample of RNA quality test. **A)** Digital data produced from electrophoresis conducted in microchips. RNA integrity is quantitated by comparing the area of the peaks that correspond to the small and large subunit ribosomal RNAs (rRNAs). A ratio around 2 indicates intact RNA. The RQI is a score from 1-10, highest being intact RNA and lowest degraded RNA, calculated by comparing the electrophoresis vales to a series of standardized RNA samples. **B)** Left, ladder for agarose gel. Right, virtual gel image indicating two bands, the bottom weaker intensity band corresponds to the small subunit and the upper band, with double the intensity, corresponding to the large subunit of the rRNA. The presence of both of these bands indicates that the RNA is not degraded.

average yield was 450 ng RNA per hindbrain (n=4). Since the amount of total RNA required for Illumina sequencing is 2-5 µg/sample, and the RNA yield from rhombomere fragments will be even lower than from whole hindbrains tested, we decided to pool 8 hindbrain fragments of each genotype to obtain sufficient RNA. Given the large number of hindbrains needed, it was not possible to obtain all *Celsr1*$^{+/Crash}$*; GFP*$^{+/-}$ and *Celsr1*$^{+/+}$*; GFP*$^{+/-}$ sibling tissues from one female. Therefore, one *Celsr1*$^{+/+}$*; GFP*$^{+/-}$ male was mated with several *Celsr1*$^{+/Crash}$*; GFP*$^{+/-}$ female siblings in order to produce enough embryos of each genotype while maintaining a high degree of genetic relatedness so as to minimize the effects of random genetic variation on gene expression changes within each group. From two females, 8 *Celsr1*$^{+/+}$*; GFP*$^{+/-}$ and 8 *Celsr1*$^{+/Crash}$*; GFP*$^{+/-}$ embryos were collected. The tissues from each female were processed separately and the isolated RNAs were evaluated for quality (**Table 4.1, Figure 4.1**). Each sample gave more than 40 ng/µL of RNA, and all were of excellent quality for generating a cDNA library, as shown by the RNA Quality Indicator (RQI) score, which was between 9.7-10 in each sample (**Table 4.1**). The best samples for each condition were pooled in order to obtain enough RNA at sufficient concentration for submission for RNA sequencing by the University of Missouri DNA Core facility.

Table 4.1. RNA Quality

	WA		WP		MA		MP	
Female #	**Concentration (ng/µL)**	**RQI**	**Concentration (ng/µL)**	**RQI**	**Concentration (ng/µL)**	**RQI**	**Concentration (ng/µL)**	**RQI**
1	52.4	8.5	41.28	8.5	39.58	9.1	69.87	8.6
2	33.12	9.8	N/A	N/A	N/A	N/A	42.14	9.7
3*	59.45	10	68.39	9.8	67.75	10	69.77	10
4*	118.81	9.7	91.61	9.8	67.75	10	41.29	10

*The embryos from these females were used for RNA seq submission. 4 WT and 6 *Celsr1*$^{+/Crash}$ embryos were collected from female 3. 4 WT and 2 Celsr1$^{+/Crash}$ embryos were collected from female 4.

Table 4.1. RNA Quality

Hindbrain tissues were collected from 4 *Celsr1*$^{+/Crash}$ females at E11.5. RNA was isolated from the tissues and submitted to the University of Missouri DNA core for quality validation. The results for each female are shown. The RNA from females 3 and 4 in each category were combined and submitted for RNA sequencing. The concentration and RNA Quality Index (RQI) score were excellent in all of these samples.

Abbreviations: W: WT, or *GFP*$^{+/-}$. M: mutant, or *Celsr1*$^{+/Crash}$*; GFP*$^{+/-}$. a: anterior hindbrain, from r2-mid r4. p: posterior hidnbrain, from mid r4-r6.

4.2.3. RNA sequencing

Sequencing was performed by the University of Missouri DNA Core using the Illumina HiSeq2000, a high-throughput sequencer. During this process, mRNA is purified from the total and converted into cDNA (Illumina, TruSeq RNA). A cDNA library composed of 200-500 base pair fragments of cDNAs is then prepared. The Illumina sequencing platform allows for multiple samples to be run in the same lane by incorporating a unique barcode sequence into each fragment during cDNA library construction. Each cDNA fragment is sequenced, creating “reads” of 30-400 base pairs. A single lane can yield ~150 million reads making multiplexing efficient and cost-effective. In addition, running all of the samples in a single lane decreases the chances of technical errors that could arise if each sample were run in a separate well. As each fragment is sequenced, computer software allows for the identification and removal of the barcode. Reads can then be assembled to produce a transcriptome, or set of transcripts within a cell, using a reference genome. In this case, the reference genome was the Genome Reference Consortium Mouse Build 38 patch release 1 (GRCm38.p1) (http://www.ncbi.nlm.nih.gov/assembly/GCF_000001635.21/). This genome-wide transcriptional map indicates the structure of each transcript, including splicing patterns and other post-transcriptional modification, and the level of expression for each gene (Wang et al., 2009).

4.2.4. Bioinformatics analysis

The transcriptome generated during the RNA sequencing was submitted to the University of Missouri Bioinformatics Core for analysis. We worked closely with Dr. Scott Givan (Associate Director, Informatics Research Core facility, MU) to analyze the raw data. A standard sequence analysis suite, including TopHat (http://tophat.cbcb.umd.edu) (Trapnell et al., 2009), Cufflinks and CuffDiff (http://cufflinks.cbcb.umd.edu) (Trapnell et al., 2012; Trapnell et al., 2010), was applied to the sequence data. TopHat uses the BowTie program (http://bowtie-bio.sourceforge.net) to align the fragment reads to the reference genome, in this case the Genome Reference Consortium Mouse Build 38 patch release 1 (GRCm38.p1) (http://www.ncbi.nlm.nih.gov/assembly/GCF_000001635.21/), and identify splice junctions between exons. The quality of the reads, and fraction of reads that were mapped to the genome, were excellent, as indicated by the RNA Quality Index (RQI) score near 10, meaning that the RNA had not been degraded (**Table 4.2**). There were over 1,200,000 reads from each of the four samples, and over 94% of the reads could be mapped in each sample. Cufflinks was used to assemble the alignments into a set of transcripts and test for differential expression of exons, indicative of isoform-specific gene regulation. The abundance of each transcript is based upon the number of corresponding reads generated in each sample (Trapnell et al., 2012). This analysis was performed on all samples (Wa, Wp, Ma, Mp). Next, CuffDiff was used to compare the transcriptome assemblies between samples to identify genes that were

Table 4.2. Bioinformatics Analysis, Read Accounting

A) Read quality

		No. of Reads Removed		
Sample	Raw Reads	Trim[1]	Filter[2]	Match[3]
Wa	42,973,711	1,843,956	790,474	1,588,839
Wp	42,343,897	1,356,187	434,063	1,266,139
Ma	55,645,936	2,445,579	1,011,838	2,156,784
Mp	67,234,788	3,054,490	1,228,745	2,327,718

B) Read Mapping

Sample	QC Reads[4]	Mapped[5]	% Mapped[6]
Wa	38,750,442	38,007,156	98.1%
Wp	39,287,508	37,276,372	94.9%
Ma	50,031,735	49,059,122	98.1%
Mp	60,623,835	59,424,340	98.0%

[1]Reads trimmed with fastx_trimmer. Minimum Quality Threshold = 13, Minimum length = 32. [2]Reads filtered with fastq_quality_filter. Quality cut-off = 13, Minimum percentage = 90. [3]Reads filtered by match to mitochondrial and/or plastid genomes, repeat elements, or the PhiX genome using bowtie. [4]Number of reads that pass all QC measures (the raw reads minus the reads removed[1,2,3]). [5]Number of QC reads that map to the reference genome. [6]Percentage of QC reads that map to the reference genome.

Table 4.2. Bioinformatics analysis, Read Accounting

(A) Read quality. Indicates the number of reads that were generated in the RNA sequencing. Reads were then trimmed to remove the adaptor sequences, filtered based on a quality threshold, and matched to the reference genome. **(B)** Read Mapping. Indicates the number of genes that passed the quality tests and the amount of those that were mapped to the reference genome.

differentially expressed. Several pairwise comparisons were examined in order to identify genes potentially involved in different aspects of FBM neuron migration (**Figure 4.2**). For example, one would expect in the Wa-Ma comparison to see genes that are involved in directionality, while in the Wa-Wp comparison, one may identify genes that are involved in the initiation and termination of normal FBM neuron migration.

4.2.5. Bioinformatics report

The bioinformatics analyses generated a report that listed all genes that were identified and mapped to the mouse genome. The four pairwise comparisons (**Figure 4.2**) were expected to provide insight into FBM neuron migration mechanisms. Importantly, the Wa-Ma comparison may identify genes potentially involved in the suppression of rostral migration of FBM neurons in wild type embryos. For each comparison, a spreadsheet was generated showing all of the transcripts that were differentially regulated between the two samples. For every gene expressed in either of the two conditions under comparison, statistical tests were performed to evaluate whether differences in expression of the gene between the two conditions was statistically significant (q-value <0.05). Truncated gene lists containing up- and down-regulated genes corresponding to the four comparisons examined are shown in **Tables 4.3-4.6**.

Figure 4.2: Pairwise comparisons may identify candidate genes involved in FBM neuron migration

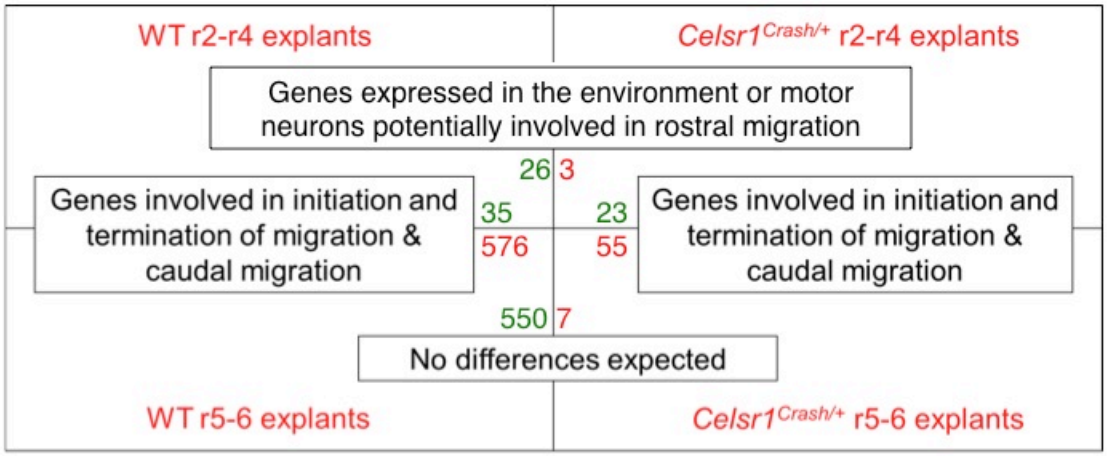

Figure 4.2: Pairwise comparisons may identify candidate genes involved in FBM neuron migration

Anterior and posterior portions of WT and Celsr1$^{+/Crash}$ hindbrains were submitted for RNA sequencing and bioinformatics analysis. The 4 samples allowed for several pairwise comparisons to be made, as indicated here. For instance, when comparing the anterior portions of the WT hindbrains to the Celsr1$^{+/Crash}$ hindbrains, we would expect to identify candidate genes involved in determining the directionality of FBM neuron migration. Other comparisons, such as the anterior vs the posterior portion of WT embryos, may identify candidates involved in the initiation or termination of migration. The numbers of genes that were identified as significant in each comparison are indicated (red: downregulated genes; green: upregulated genes).

Table 4.3. Genes exhibiting largest changes in expression levels between Wa and Ma

gene_id	gene	locus	value_1: Wa	value_2: Ma	log2(fold_change) (Ma/Wa)	test_stat	p_value	q_value
ENSMUSG00000078193	Gm2000	1:156310726-156421159	338.309	0.150365	-11.1357	8.05593	8.88E-16	4.40E-13
ENSMUSG00000080977	Gm13772	2:90782726-90834437	46.104	0.148025	-8.28291	3.65409	0.000258092	0.01383
ENSMUSG00000082872	Gm15773	7:12581469-12606544	0.701984	0.0226107	-4.95636	4.15117	3.31E-05	0.00223362
ENSMUSG00000037742	Eef1a1	9:78478448-78489151	4660.53	4749.2	0.027191	-4.36108	1.29E-05	0.000964412
ENSMUSG00000072235	Tuba1a	15:98949840-98953551	6528.09	6951.14	0.0905886	-16.8436	0	0
ENSMUSG00000029838	Ptn	6:36715662-36811361	23.3138	38.1488	0.710452	-3.45916	0.000541859	0.0263427
ENSMUSG00000074280	Gm6166	9:57483912-57484585	83.7496	144.102	0.782932	-3.86336	0.000111838	0.00663136
ENSMUSG00000060128	Gm10075	1:19063298-19166346	93.8065	166.847	0.830764	-4.24706	2.17E-05	0.0015386
ENSMUSG00000026043	Col3a1	1:45311537-45349706	0.885595	2.22001	1.32585	-3.3736	0.000741914	0.0346192
ENSMUSG00000084116	Gm12460	4:51190106-51190463	14.7659	43.8799	1.57129	-3.39792	0.000679014	0.032002
ENSMUSG00000023484	Prph	15:99055173-99058978	1.62602	4.8631	1.58053	-3.44831	0.000564103	0.027228
ENSMUSG00000081683	Fzd10	5:128601105-128604093	2.50215	8.20091	1.71262	-4.85633	1.20E-06	0.000115802

ENSMUSG00000021867	Gm9746	14:26082296-26235735	2.47393	8.77198	1.8261	-3.63438	0.000278647	0.0147775
ENSMUSG00000021943	Gdf10	14:33923586-33935280	0.322538	1.44582	2.16435	-3.85931	0.000113707	0.0067311
ENSMUSG00000048450	Msx1	5:37820484-37824583	0.329105	1.51084	2.19873	-3.68385	0.000229742	0.0124843
ENSMUSG00000032368	Zic1	9:91358057-91389348	4.03334	21.2361	2.39647	-3.53986	0.000400343	0.0202374
ENSMUSG00000061524	Zic2	14:122475434-122479852	0.858456	6.01669	2.80915	-5.76968	7.94E-09	1.19E-06
ENSMUSG00000028707	Dmbx1	4:115914543-115939926	0.412071	3.11504	2.91828	-6.23069	4.64E-10	9.08E-08
ENSMUSG00000042240	Crybb2	5:113058257-113070117	0.529829	6.12855	3.53195	-4.16227	3.15E-05	0.00213847
ENSMUSG00000041703	Zic5	14:122456794-122465677	0.152897	1.78581	3.54595	-5.27349	1.34E-07	1.58E-05
ENSMUSG00000028871	Rspo1	4:124957646-125009099	0.0415587	0.528383	3.66836	-3.57358	0.000352132	0.0181227
ENSMUSG00000018166	Erbb3	10:128567522-128589652	0.0559755	0.730407	3.70583	-6.1289	8.85E-10	1.60E-07
ENSMUSG00000036480	Prss56	1:87183492-87188404	0.0629047	0.85507	3.7648	-4.73411	2.20E-06	0.000201668
ENSMUSG00000009900	Wnt3a	11:59248032-59290752	0.020482	0.317621	3.95488	-3.80545	0.000141545	0.00818167
ENSMUSG00000024747	Aldh1a7	19:20692952-20727562	0.0280463	0.824864	4.87827	-4.88958	1.01E-06	9.95E-05
ENSMUSG00000094597	CT025616.1	13:64509722-64511099	0.0335165	1.16612	5.1207	-4.92055	8.63E-07	8.65E-05
ENSMUSG00000026979	Psd4	2:24367579-24409182	0.0271534	1.09121	5.32865	-3.45081	0.000558903	0.0270433

ENSMUSG00000075014	Gm10800	2:98666546-98667301	0.100241	4.03686	5.33169	-3.81098	0.000138416	0.00803088
ENSMUSG00000083545	Gm13320	2:14174523-14221971	0.157841	51.0186	8.33641	-4.71606	2.40E-06	0.000217451
ENSMUSG00000062962	Gm6378	18:21072343-21100199	0	4.71216	1.79769e+308	1.79769e+308	0.000161818	0.00917661
ENSMUSG00000070522	Gm6505	3:28697902-28781108	0	9.50487	1.79769e+308	1.79769e+308	2.14E-08	3.01E-06
ENSMUSG00000080816	Gm12447	4:46300006-46346412	0	2.98064	1.79769e+308	1.79769e+308	0.000372785	0.0190224
ENSMUSG00000082154	Gm16464	7:104470013-104507849	0	1.66166	1.79769e+308	1.79769e+308	0.0001166	0.00688723
ENSMUSG00000082768	Gm12727	4:106088713-106105068	0	4.73475	1.79769e+308	1.79769e+308	0.000499817	0.0246146

Table 4.3. Genes exhibiting largest changes in expression levels between Wa and Ma

An example of the results following analysis of an RNA-seq. This table indicates the expression data for the comparison between the wild type anterior (Wa) and Mutant anterior (Ma), in which we expected to identify genes involved in the directionality of migration. The data is sorted by the log 2 value, or fold change, and only significant results are listed. Red shading indicates that the specific gene was downregulated in sample 2 compared to sample 1, while green indicates a gene that is upregulated in sample 2 compared to sample 1. "Locus" is the location of the gene or transcript on the genome. "Value" is a measure of transcript abundance, given in units of Fragments Per Kilobase of exon per Million fragments mapped (FPKM), and corresponds to the level of gene expression. "Log2" is the fold change of the values in the two samples being compared. Because RNA-sequencing can identify differentially spliced or differentially regulated genes, Cufflinks also prepares a "Test stat" which reflects the changes of the abundance of different isoforms expressed within each gene. Thus, the "p-value" is the uncorrected p-value of the test stat and the "q-value" is the false positive corrected p-value. Significance was then established as being a q-value <0.05).

Table 4.4. Genes exhibiting largest changes in expression levels between Wa and Wp

gene_id	gene	locus	value_1: Wa	value_2: Wp	log2(fold_change) (Wp/Wa)	test_stat	p_value	q_value
ENSMUSG00000080848	Gm9385	9:115909454-116076176	640.531	0.481539	-10.3774	13.1556	0	0
ENSMUSG00000089999	Gm6485	3:104752726-104753165	74.1053	0.119099	-9.28127	7.1773	7.11E-13	2.29E-10
ENSMUSG00000044609	Gm9294	7:42953596-42954388	12.3754	0.0317462	-8.60668	3.5475	0.000388901	0.01977
ENSMUSG00000058932	Gm2174	X:56447887-56448366	54.495	0.142963	-8.57433	3.55453	0.000378659	0.0192766
ENSMUSG00000050900	Gm7327	X:61785380-61786032	8.49811	0.0240546	-8.46468	4.11755	3.83E-05	0.00254754
ENSMUSG00000063739	Gm4963	5:137993046-137993424	43.7658	0.130795	-8.38635	6.48681	8.77E-11	2.01E-08
ENSMUSG00000078193	Gm2000	1:156310726-156421159	338.309	1.01862	-8.37558	13.736	0	0
ENSMUSG00000066245	Gm10156	7:107863038-107863500	6.59062	0.0275813	-7.90058	3.33656	0.000848226	0.0388081
ENSMUSG00000091639	Gm3756	9:31936458-31936755	543.362	2.76414	-7.61894	13.873	0	0
ENSMUSG00000084691	SNORD113	12:109646128-109646202	5243.6	31.1879	-7.39343	5.47621	4.35E-08	5.71E-06
ENSMUSG00000091058	Gm17538	17:77674375-77674702	26.5115	0.160114	-7.37138	4.85933	1.18E-06	0.000114294
ENSMUSG00000081244	Gm13529	2:33652388-33652798	18.962	0.11677	-7.34329	5.45252	4.97E-08	6.46E-06

ENSMUSG00000069125	Rps24-ps2	3:3791896-3792295	18.905	0.119348	-7.30746	5.461	4.73E-08	6.20E-06
ENSMUSG00000074412	Gm10689	8:25454272-25454704	34.3168	0.23683	-7.17892	8.02797	8.88E-16	4.40E-13
ENSMUSG00000081629	Eif3s6-ps1	11:9737151-9737621	6.64024	0.0458576	-7.17793	3.56405	0.000365174	0.0186959
ENSMUSG00000046721	Rpl14-ps1	7:45303154-45333780	53.3927	0.408801	-7.0291	4.45142	8.53E-06	0.000670364
ENSMUSG00000086922	Gm13835	6:31141978-31142663	9.82326	0.0769372	-6.99638	4.21795	2.47E-05	0.00172184
ENSMUSG00000059585	Ube2nl	7:61549242-61549701	14.3273	0.115526	-6.9544	5.17893	2.23E-07	2.53E-05
ENSMUSG00000092278	Gm8752	17:35445855-35448926	0.913061	0.00749567	-6.92851	3.5775	0.000346894	0.0178958
ENSMUSG00000081819	Gm12722	4:105374453-105374946	10.4028	0.0882297	-6.88149	5.08365	3.70E-07	4.01E-05
ENSMUSG00000061013	Mkx	18:6910458-7004726	0.125306	1.26794	3.33895	-3.52743	0.000419618	0.0210834
ENSMUSG00000023484	Prph	15:99055173-99058978	1.62602	26.8929	4.04781	-10.1331	0	0
ENSMUSG00000038692	Hoxb4	11:96316683-96321638	0.0209053	0.490201	4.55143	-4.9989	5.77E-07	6.01E-05
ENSMUSG00000075277	6720416L17Rik	2:74748421-74762896	0.394944	12.8474	5.02369	-9.89133	0	0
ENSMUSG00000079277	Hoxd3	2:74703247-74748274	1.60534	60.3594	5.23263	-9.62001	0	0
ENSMUSG00000029671	Wnt16	6:22288226-22298522	0.0342192	1.51656	5.46985	-3.50829	0.000450992	0.0225027
ENSMUSG00000068165	Gm10233	14:66027328-66077733	0	2.28475	1.79769e+308	1.79769e+308	0.000185244	0.0103261

ENSMUSG00000081254	Gm12112	11:32903136-32926160	0	17.3787	1.79769e+308	1.79769e+308	0.000288526	0.0152266
ENSMUSG00000082154	Gm16464	7:104470013-104507849	0	0.55986	1.79769e+308	1.79769e+308	0.00104882	0.0468156
ENSMUSG00000085281	Gm13316	2:14603989-14987908	0	11.6943	1.79769e+308	1.79769e+308	1.26E-05	0.000940049
ENSMUSG00000022738	Gsc2	16:17913113-17915059	0.839433	0	-1.79769e+308	-1.79769e+308	0.00055578	0.0269225
ENSMUSG00000044268	Gm4895	10:22153279-22154047	1.0098	0	-1.79769e+308	-1.79769e+308	0.000812578	0.0374629
ENSMUSG00000067575	Rpl35a-ps3	17:29135055-29148980	85.6572	0	-1.79769e+308	-1.79769e+308	3.62E-10	7.20E-08
ENSMUSG00000080065	Gm11864	4:16390444-16391664	0.614351	0	-1.79769e+308	-1.79769e+308	0.000516348	0.0253076
ENSMUSG00000080839	Gm11625	11:101476225-101476521	8.82034	0	-1.79769e+308	-1.79769e+308	0.000296915	0.0156159
ENSMUSG00000081376	Gm11694	11:115493023-115493182	58.025	0	-1.79769e+308	-1.79769e+308	0.000568849	0.0274326
ENSMUSG00000082500	Gm15195	X:160269700-160269963	16.6138	0	-1.79769e+308	-1.79769e+308	0.000126947	0.00744949
ENSMUSG00000082524	Gm6272	5:144723626-144723812	862.559	0	-1.79769e+308	-1.79769e+308	5.51E-15	2.33E-12
ENSMUSG00000083880	Hspe1-ps6	4:96027533-96077546	10.7561	0	-1.79769e+308	-1.79769e+308	0.000714127	0.0334669
ENSMUSG00000084559	Mir1906-2	X:88759473-88759553	579.455	0	-1.79769e+308	-1.79769e+308	0.000817435	0.0376386
ENSMUSG00000092972	Mir3078	14:64591184-64591271	440.568	0	-1.79769e+308	-1.79769e+308	0.000516348	0.0253076

Table 4.4. Genes exhibiting largest changes in expression levels between Wa and Wp

An example of the results following analysis of an RNA-seq. This table indicates the expression data for the ~20 most up (green) and down (red) regulated transcripts for the comparison between the wild type anterior (Wa) and wild type posterior (Wp), in which we expected to identify genes potentially involved in the initiation of termination of migration.

Table 4.5. Genes exhibiting largest changes in expression levels between Ma and Mp

gene_id	gene	locus	value_1: Ma	value_2: Mp	log2(fold_change) (Mp/Ma)	test_stat	p_value	q_value
ENSMUSG00000029378	Areg	5:91139614-91148432	0.708598	0.0144237	-5.61845	3.27624	0.00105198	0.0469177
ENSMUSG00000005917	Otx1	11:21994763-22002897	2.10333	0.055488	-5.24436	6.57476	4.87E-11	1.17E-08
ENSMUSG00000080816	Gm12447	4:46300006-46346412	2.98064	0.105337	-4.82253	3.40793	0.000654565	0.030985
ENSMUSG00000039095	En2	5:28165695-28173612	2.80931	0.118745	-4.56428	8.487	0	0
ENSMUSG00000051490	Foxd4	19:24898964-24901309	2.79769	0.118447	-4.56192	7.20138	5.96E-13	1.94E-10
ENSMUSG00000036480	Prss56	1:87183492-87188404	0.85507	0.0412707	-4.37285	4.23708	2.26E-05	0.00160437
ENSMUSG00000056569	Mpz	1:171150710-171161130	2.21654	0.136701	-4.01921	4.77862	1.77E-06	0.000164573
ENSMUSG00000024134	Six2	17:85684267-85688274	1.7178	0.109849	-3.96696	4.90156	9.51E-07	9.45E-05
ENSMUSG00000063661	Krt73	15:101793307-101802343	0.673191	0.0458484	-3.87607	4.87979	1.06E-06	0.000104053
ENSMUSG00000041703	Zic5	14:122456794-122465677	1.78581	0.125439	-3.83152	4.63478	3.57E-06	0.00030915
ENSMUSG00000024747	Aldh1a7	19:20692952-20727562	0.824864	0.0583385	-3.82164	4.97024	6.69E-07	6.88E-05
ENSMUSG00000018166	Erbb3	10:128567522-128589652	0.730407	0.0529648	-3.78559	6.21662	5.08E-10	9.85E-08

ENSMUSG00000009900	Wnt3a	11:59248032-59290752	0.317621	0.0265736	-3.57924	3.82233	0.000132199	0.00771578
ENSMUSG00000085555	2610035F20Rik	14:122470283-122475199	0.945198	0.102801	-3.20076	3.71073	0.000206663	0.0114082
ENSMUSG00000041731	Pgm5	19:24683015-24861855	3.49877	0.400559	-3.12676	4.89564	9.80E-07	9.69E-05
ENSMUSG00000023828	Slc22a3	17:12419971-12507704	1.82357	0.210067	-3.11784	5.66718	1.45E-08	2.10E-06
ENSMUSG00000020218	Wif1	10:121033959-121100650	0.644934	0.0755037	-3.09453	3.53611	0.000406071	0.0204599
ENSMUSG00000081683	Fzd10	5:128601105-128604093	8.20091	0.962893	-3.09034	7.48898	6.95E-14	2.54E-11
ENSMUSG00000073738	Gm10567	1:9960170-9962809	22.6565	2.70302	-3.06728	8.96366	0	0
ENSMUSG00000034384	Barhl2	5:106452513-106458440	1.08605	0.141928	-2.93586	4.75104	2.02E-06	0.000186918
ENSMUSG00000082280	Gm7901	8:75448693-75984503	2.64988	11.3395	2.09735	-5.58303	2.36E-08	3.26E-06
ENSMUSG00000050852	Gm12115	11:33172917-33173368	1.24095	6.61529	2.41436	-3.68079	0.00023251	0.0126094
ENSMUSG00000079560	Hoxa3	6:52162350-52221854	4.72989	26.3037	2.47539	-6.29321	3.11E-10	6.28E-08
ENSMUSG00000025221	Kcnip2	19:45791838-45816061	2.26845	12.6624	2.48077	-3.79676	0.000146599	0.00844667
ENSMUSG00000024985	Tcf7l2	19:55741809-55933654	3.12301	17.4912	2.48562	-4.26916	1.96E-05	0.00140399
ENSMUSG00000087333	Gm13652	2:75124870-75137798	0.0531871	0.318429	2.58182	-3.53301	0.000410854	0.0206912
ENSMUSG00000042448	Hoxd1	2:74762979-74765143	0.0562328	0.493447	3.13341	-3.55873	0.000372656	0.0190224

ENSMUSG00000026934	Lhx3	2:26200211-26208289	2.10564	20.6374	3.29293	-7.38783	1.49E-13	5.11E-11
ENSMUSG00000034173	2410018M08Rik	5:129846989-129903623	3.54274	40.9299	3.53022	-5.8706	4.34E-09	6.91E-07
ENSMUSG00000069132	Nxph2	2:23321245-23401973	0.0304763	0.484104	3.98955	-4.11858	3.81E-05	0.00254088
ENSMUSG00000081470	Gm14131	2:149356686-149357405	0.379641	6.96714	4.19786	-6.59161	4.35E-11	1.07E-08
ENSMUSG00000079277	Hoxd3	2:74703247-74748274	2.52936	47.8655	4.24214	-5.24015	1.60E-07	1.86E-05
ENSMUSG00000075277	6720416L17Rik	2:74748421-74762896	0.581446	11.2334	4.272	-9.12318	0	0
ENSMUSG00000080977	Gm13772	2:90782726-90834437	0.148025	55.9102	8.56113	-3.78078	0.000156336	0.00893612
ENSMUSG00000063180	Gm10126	13:73963850-73992989	0	1100.73	1.79769e+308	1.79769e+308	3.58E-16	1.96E-13
ENSMUSG00000068165	Gm10233	14:66027328-66077733	0	7.23797	1.79769e+308	1.79769e+308	3.58E-06	0.000309213
ENSMUSG00000081254	Gm12112	11:32903136-32926160	0	50.8889	1.79769e+308	1.79769e+308	2.10E-05	0.0014961
ENSMUSG00000085281	Gm13316	2:14603989-14987908	0	13.974	1.79769e+308	1.79769e+308	9.05E-06	0.000701237

Table 4.5. Genes exhibiting largest changes in expression levels between Ma and Mp

An example of the results following analysis of an RNA-seq. This table indicates the expression data for the ~20 most up (green) and down (red) regulated transcripts for the comparison between the mutant anterior (Ma) and mutant posterior (Mp), in which we expected to identify genes potentially involved in the initiation of termination of migration.

Table 4.6. Genes exhibiting largest changes in expression levels between Wp and Mp

gene_id	gene	locus	value_1: Wp	value_2: Mp	log2(fold_change) (Mp/Wp)	test_stat	p_value	q_value
ENSMUSG00000038692	Hoxb4	11:96316683-96321638	0.490201	0.0903724	-2.43942	3.75143	0.000175832	0.00989178
ENSMUSG00000081683	Fzd10	5:128601105-128604093	4.55501	0.962893	-2.24201	5.14326	2.70E-07	2.99E-05
ENSMUSG00000020460	Rps27a	11:29545845-29578367	98.746	25.6578	-1.94432	6.19108	5.98E-10	1.14E-07
ENSMUSG00000028707	Dmbx1	4:115914543-115939926	1.90863	0.544094	-1.81061	3.78981	0.000150765	0.00863599
ENSMUSG00000059325	Hopx	5:77086442-77115161	19.8921	5.95314	-1.74047	4.2078	2.58E-05	0.00179407
ENSMUSG00000095159	AC133939.1	5:7179364-7180699	42.4273	15.3774	-1.46418	5.82491	5.71E-09	8.89E-07
ENSMUSG00000091957	Gm8841	18:61220481-61289924	445.992	192.51	-1.21209	7.3467	2.03E-13	6.88E-11
ENSMUSG00000063480	Nhp2l1	15:82041318-82047598	46.2057	20.9578	-1.14058	4.51872	6.22E-06	0.00050585
ENSMUSG00000083563	Gm13340	2:22227502-22618252	48.2319	24.7375	-0.963287	4.05704	4.97E-05	0.00322296
ENSMUSG00000025927	Tfap2b	1:19208913-19238734	6.74404	3.60286	-0.904469	3.43947	0.000582859	0.0279832
ENSMUSG00000029838	Ptn	6:36715662-36811361	37.2125	22.4959	-0.726123	3.51104	0.000446364	0.0223027
ENSMUSG00000073702	Rpl31	1:39367850-39478747	398.279	242.036	-0.718558	4.43331	9.28E-06	0.000717227

ENSMUSG00000063696	Gm8730	8:102864778-102865853	324.848	198.905	-0.707686	4.47784	7.54E-06	0.000599075
ENSMUSG00000034892	Rps29	12:69157721-69159186	1377.85	858.023	-0.683332	4.11812	3.82E-05	0.00254433
ENSMUSG00000069117	Gm17352	13:97760129-97760588	398.341	254.703	-0.645189	3.57765	0.000346698	0.0178942
ENSMUSG00000062353	Gm15772	5:3236388-3236907	784.019	502.971	-0.640413	3.49996	0.000465332	0.023154
ENSMUSG00000032518	Rpsa	9:120127765-120132369	513.448	348.528	-0.558944	3.74061	0.000183573	0.0102595
ENSMUSG00000062070	Pgk1	X:106187099-106203699	188.182	130.065	-0.532891	3.29298	0.000991316	0.0446161
ENSMUSG00000049517	Rps23	13:90923130-90924942	553.926	386.599	-0.518855	3.32652	0.000879369	0.0401819
ENSMUSG00000072235	Tuba1a	15:98949840-98953551	8681.42	7534.65	-0.204391	42.8791	0	0
ENSMUSG00000069125	Rps24-ps2	3:3791896-3792295	0.119348	18.3542	7.2648	-5.42626	5.75E-08	7.39E-06
ENSMUSG00000086922	Gm13835	6:31141978-31142663	0.0769372	11.9918	7.28415	-4.39741	1.10E-05	0.000831834
ENSMUSG00000081470	Gm14131	2:149356686-149357405	0.0432349	6.96714	7.33223	-5.42747	5.72E-08	7.36E-06
ENSMUSG00000081244	Gm13529	2:33652388-33652798	0.11677	20.4656	7.45338	-5.53882	3.05E-08	4.12E-06
ENSMUSG00000091639	Gm3756	9:31936458-31936755	2.76414	626.72	7.82485	-14.2828	0	0
ENSMUSG00000084691	SNORD113	12:109646128-109646202	31.1879	7171.63	7.84517	-5.83736	5.30E-09	8.30E-07
ENSMUSG00000066245	Gm10156	7:107863038-107863500	0.0275813	6.98524	7.98448	-3.37262	0.00074456	0.0347274

ENSMUSG00000050900	Gm7327	X:61785380-61786032	0.0240546	7.42047	8.26905	-4.01936	5.84E-05	0.00372405
ENSMUSG00000063739	Gm4963	5:137993046-137993424	0.130795	45.3642	8.4381	-6.52853	6.64E-11	1.55E-08
ENSMUSG00000058932	Gm2174	X:56447887-56448366	0.142963	50.9113	8.4762	-3.51244	0.000444019	0.0222061
ENSMUSG00000044609	Gm9294	7:42953596-42954388	0.0317462	12.2389	8.59068	-3.54078	0.000398945	0.0201762
ENSMUSG00000080848	Gm9385	9:115909454-116076176	0.481539	206.477	8.74411	-10.5025	0	0
ENSMUSG00000089999	Gm6485	3:104752726-104753165	0.119099	65.8537	9.11096	-7.03628	1.97E-12	6.00E-10
ENSMUSG00000044268	Gm4895	10:22153279-22154047	0	1.11398	1.79769e+308	1.79769e+308	0.000649982	0.0307815
ENSMUSG00000063180	Gm10126	13:73963850-73992989	0	1100.73	1.79769e+308	1.79769e+308	3.58E-16	1.96E-13
ENSMUSG00000067575	Rpl35a-ps3	17:29135055-29148980	0	81.8776	1.79769e+308	1.79769e+308	6.50E-10	1.23E-07
ENSMUSG00000080065	Gm11864	4:16390444-16391664	0	0.427435	1.79769e+308	1.79769e+308	0.00105918	0.047083
ENSMUSG00000080839	Gm11625	11:101476225-101476521	0	9.46724	1.79769e+308	1.79769e+308	0.000253004	0.0135911
ENSMUSG00000081376	Gm11694	11:115493023-115493182	0	50.9536	1.79769e+308	1.79769e+308	0.00077366	0.0358369
ENSMUSG00000082500	Gm15195	X:160269700-160269963	0	32.8376	1.79769e+308	1.79769e+308	2.59E-05	0.00180241
ENSMUSG00000082524	Gm6272	5:144723626-144723812	0	410.732	1.79769e+308	1.79769e+308	1.92E-09	3.23E-07
ENSMUSG00000083880	Hspe1-ps6	4:96027533-96077546	0	13.7208	1.79769e+308	1.79769e+308	0.000308459	0.0161757

ENSMUSG00000084559	Mir1906-2	X:88759473-88759553	0	576.792	1.79769e+308	1.79769e+308	0.000812006	0.0374525
ENSMUSG00000092972	Mir3078	14:64591184-64591271	0	319.309	1.79769e+308	1.79769e+308	0.00100334	0.0450461
ENSMUSG00000093337	Mir5109	5:17776748-17776835	0	426.824	1.79769e+308	1.79769e+308	0.00049993	0.0246146
ENSMUSG00000095344	Gm6838	12:22286892-22326064	0	0.682669	1.79769e+308	1.79769e+308	0.00105501	0.0469792

Table 4.6. Genes exhibiting largest changes in expression levels between Wp and Mp

An example of the results following analysis of an RNA-seq. This table indicates the expression data for the ~20 most up (green) and down (red) regulated transcripts for the comparison between the wild type posterior (Wp) and Mutant posterior (Mp), in which we did not expect to see any differences.

4.3. Results

4.3.1 Validation of the RNA Seq analysis

RNA sequencing data gives us the ability to identify alternatively spliced transcripts, mutations, and changes in gene expression levels. For our purposes, we were interested in determining if the loss of *Celsr1* alters the expression levels of other genes, and hoped to identify genes that are involved in the suppression of rostral migration. Even small changes in transcript levels can be detected via RNA-sequencing. Although this method measures changes in RNA transcript levels, and not protein, it can help in the identification of candidate genes of potential biological relevance.

4.3.2 Overview of gene expression changes between different experimental conditions

Several of the genes that were identified through the bioinformatics analysis of the RNA-seq were present in multiple pairwise comparisons. The Venn diagram in **Figure 4.3** indicates the number of genes that overlapped in each category, and whether they were upregulated (green) or downregulated (red) in each comparison. Genes which were expressed in two categories had similar expression patterns, with the exception of the two overlapping categories indicated by an *. In these categories, each gene was upregulated in one category, and downregulated in the other. This overlap in expression is expected because of the way the pairwise comparisons were made. For instance, for a

Figure 4.3. Several genes are differentially expressed in multiple comparisons

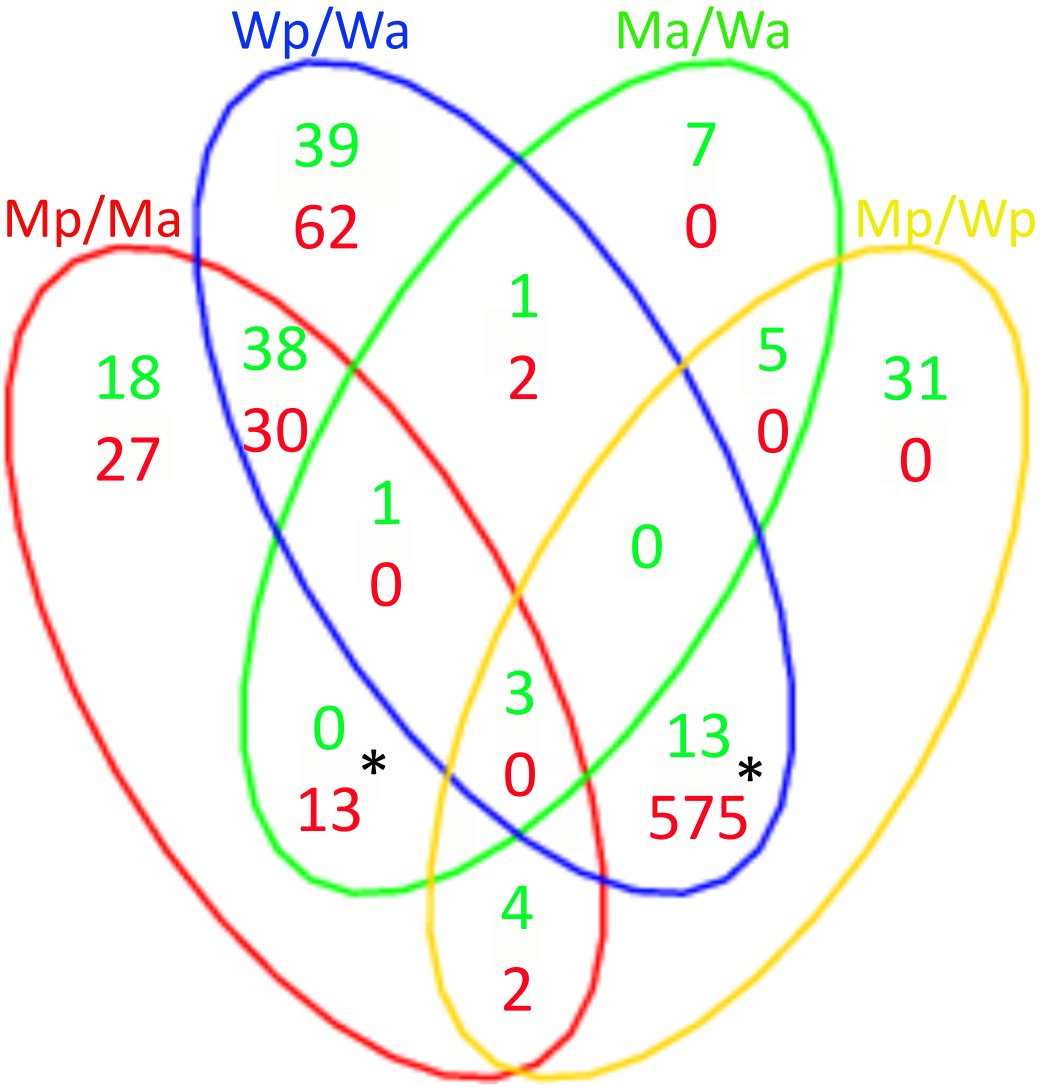

Figure 4.3. Several genes are differentially expressed in multiple comparisons

Venn diagram showing the number of genes that were differentially expressed in each comparison. The number of genes that are upregulated in each category are indicated in green, while downregulated genes are in red. For categories with genes present in multiple comparisons, the expression pattern stayed the same, with the exception of 2 categories (*), in which the expression patterns are reversed (upregulated in one category and downregulated in the other).

gene that is downregulated in the Mp compared to the Ma, it could be reasonably expected to also be downregulated when compared to the Wa. In addition, the presence of the same gene in multiple categories validates the RNA sequencing results, because given the restricted expression pattern of *Celsr1*, we would expect the loss of *Celsr1* function to alter the expression levels of a relatively small number of genes.

4.3.3. Candidate genes with potential roles in FBM neuron migration

After the analysis by the Bioinformatics Core at the University of Missouri, we were presented with lists of genes that were significant in each comparison category. The diagram above shows the number of genes that were expressed in the different comparisons (**Figure 4.4**). For our purposes, the lists were narrowed down first to genes that were known to be expressed within the hindbrain by extensive literature searches using search engines such as Mouse Genome Informatics (MGI, http://www.informatics.jax.org), Allen Brain Atlas (http://developingmouse.brain-map.org), and Eurexpress (http://www.eurexpress.org/ee). The data was then sorted by the log2 value (Value 2 / Value 1) in order to determine the genes that were the most up- or down-regulated in a sample, and eliminated all genes that had a log2 value of less than 1, keeping only those that had greater than a two-fold change in expression. An extensive literature search of each gene was then completed in order to determine their known function and if they could possibly be involved in migration. Genes were identified that may be involved in processes that could

Figure 4.4. RNA Sequencing Identifies Candidate Molecules involved in Directed Migration of Facial Branchiomotor Neurons

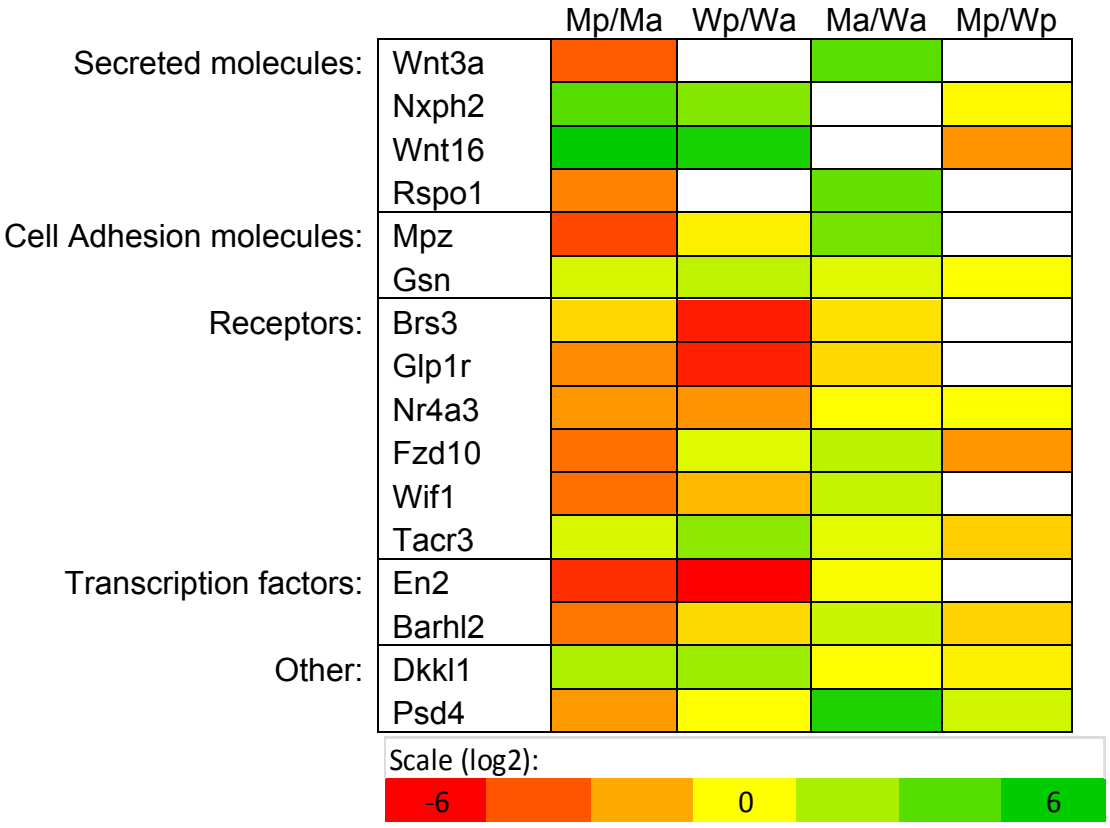

Figure 4.4. RNA Sequencing Identifies Candidate Molecules involved in Directed Migration of Facial Branchiomotor Neurons

Schematic of our top candidates and the expression values (log2) of the gene in each comparison (Value 2/Value 1). *Wnt3a, Wingless-related MMTV integration site 3A. Nxph2, Neurexophilin 2. Wnt16, Wingless-related MMTV integration site 16. Rspo1, R-spondin homolog. Mpz, myelin protein zero. Gsn, Gelsolin. Brs3, Bombesin-like receptor 3. Glp1r, Glucagon-like peptide 1 receptor. Nr4a3, nuclear receptor subfamily 4, group A, member 3 (synonym: nor-1). Fzd10, Frizzled homolog 10. Wif1, Wnt inhibitory factor 1. Tacr3, Tachykinin receptor 3. En2, engrailed 2. Barhl2, BarH-like 2. Nxph2, Neurexophilin 2. Dkkl1, Dickkopf-like 1. Psd4, Pleckstrin and Sec7 domain containing 4.* White box indicates that the test was unsuccessful for that specific gene or that the gene was not found in the comparison.

Abbreviations: Wa, wild type anterior (*GFP*$^{+/-}$ r2-r4). Wp, wild type posterior (*GFP*$^{+/-}$ r4-r6). Ma, mutant anterior (*Celsr1*$^{+/Crash}$*; GFP*$^{+/-}$ r2-r4). Mp, mutant posterior (*Celsr1*$^{+/Crash}$*; GFP*$^{+/-}$, r4-r6).

play a role in FBM neuron migration based upon their known functions. These include cell adhesion, receptors, enzymes, and transcription. Sixteen genes were chosen as being candidate molecules for the suppression of rostral migration based on the classifications described above. The function and expression level of each of these are shown below (**Figure 4.4**). The relative expression levels of each candidate gene are indicated for each comparison. White boxes indicate that the gene was not found in the specific comparison.

If *Celsr1* is acting to suppress Wnt activity in the rostral hindbrain, we would expect to see more Wnt activity in this area upon the loss of *Celsr1*. Indeed, *Wnt3a* is highly upregulated in the Ma when compared to the Wa. It is also highly downregulated in the Mp when compared to Ma, and is not differentially regulated between Wa-Wp or Wp-Mp comparisons (**Figure 4.4**). *Wnt3a* has been shown to be expressed in the developing mouse along the cortical hem of the telencephalon, extending dorsally along the midline of the neural tube (Grove et al., 1998). *Wnt3a* is involved in both the canonical and non-canonical PCP pathways, by activating β-catenin (Holmen et al., 2002; Le Grand et al., 2009) or Rho-Kinase (Kishida et al., 2004), respectively. In addition, it may play a role in axon guidance (Purro et al., 2008) and neurite projections (Kishida et al., 2004). Given its expression in the hindbrain and its known functions, *Wnt3a* may be a candidate for our model of *Celsr1*-mediated suppression of rostral migration.

Another possibility is that if *Celsr1* is acting to suppress Wnt activity in the rostral hindbrain, perhaps it is doing so by suppressing molecules that activate

Wnt activity. A Wnt agonist that was identified through the RNA sequencing process is *R-spondin homolog* (*Rspo1*), which is upregulated in the mutant anterior compared to the wild type (**Figure 4.4**), consistent with a role for it activating Wnt activity in the absence of *Celsr1*. *Rspo1* is a secreted agonist that is expressed in the hindbrain along the boundaries of the roof plate, as well as in the midbrain and dorsal spinal cord (Kamata et al., 2004; Nam et al., 2007). Interestingly, *Rspo1* signal is reduced in *Wnt1* mutant and *Wnt1/3* double mutant mice. Rspo1 binds to the receptor Lgr and forms a complex with Fzd and Wnt to initiate the canonical Wnt signaling pathway (Carmon et al., 2011; de Lau et al., 2012). In addition, *Rspo1* may act by antagonizing the degradation of Wnt receptors (MacDonald and He, 2012) or antagonizing Wnt inhibitors (Krönke et al., 2010).

Interestingly, *Engrailed2* (*En2*), is a homeobox transcription factor which is expressed in the neuroepithelium of hindbrain and at the midbrain/hindbrain border (Erickson et al., 1997), is highly downregulated in Mp and Wp samples, compared to Ma and Wa samples, respectively (**Figure 4.4**). *En2* is involved in the development of the hindbrain, midbrain, and neurons (Albéri et al., 2004; Simon et al., 2005). It is possible that it is upregulated in both anterior sections to regulate A-P specification. However, since there is not a significant difference in expression between the anterior portions of the WT and the mutant, it is unlikely that En2 is involved in the rostral migration phenotype. Therefore, another possibility is that during the dissection of the anterior hindbrain fragments, portions of the midbrain/hindbrain boundary were also collected since

we attempted to cut above r2, using the trigeminal neurons as a guide. Further analyses of these and other candidate molecules is required to determine if they do indeed play a role in the *Celsr1*-mediated suppression of rostral migration.

CHAPTER 5: Conclusions and Future Directions

Neuronal migration is critical to the proper development of the brain. In the developing mouse embryo, the FBM neurons provide a model to study multiple aspects of neuronal migration. Several molecules of the Wnt/PCP signaling pathway have been identified as playing a role in the caudal migration of the FBM neurons. One of these molecules, *Celsr1*, has also recently been implicated in determining the direction in which the neurons choose to migrate. In *Celsr1* mutants, the majority of the FBM neurons migrate caudally as normal, but a significant subset of neurons aberrantly migrates rostrally (Qu et al., 2010). Our results indicate that *Celsr1* normally functions in the ventricular zone of rhombomeres 3 and 4 of the (**Chapter 3**). Interestingly, inactivation of *Dvl2*, another core Wnt/PCP component, in *Celsr1* mutants suppresses the rostral migration phenotype, indicating that this aberrant migration is Dvl-dependent. We propose a model in which wild type Celsr1 directly or indirectly inhibits the activity of a Wnt5a cue expressed in the rostral hindbrain, preventing the rostral migration of FBM neurons. We employed several approaches to test and clarify this model. First, I examined the ability of Wnt5a-coated beads placed in r3 to overcome putative *Celsr1*-mediated suppression of FBM neuron migration in wild type hindbrain explants. Next, the ability of FBM neurons to migrate rostrally toward Wnt5a beads was analyzed in *Dvl2* mutant embryos. Consistent with our model, Wnt5a-coated beads placed in the rostral hindbrain of *Dvl2* mutants fail to attract FBM neurons (**Chapter 3**).

In our model, the mechanism of *Celsr1*-mediated suppression of Wnt5a activity is not defined. To address this question, we examined whether *Celsr1* may act through Wnt antagonists such as secreted Frizzled Related Proteins (sFRPs). Although *sFRP1* and *sFRP2* are expressed in the hindbrain, they do not play a role in suppressing the rostral migration of FBM neurons (**Chapter 3).** It is possible that *Celsr1* acts through other pathways to inhibit Wnt activity. To identify possible candidates, we performed a high throughput expression profiling screen for genes that are misregulated in *Celsr1*$^{+/Crash}$ hindbrains (**Chapter 4**). We have identified several candidates, which must be characterized in detail to define potential roles in *Celsr1*-mediated suppression of rostral migration.

Several approaches are available for analysis of the candidate molecules.

1) For secreted molecules, one could employ the hindbrain explant system described in **Chapter 4** with beads soaked in candidate molecules, and examining FBM neuron migration. Candidates that test positive may represent chemoattractants (in addition to Wnt5a) in the rostral hindbrain. Candidates that show no effect may be involved in inhibiting Wnt activity, and could be re-tested by coating beads with both Wnt5a and the candidate protein.

2) Candidate genes could be tested in zebrafish. Although a Celsr-mediated mechanism likely plays no role in suppressing rostral migration of FBM neurons in zebrafish, the expression-profiling screen has identified several genes with potential roles in FBM neuron migration, in general. The expression patterns of the orthologous zebrafish genes will be characterized in detail. Promising genes will be targeted for site-specific genomic modifications using TALEN (Joung &

Sander, 2013) or CRISPR (Jao et al., 2013) technologies. This will allow us to efficiently test several candidate genes for roles in regulating FBM neuron migration.

3) While our model proposes that *Celsr1* is inhibiting a chemoattractant (Wnt5a) in the rostral hindbrain from attracting FBM neurons, it is also possible that there are chemorepulsive cues in the rostral hindbrain that normally repel the FBM neurons so that they migrate in a caudal direction. To examine this possibility, we can establish a different explant system, in which rhombomere 4 tissue containing GFP-expressing FBM neurons would be microdissected and cultured in 3D matrices such as collagen or Matrigel to allow for individual FBM neurons to migrate out of the tissue. Under these conditions, one can examine whether candidate molecules have attractive or repulsive effects in the emigrating FBM neurons.

REFERENCES

Albéri, L., Sgadò, P., & Simon, H. H. (2004). Engrailed genes are cell-autonomously required to prevent apoptosis in mesencephalic dopaminergic neurons. *Development, 131*(13), 3229-3236. doi: 10.1242/dev.01128

Anders, S., & Huber, W. (2010). Differential expression analysis for sequence count data. *Genome Biol, 11*(10), R106. doi: 10.1186/gb-2010-11-10-r106

Barrow, J. R. (2006). Wnt/PCP signaling: a veritable polar star in establishing patterns of polarity in embryonic tissues. *Semin Cell Dev Biol, 17*(2), 185-193. doi: 10.1016/j.semcdb.2006.04.002

Behrens, J., von Kries, J. P., Kuhl, M., Bruhn, L., Wedlich, D., Grosschedl, R., & Birchmeier, W. (1996). Functional interaction of [beta]-catenin with the transcription factor LEF-1. *Nature, 382*(6592), 638-642.

Bhattacharyya, B. J., Banisadr, G., Jung, H., Ren, D., Cronshaw, D. G., Zou, Y., & Miller, R. J. (2008). The chemokine stromal cell-derived factor-1 regulates GABAergic inputs to neural progenitors in the postnatal dentate gyrus. *J Neurosci, 28*(26), 6720-6730. doi: 10.1523/JNEUROSCI.1677-08.2008

Bingham, S., Higashijima, S., Okamoto, H., & Chandrasekhar, A. (2002). The Zebrafish trilobite gene is essential for tangential migration of branchiomotor neurons. *Dev Biol, 242*(2), 149-160. doi: 10.1006/dbio.2001.0532

Bodine, P. V., Zhao, W., Kharode, Y. P., Bex, F. J., Lambert, A. J., Goad, M. B., . . . Komm, B. S. (2004). The Wnt antagonist secreted frizzled-related protein-1 is a negative regulator of trabecular bone formation in adult mice. *Mol Endocrinol, 18*(5), 1222-1237. doi: 10.1210/me.2003-0498

Brady, J. (1965). A SimpleTechnique for Making Very Fine, Durable Dissecting Needles by Sharpening Tungsten Wire Electrolytically. *Bulletin of the World Health Organization, 32*(1), 143-144.

Cadigan, K. M., & Nusse, R. (1997). Wnt signaling: a common theme in animal development. *Genes & Development, 11*(24), 3286-3305. doi: 10.1101/gad.11.24.3286

Carmon, K. S., Gong, X., Lin, Q., Thomas, A., & Liu, Q. (2011). R-spondins function as ligands of the orphan receptors LGR4 and LGR5 to regulate Wnt/β-catenin signaling. *PNAS, 108*(28), 11452-11457.

Carreira-Barbosa, F., Concha, M. L., Takeuchi, M., Ueno, N., Wilson, S. W., & Tada, M. (2003). Prickle 1 regulates cell movements during gastrulation and neuronal migration in zebrafish. *Development, 130*(17), 4037-4046. doi: 10.1242/dev.00567

Chandrasekhar, A. (2004). Turning heads: development of vertebrate branchiomotor neurons. *Dev Dyn, 229*(1), 143-161. doi: 10.1002/dvdy.10444

Charron, F., & Tessier-Lavigne, M. (2005). Novel brain wiring functions for classical morphogens: a role as graded positional cues in axon guidance. *Development, 132*(10), 2251-2262.

Curtin, J. A., Quint, E., Tsipouri, V., Arkell, R. M., Cattanach, B., Copp, A. J., . . . Murdoch, J. N. (2003). Mutation of Celsr1 Disrupts Planar Polarity of Inner Ear Hair Cells and Causes Severe Neural Tube Defects in the Mouse. *Current Biology, 13*(13), 1129-1133. doi: 10.1016/s0960-9822(03)00374-9

de Lau, W. B., Snel, B., & Clevers, H. C. (2012). The R-spondin protein family. *Genome Biology, 13*(242).

Devenport, D., & Fuchs, E. (2008). Planar polarization in embryonic epidermis orchestrates global asymmetric morphogenesis of hair follicles. *Nat Cell Biol, 10*(11), 1257-1268. doi: 10.1038/ncb1784

Di Bonito, M., Narita, Y., Avallone, B., Sequino, L., Mancuso, M., Andolfi, G., . . . Studer, M. (2013). Assembly of the auditory circuitry by a Hox genetic network in the mouse brainstem. *PLoS Genet, 9*(2), e1003249. doi: 10.1371/journal.pgen.1003249

Dobyns, W. B., & Das, S. (2009). LIS1-Associated Lissencephaly/Subcortical Band Heterotopia. *GeneReviews™ [Internet]*.

Erickson, S. L., O'Shea, K. S., Ghaboosi, N., Loverro, L., Frantz, G., Bauer, M., . . . Moore, M. W. (1997). ErbB3 is required for normal cerebellar and cardiac development: a comparison with ErbB2-and heregulin-deficient mice. *Development, 124*(24), 4999-5011.

Etheridge, S. L., Ray, S., Li, S., Hamblet, N. S., Lijam, N., Tsang, M., . . . Wynshaw-Boris, A. (2008). Murine dishevelled 3 functions in redundant pathways with dishevelled 1 and 2 in normal cardiac outflow tract, cochlea, and neural tube development. *PLoS Genet, 4*(11), e1000259. doi: 10.1371/journal.pgen.1000259

Fenstermaker, A. G., Prasad, A. A., Bechara, A., Adolfs, Y., Tissir, F., Goffinet, A., . . . Pasterkamp, R. J. (2010). Wnt/planar cell polarity signaling controls the anterior-posterior organization of monoaminergic axons in the brainstem. *J Neurosci, 30*(47), 16053-16064. doi: 10.1523/JNEUROSCI.4508-10.2010

Fogarty, M., Grist, M., Gelman, D., Marin, O., Pachnis, V., & Kessaris, N. (2007). Spatial genetic patterning of the embryonic neuroepithelium generates GABAergic interneuron diversity in the adult cortex. *J Neurosci, 27*(41), 10935-10946. doi: 10.1523/JNEUROSCI.1629-07.2007

Fritzsch, B., Muirhead, K. A., Feng, F., Gray, B. D., & Ohlsson-Wilhelm, B. M. (2005). Diffusion and imaging properties of three new lipophilic tracers, NeuroVue Maroon, NeuroVue Red and NeuroVue Green and their use for double and triple labeling of neuronal profile. *Brain Res Bull, 66*(3), 249-258. doi: 10.1016/j.brainresbull.2005.05.016

Gao, C., & Chen, Y. G. (2010). Dishevelled: The hub of Wnt signaling. *Cell Signal, 22*(5), 717-727. doi: 10.1016/j.cellsig.2009.11.021

Ghashghaei, H. T., Lai, C., & Anton, E. S. (2007). Neuronal migration in the adult brain: are we there yet? *Nat Rev Neurosci, 8*(2), 141-151. doi: 10.1038/nrn2074

Glasco, D. M. (2011). *The Role of Wnt/ Planar Cell Polarity Signaling in Mouse Facial Branchiomotor Neuron Migration.* (Doctoral Doctoral Dissertation), University of Missouri-Columbia. Retrieved from http://hdl.handle.net/10355/14286 (GlascoD-062811-D255)

Glasco, D. M., Sittaramane, V., Bryant, W., Fritzsch, B., Sawant, A., Paudyal, A., . . . Chandrasekhar, A. (2012). The mouse Wnt/PCP protein Vangl2 is necessary for migration of facial branchiomotor neurons, and functions independently of Dishevelled. *Dev Biol, 369*(2), 211-222. doi: 10.1016/j.ydbio.2012.06.021

Grove, E. A., Tole, S., Limon, J., Yip, L.-w., & Ragsdale, C. W. (1998). The hem of the embryonic cerebral cortex is defined by the expression of multiple Wnt genes and is compromised in Gli3-deficient mice. *Development, 125*, 2315-2325.

Guerrini, R., & Parrini, E. (2010). Neuronal migration disorders. *Neurobiol Dis, 38*(2), 154-166. doi: 10.1016/j.nbd.2009.02.008

Hamblet, N. S., Lijam, N., Ruiz-Lozano, P., Wang, J., Yang, Y., Luo, Z., . . . Wynshaw-Boris, A. (2002). Dishevelled 2 is essential for cardiac outflow tract development, somite segmentation and neural tube closure. *Development, 129*(24), 5827-5838. doi: 10.1242/dev.00164

Harfe, B. D., Scherz, P. J., Nissim, S., Tian, H., McMahon, A. P., & Tabin, C. J. (2004). Evidence for an expansion-based temporal Shh gradient in specifying vertebrate digit identities. *Cell, 118*(4), 517-528. doi: 10.1016/j.cell.2004.07.024

Holmen, S. L., Salic, A., Zylstra, C. R., Kirschner, M. W., & Williams, B. O. (2002). A Novel Set of Wnt-Frizzled Fusion Proteins Identifies Receptor Components That Activate β-Catenin-dependent Signaling. *Journal of Biological Chemistry, 277*(38), 34727-34735. doi: 10.1074/jbc.M204989200

Jao, L., Wente, S. R., & Chen, W. (2013). Efficient multiplex biallelic zebrafish genome editing using a CRiSPR nuclease system. *PNAS, 110*(34), 13904-13909.

Jessen, J. R., Topczewski, J., Bingham, S., Sepich, D. S., Marlow, F., Chandrasekhar, A., & Solnica-Krezel, L. (2002). Zebrafish trilobite identifies new roles for Strabismus in gastrulation and neuronal movements. *Nat Cell Biol, 4*(8), 610-615. doi: 10.1038/ncb828

Joung, J. K., & Sander, J. D. (2013). TALENs: a widely applicable technology for targeted genome editing. *Nat Rev Mol Cell Biol, 14*(1), 49-55. doi: 10.1038/nrm3486

Kamata, T., Katsube, K.-i., Michikawa, M., Yamada, M., Takada, S., & Mizusawa, H. (2004). R-spondin, a novel gene with thrombospondin type 1 domain, was expressed in the dorsal neural tube and affected in Wnts mutants. *Biochimica et Biophysica Acta (BBA) - Gene Structure and Expression, 1676*(1), 51-62. doi: 10.1016/j.bbaexp.2003.10.009

Keeble, T. R., Halford, M. M., Seaman, C., Kee, N., Macheda, M., Anderson, R. B., . . . Cooper, H. M. (2006). The Wnt receptor Ryk is required for Wnt5a-mediated axon guidance on the contralateral side of the corpus callosum. *The Journal of neuroscience, 26*(21), 5840-5848.

Kishida, S., Yamamoto, H., & Kikuchi, A. (2004). Wnt-3a and Dvl Induce Neurite Retraction by Activating Rho-Associated Kinase. *Molecular and Cellular Biology, 24*(10), 4487-4501. doi: 10.1128/mcb.24.10.4487-4501.2004

Kobayashi, K., Luo, M., Zhang, Y., Wilkes, D. C., Ge, G., Grieskamp, T., . . . Sato, T. N. (2009). Secreted Frizzled-related protein 2 is a procollagen C proteinase enhancer with a role in fibrosis associated with myocardial infarction. *Nat Cell Biol, 11*(1), 46-55. doi: 10.1038/ncb1811

Krönke, G., Uderhardt, S., Kim, K.-A., Stock, M., Scholtysek, C., Zaiss, M. M., . . . Abo, A. (2010). R-spondin 1 protects against inflammatory bone damage during murine arthritis by modulating the Wnt pathway. *Arthritis & Rheumatism, 62*(8), 2303-2312. doi: 10.1002/art.27496

Lambert de Rouvroit, C., & Goffinet, A. M. (2001). Neuronal migration. *Mechanisms of Development, 105*, 47-56.

Le Grand, F., Jones, A. E., Seale, V., Scime, A., & Rudnicki, M. A. (2009). Wnt7a activates the planar cell polarity pathway to drive the symmetric expansion of satellite stem cells. *Cell Stem Cell, 4*(6), 535-547. doi: 10.1016/j.stem.2009.03.013

Lei, Q., Jeong, Y., Misra, K., Li, S., Zelman, A. K., Epstein, D. J., & Matise, M. P. (2006). Wnt signaling inhibitors regulate the transcriptional response to morphogenetic Shh-Gli signaling in the neural tube. *Dev Cell, 11*(3), 325-337. doi: 10.1016/j.devcel.2006.06.013

Leimeister, C., Bach, A., & Gessler, M. (1998). Developmental expression patterns of mouse sFRP genes encoding members of the secreted frizzled related protein family. *Mechanisms of Development, 75*, 29-42.

Li, B., & Dewey, C. N. (2011). RSEM: accurate transcript quantification from RNA-Seq data with or without a reference genome. *BMC Bioinformatics, 12*, 323. doi: 10.1186/1471-2105-12-323

MacDonald, B. T., & He, X. (2012). Frizzled and LRP5/6 Receptors for Wnt/β-Catenin Signaling. *Cold Spring Harbor Perspectives in Biology, 4*(12). doi: 10.1101/cshperspect.a007880

Mapp, O. M., Wanner, S. J., Rohrschneider, M. R., & Prince, V. E. (2010). Prickle1b mediates interpretation of migratory cues during zebrafish facial branchiomotor neuron migration. *Dev Dyn, 239*(6), 1596-1608. doi: 10.1002/dvdy.22283

Marin, O., & Rubenstein, J. L. (2001). A long, remarkable journey: Tangential migration in the telencephalon. *Nat Rev Neurosci, 2*(11), 780-790.

Marin, O., & Rubenstein, J. L. (2003). Cell migration in the forebrain. *Annu Rev Neurosci, 26*, 441-483. doi: 10.1146/annurev.neuro.26.041002.131058

Misra, K., & Matise, M. P. (2010). A critical role for sFRP proteins in maintaining caudal neural tube closure in mice via inhibition of BMP signaling. *Dev Biol, 337*(1), 74-83. doi: 10.1016/j.ydbio.2009.10.015

Murakami, S., Ohki-Hamazaki, H., Watanabe, K., Ikenaka, K., & Ono, K. (2010). Netrin 1 provides a chemoattractive cue for the ventral migration of GnRH neurons in the chick forebrain. *The Journal of Comparative Neurology, 518*(11), 2019-2034. doi: 10.1002/cne.22319

Muzumdar, M. D., Tasic, B., Miyamichi, K., Li, L., & Luo, L. (2007). A global double-fluorescent Cre reporter mouse. *Genesis, 45*(9), 593-605. doi: 10.1002/dvg.20335

Nam, J. S., Turcotte, T. J., & Yoon, J. K. (2007). Dynamic expression of R-spondin family genes in mouse development. *Gene Expr Patterns, 7*(3), 306-312. doi: 10.1016/j.modgep.2006.08.006

Penton, A., Wodarz, A., & Nusse, R. (2002). Analysis of dishevelled in Drosophila Defines Novel Domains in the Dishevelled Protein as Well as Novel Suppressing Alleles of axin. *Genetics Society of America, 161*, 747-762.

Purro, S. A., Ciani, L., Hoyos-Flight, M., Stamatakou, E., Siomou, E., & Salinas, P. C. (2008). Wnt Regulates Axon Behavior through Changes in Microtubule Growth Directionality: A New Role for Adenomatous Polyposis Coli. *The Journal of neuroscience, 28*(34), 8644-8654. doi: 10.1523/jneurosci.2320-08.2008

Qu, Y., Glasco, D. M., Zhou, L., Sawant, A., Ravni, A., Fritzsch, B., . . . Tissir, F. (2010). Atypical cadherins Celsr1-3 differentially regulate migration of facial branchiomotor neurons in mice. *J Neurosci, 30*(28), 9392-9401. doi: 10.1523/JNEUROSCI.0124-10.2010

Ravni, A., Qu, Y., Goffinet, A. M., & Tissir, F. (2009). Planar cell polarity cadherin Celsr1 regulates skin hair patterning in the mouse. *J Invest Dermatol, 129*(10), 2507-2509. doi: 10.1038/jid.2009.84

Robinson, M. D., McCarthy, D. J., & Smyth, G. K. (2010). edgeR: a Bioconductor package for differential expression analysis of digital gene expression data. *Bioinformatics, 26*(1), 139-140. doi: 10.1093/bioinformatics/btp616

Schwarz, Q., Gu, C., Fujisawa, H., Sabelko, K., Gertsenstein, M., Nagy, A., . . . Ruhrberg, C. (2004). Vascular endothelial growth factor controls neuronal migration and cooperates with Sema3A to pattern distinct compartments of the facial nerve. *Genes Dev, 18*(22), 2822-2834. doi: 10.1101/gad.322904

Schwarz, Q., Waimey, K. E., Golding, M., Takamatsu, H., Kumanogoh, A., Fujisawa, H., . . . Ruhrberg, C. (2008). Plexin A3 and plexin A4 convey semaphorin signals during facial nerve development. *Dev Biol, 324*(1), 1-9. doi: 10.1016/j.ydbio.2008.08.020

Shirasaki, R., Lewcock, J. W., Lettieri, K., & Pfaff, S. L. (2006). FGF as a target-derived chemoattractant for developing motor axons genetically programmed by the LIM code. *Neuron, 50*(6), 841-853. doi: 10.1016/j.neuron.2006.04.030

Simon, H. H., Scholz, C., & O'Leary, D. D. M. (2005). Engrailed genes control developmental fate of serotonergic and noradrenergic neurons in mid- and hindbrain in a gene dose-dependent manner. *Molecular and Cellular Neuroscience, 28*(1), 96-105. doi: http://dx.doi.org/10.1016/j.mcn.2004.08.016

Sittaramane, V., Pan, X., Glasco, D. M., Huang, P., Gurung, S., Bock, A., . . . Chandrasekhar, A. (2013). The PCP protein Vangl2 regulates migration of hindbrain motor neurons by acting in floor plate cells, and independently of cilia function. *Dev Biol, 382*(2), 400-412. doi: 10.1016/j.ydbio.2013.08.017

Sittaramane, V., Sawant, A., Wolman, M. A., Maves, L., Halloran, M. C., & Chandrasekhar, A. (2009). The cell adhesion molecule Tag1, transmembrane protein Stbm/Vangl2, and Lamininalpha1 exhibit genetic interactions during migration of facial branchiomotor neurons in zebrafish. *Dev Biol, 325*(2), 363-373. doi: 10.1016/j.ydbio.2008.10.030

Song, M.-R. (2007). Moving Cell Bodies: Understanding the Migratory Mechanisms of Facial Motor Neurons. *Archives of Pharmacal Research, 30*(10), 1273-1282.

Song, M. R., Shirasaki, R., Cai, C. L., Ruiz, E. C., Evans, S. M., Lee, S. K., & Pfaff, S. L. (2006). T-Box transcription factor Tbx20 regulates a genetic program for cranial motor neuron cell body migration. *Development, 133*(24), 4945-4955. doi: 10.1242/dev.02694

Studer, M., Gavalas, A., Marshall, H., Ariza-McNaughton, L., Rijil, F. M., Chambon, P., & Krumlauf, R. (1998). Genetic interactions between Hoxa1 and Hoxb1 reveal new roles in regulation of early hindbrain patterning. *Development, 125*, 1025-1036.

Tissir, F., Bar, I., Jossin, Y., De Backer, O., & Goffinet, A. M. (2005). Protocadherin Celsr3 is crucial in axonal tract development. *Nat Neurosci, 8*(4), 451-457. doi: 10.1038/nn1428

Tissir, F., & Goffinet, A. M. (2006). Expression of planar cell polarity genes during development of the mouse CNS. *Eur J Neurosci, 23*(3), 597-607. doi: 10.1111/j.1460-9568.2006.04596.x

Tissir, F., & Goffinet, A. M. (2013). Atypical Cadherins Celsr1-3 and Planar Cell Polarity in Vertebrates. *Progress in Molecular Biology abd Translational Science, 116*.

Tissir, F., Qu, Y., Montcouquiol, M., Zhou, L., Komatsu, K., Shi, D., . . . Goffinet, A. M. (2010). Lack of cadherins Celsr2 and Celsr3 impairs ependymal ciliogenesis, leading to fatal hydrocephalus. *Nat Neurosci, 13*(6), 700-707. doi: 10.1038/nn.2555

Trapnell, C., Pachter, L., & Salzberg, S. L. (2009). TopHat: discovering splice junctions with RNA-Seq. *Bioinformatics, 25*(9), 1105-1111. doi: 10.1093/bioinformatics/btp120

Trapnell, C., Roberts, A., Goff, L., Pertea, G., Kim, D., Kelley, D. R., . . . Pachter, L. (2012). Differential gene and transcript expression analysis of RNA-seq experiments with TopHat and Cufflinks. *Nat Protoc, 7*(3), 562-578. doi: 10.1038/nprot.2012.016

Trapnell, C., Williams, B. A., Pertea, G., Mortazavi, A., Kwan, G., van Baren, M. J., . . . Pachter, L. (2010). Transcript assembly and quantification by RNA-Seq reveals unannotated transcripts and isoform switching during cell differentiation. *Nat Biotechnol, 28*(5), 511-515. doi: 10.1038/nbt.1621

Valiente, M., & Marin, O. (2010). Neuronal migration mechanisms in development and disease. *Curr Opin Neurobiol, 20*(1), 68-78. doi: 10.1016/j.conb.2009.12.003

Vivancos, V., Chen, P., Spassky, N., Qian, D., Dabdoub, A., Kelley, M., . . . Guthrie, S. (2009). Wnt activity guides facial branchiomotor neuron migration, and involves the PCP pathway and JNK and ROCK kinases. *Neural Dev, 4*, 7. doi: 10.1186/1749-8104-4-7

Voiculescu, O., Charney, P., & Schneider-Maunoury, S. (2000). Expression Pattern of a Krox-20/Cre Knock-in llele in the Developing Hindbrain, Bones, and Peripheral Nervous System. *Genesis, 26*, 123-126.

Wada, H., Tanaka, H., Nakayama, S., Iwasaki, M., & Okamoto, H. (2006). Frizzled3a and Celsr2 function in the neuroepithelium to regulate migration of facial motor neurons in the developing zebrafish hindbrain. *Development, 133*(23), 4749-4759. doi: 10.1242/dev.02665

Wang, J., Mark, S., Zhang, X., Qian, D., Yoo, S. J., Radde-Gallwitz, K., . . . Chen, P. (2005). Regulation of polarized extension and planar cell polarity in the cochlea by the vertebrate PCP pathway. *Nat Genet, 37*(9), 980-985. doi: 10.1038/ng1622

Wang, Z., Gerstein, M., & Snyder, M. (2009). RNA-Seq: a revolutionary tool for transcriptomics. *Nature Reviews Genetics, 10*, 57-63.

Zerbino, D. R., & Birney, E. (2008). Velvet: algorithms for de novo short read assembly using de Bruijn graphs. *Genome Res, 18*(5), 821-829. doi: 10.1101/gr.074492.107